

2004

The influences of preparation on the bond strength of zinc twin-wire arc spray coating on steel

Tram Tran
San Jose State University

Follow this and additional works at: https://scholarworks.sjsu.edu/etd_theses

Recommended Citation

Tran, Tram, "The influences of preparation on the bond strength of zinc twin-wire arc spray coating on steel" (2004). *Master's Theses*. 2739.

DOI: <https://doi.org/10.31979/etd.k4fh-t4es>

https://scholarworks.sjsu.edu/etd_theses/2739

This Thesis is brought to you for free and open access by the Master's Theses and Graduate Research at SJSU ScholarWorks. It has been accepted for inclusion in Master's Theses by an authorized administrator of SJSU ScholarWorks. For more information, please contact scholarworks@sjsu.edu.

NOTE TO USERS

This reproduction is the best copy available.

UMI[®]

THE INFLUENCES OF PREPARATION ON THE BOND STRENGTH OF ZINC
TWIN-WIRE ARC SPRAY COATING ON STEEL

A Thesis

Presented to

The Faculty of the Department of Chemical and Materials Engineering
San Jose State University

In Partial Fulfillment

of the Requirements for the Degree

Master of Science

By Tram Tran

August 2004

UMI Number: 1427194

Copyright 2004 by
Tran, Tram

All rights reserved.

INFORMATION TO USERS

The quality of this reproduction is dependent upon the quality of the copy submitted. Broken or indistinct print, colored or poor quality illustrations and photographs, print bleed-through, substandard margins, and improper alignment can adversely affect reproduction.

In the unlikely event that the author did not send a complete manuscript and there are missing pages, these will be noted. Also, if unauthorized copyright material had to be removed, a note will indicate the deletion.

UMI[®]

UMI Microform 1427194

Copyright 2005 by ProQuest Information and Learning Company.

All rights reserved. This microform edition is protected against
unauthorized copying under Title 17, United States Code.

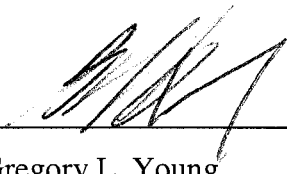
ProQuest Information and Learning Company
300 North Zeeb Road
P.O. Box 1346
Ann Arbor, MI 48106-1346

© 2004

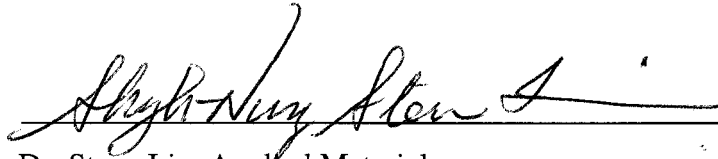
Tram Tran

ALL RIGHTS RESERVED

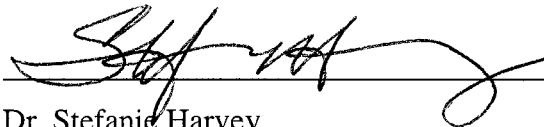
APPROVED FOR THE DEPARTMENT OF CHEMICAL
AND MATERIALS ENGINEERING



Dr. Gregory L. Young



Dr. Steve Lin, Applied Materials



Dr. Stefanie Harvey

APPROVED FOR THE UNIVERSITY



ABSTRACT

THE INFLUENCE OF PREPARATION ON THE BOND STRENGTH OF ZINC TWIN-WIRE ARC SPRAY

By Tram Tran

Twin-wire arc spray (TWAS) is a process of depositing a metallic coating on a substrate. TWAS has a variety of applications for corrosion and abrasion protection. The bond strength between the coating and the substrate is essential since a coating's success relies primarily upon mechanical bonding of the coating to the substrate. Substrate preparation, coating thickness, and surface morphology are among the critical factors. This study focuses on characterizing coating adhesion strength as a function of substrate preparation. The influence of substrate preparation by grit blasting to enhance roughening of the substrate on the coating bond strength is investigated. A tensile adhesion test is used to measure bond strength of the coating. The relationship between substrate surface cleanliness and bond strength is explored. The surface profile is characterized by a 2-D profilometer. The coating interfacial and cross-sectioned microstructures are also examined with the use of a scanning-electron microscope (SEM).

ACKNOWLEDGEMENT

I would like to thank

- APS Materials and Heath Phillips
- CSL, Inc. and Mahesh Naik
- Dr. Gregory Young
- Dr. Steve Lin
- Dr. Stefanie Harvey

for guidance and effort in supporting this research.

Also, I wish to thank my parents for always encouraging me.

TABLE OF CONTENTS

LIST OF FIGURES	xi
LIST OF TABLES	xvi
GLOSSARY OF ACRONYMS	xvii
1. INTRODUCTION.....	1
1.1. Thermal Spray Technology	1
1.2. Concept of Twin-Wire Arc Spray (TWAS)	4
1.2.1. Advantages of Twin-Wire Arc Spraying	7
1.2.2. Disadvantages of Twin-Wire Arc Spraying.....	8
1.3. Applications of Twin-Wire Arc Spraying	8
1.4. Coating Material	9
2. LITERATURE REVIEW	11
2.1. Bond Strength.....	11
2.2. The Major Parameters Affecting Bond Strength.....	13
2.2.1 Substrate Surface Preparation.....	14
2.2.1.1 Substrate Surface Cleanliness	15
2.2.1.2 Substrate Surface Roughness.....	16
2.2.2 Coating Thickness.....	17
2.2.2.1 Spray Particles	21
2.2.3 Coating Surface Characterization	23
2.2.3.1. 2-D Surface Profile	24
2.2.3.2. 3-D Surface Topography.....	26

2.3	Summary.....	30
3.	RESEARCH FOCUS.....	31
3.1.	Hypothesis	31
3.2.	Objective.....	32
3.3.	Justification.....	33
4.	EXPERIMENTAL METHODOLOGY.....	34
4.1.	Approach	34
4.2.	Substrate Materials	34
4.3.	Experimental Design	35
4.3.1.	Baseline Experiments.....	36
4.3.2.	Experimental Testing.....	41
4.3.2.1.	Tensile Adhesion Test.....	41
4.3.2.2.	Surface Characterization.....	42
4.3.2.2.1.	Surface Roughness Measurement	42
4.3.2.2.2.	Surface Microstructure Examination	45
4.4.	Analytical Instrumentation	47
4.4.1.	Profilometer for Surface Roughness Measurement	47
4.4.2.	SEM for Surface Microstructure Examination	51
4.4.3.	Micrometer for Thickness Measurement	52
4.5.	Experimental Procedure	52
4.5.1.	Substrate Preparation	53
4.5.2.	Measuring Substrate Roughness and Pre-Coating Thickness and Cleaning	53

4.5.3. Coating.....	54
4.5.4. Analyzing Coating Bond Strength, Thickness, Surface Profile, and Microstructure	54
5. RESULTS AND DISCUSSION	55
5.1. Roughness as a Function of Grit Size.....	55
5.2. Ra Before and After Cleaning	56
5.3. Results of Clean Coupons.....	57
5.3.1. Adhesion vs. Roughness	58
5.3.2. SEM Images Analysis.....	59
5.3.2.1. Clean 24 Grit.....	59
5.3.2.1.1. Interface	59
5.3.2.1.2. Cross-Sectional Images.....	66
5.3.2.2. Clean 36 Grit.....	67
5.3.2.2.1. Interface	67
5.3.2.2.2. Cross-Sectional Images.....	70
5.3.2.3. Clean 80 Grit.....	71
5.3.2.3.1. Interface	71
5.3.2.3.2. Cross-Sectional Images.....	74
5.4. Results of Non-Clean Coupons	75
5.4.1. Adhesion vs. Roughness	75
5.4.2. SEM Images Analysis.....	76
5.4.2.1. Non-Clean 24 Grit.....	76

5.4.2.1.1. Interface	77
5.4.2.1.2. Cross-Sectional Images.....	78
5.4.2.2. Non-Clean 36 Grit.....	80
5.4.2.2.1. Interface	80
5.4.2.2.2. Cross-Sectional Images.....	84
5.4.2.3. Non-Clean 80 Grit.....	86
5.4.2.3.1. Interface	87
5.4.2.3.2. Cross-Sectional Images.....	88
5.5. Results of Clean vs. Non-Clean Coupons	90
6. SUMMARY AND CONCLUSION	92
7. FUTURE WORK.....	96
REFERENCES.....	97
APPENDICES	103
APPENDIX A – RESULTS OF Ra BEFORE AND AFTER CLEANING.....	104
APPENDIX B – F-TESTS AND T-TESTS OF THE CHANGES IN ROUGHNESS BEFORE AND AFTER CLEANING	105
APPENDIX C – F-TEST AND T-TEST OF SIZE 24 AND SIZE 80 GRITS COUPONS.....	106
C1. F-TEST AND T-TEST OF THE BOND STRENGTH OF CLEAN COUPONS BLASTED BY SIZE 24 GRIT AND SIZE 80 GRIT	106
C2. F-TEST AND T-TEST OF THE BOND STRENGTH OF NON-CLEAN COUPONS BLASTED BY SIZE 24 GRIT AND SIZE 80 GRIT	106

APPENDIX D – CROSS-SECTIONED VIA COMPUTERIZED IMAGE ANALYSIS
..... 107

APPENDIX E - RESULTS OF SIZE 80 GRIT COUPONS..... 113

APPENDIX F – RESULTS OF SIZE 36 GRIT COUPONS 114

APPENDIX G – RESULTS OF SIZE 24 GRIT COUPONS..... 115

LIST OF FIGURES

Figure 1. Process of Thermal Spray Coating.....	1
Figure 2. Schematic Diagram of Thermal Spray Process	2
Figure 3. Spray Booth.....	3
Figure 4. Thermal Spray Coating Illustration	4
Figure 5. Sketch of Twin-Wire Arc Spraying.....	5
Figure 6. Requirement for a Typical Electric Wire Arc Spray System	6
Figure 7. An Example of the Twin-Wire Arc Method of Spray Coating	7
Figure 8. SEM Micrograph of Alumina 1400 Microns Grit Size.....	14
Figure 9. SEM Micrograph of Alumina 500 Microns Grit Size.....	15
Figure 10. Profile of Roughened Surface	17
Figure 11. Variation of Bond Strength with Coating Thickness	18
Figure 12. Schematic of Coating Deposition.....	20
Figure 13. The Lamella after Impact of Sprayed Particles	21
Figure 14. Standard Spray Pattern	22
Figure 15. Sampling (or Cut-off) Length and Evaluation Length	25
Figure 16. Roughness, Waviness, and Form of a 3-D Surface.....	27
Figure 17. Skewness of Surfaces	28
Figure 18. Kurtosis of Surfaces	28
Figure 19. Coordinate System Used for Surface Topography Representation.....	29
Figure 20. TWAS Test Coupon	35
Figure 21. Experimental Procedure Flow Diagram Phase I	37

Figure 22a. Experimental Procedure Flow Diagram Phase II for Clean Coupons	39
Figure 22b. Experimental Procedure Flow Diagram Phase II for Non-Clean Coupons..	40
Figure 23. ASTM C633 Adhesion Testing Principle.....	42
Figure 24. Illustration for the Calculation of Roughness Average Ra.....	43
Figure 25. Flow Chart of the Roughness Measurement System.....	44
Figure 26. Scanning Electron Microscope (SEM).....	46
Figure 27. SEM Electrons.....	47
Figure 28. 60mm Standard Diamond Stylus Arm	48
Figure 29. Taylor Hobson Talysurf Profilometer	49
Figure 30. Schematic Diagram of a Computerized Stylus Instrument	49
Figure 31. Schematic of Stylus Profilometer	50
Figure 32. R. J. Lee Instrument Personal SEM	51
Figure 33. Mitutoyo Micrometer	52
Figure 34. Average Substrate Roughness vs. Grit Size	56
Figure 35. Average Adhesion vs. Clean Substrate Roughness.....	58
Figure 36. Interface of Clean 24 Grit Coupon (# 041)	60
Figure 37a. SEM Secondary Image of a Textured Steel Substrate at a Nominal Magnification of 100x of a Size 24 Grit Clean Coupon	61
Figure 37b. SEM Backscattered Image of a Textured Steel Substrate at a Nominal Magnification of 100x of a Size 24 Grit Clean Coupon	61
Figure 38a. SEM Secondary Image of a Textured Steel Substrate at a Nominal Magnification of 500x of a Size 24 Grit Clean Coupon.	62

Figure 38b. SEM Backscattered Image of a Textured Steel Substrate at a Nominal Magnification of 500x of a Size 24 Grit Clean Coupon.	63
Figure 39. EDX Spectrum of Substrate (Dark Gray Areas)	64
Figure 40. EDX Spectrum of Alumina Grit (Black Spots).....	65
Figure 41. EDX Spectrum of Sprayed Zinc Coating (White Areas)	65
Figure 42. SEM Backscattered Image of a Zinc Coating Cross-Sectioned at a Nominal Magnification of 1000x of a Size 24 Grit Clean Coupon (Spot 1)	66
Figure 43. SEM Backscattered Image of a Zinc Coating Cross-Sectioned at a Nominal Magnification of 1000x of a Size 24 Grit Clean Coupon (Spot 2)	67
Figure 44. Interface of Clean 36 Grit Coupon (# 021)	68
Figure 45a. SEM Secondary Image of a Textured Steel Substrate at a Nominal Magnification of 100x of a Size 36 Grit Clean Coupon	69
Figure 45b. SEM Backscattered Image of a Textured Steel Substrate at a Nominal Magnification of 100x of a Size 36 Grit Clean Coupon	69
Figure 46. SEM Backscattered Image of a Zinc Coating Cross-Sectioned at a Nominal Magnification of 1000x of a Size 36 Grit Clean Coupon (Spot 1)	70
Figure 47. SEM Backscattered Image of a Zinc Coating Cross-Sectioned at a Nominal Magnification of 1000x of a Size 36 Grit Clean Coupon (Spot 2)	71
Figure 48. Interface of Clean 80 Grit Coupon (# 071)	72
Figure 49. SEM Backscattered Image of a Textured Steel Substrate at a Nominal Magnification of 250x of a Size 80 Grit Clean Coupon (Spot 1)	73

Figure 50. SEM Backscattered Image of a Textured Steel Substrate at a Nominal Magnification of 250x of a Size 80 Grit Clean Coupon (Spot 2)	73
Figure 51. SEM Backscattered Image of a Zinc Coating Cross-Sectioned at a Nominal Magnification of 1000x of a Size 80 Grit Clean Coupon (Spot 1)	74
Figure 52. SEM Backscattered Image of a Zinc Coating Cross-Sectioned at a Nominal Magnification of 1000x of a Size 80 Grit Clean Coupon (Spot 2)	75
Figure 53. Average Adhesion vs. Non-Clean Substrate Roughness.....	76
Figure 54. Interface of Non-Clean 24 Grit Coupon (# 056)	77
Figure 55. SEM Backscattered Image of a Textured Steel Substrate at a Nominal Magnification of 100x of a Size 24 Grit Non-Clean Coupon	78
Figure 56. SEM Backscattered Image of a Zinc Coating Cross-Sectioned at a Nominal Magnification of 1000x of a Size 24 Grit Non-Clean Coupon (Spot 1)	79
Figure 57. SEM Backscattered Image of a Zinc Coating Cross-Sectioned at a Nominal Magnification of 1000x of a Size 24 Grit Non-Clean Coupon (Spot 2)	79
Figure 58. SEM Backscattered Image of a Zinc Coating Cross-Sectioned at a Nominal Magnification of 1000x of a size 24 Grit Non-Clean Coupon (Spot 3).....	80
Figure 59. Interface of Non-Clean 36 Grit Coupon (# 006)	81
Figure 60a. SEM Secondary Image of a Textured Steel Substrate at a Nominal Magnification of 100x of a Size 36 Grit Non-Clean Coupon	82
Figure 60b. SEM Backscattered Image of a Textured Steel Substrate at a Nominal Magnification of 100x of a Size 36 Grit Non-Clean Coupon	82

Figure 61a. SEM Secondary Image of a Textured Steel Substrate at a Nominal Magnification of 500x of a Size 36 Grit Non-Clean Coupon	83
Figure 61b. SEM Backscattered Image of a Textured Steel Substrate at a Nominal Magnification of 500x of a Size 36 Grit Non-Clean Coupon	84
Figure 62. SEM Backscattered Image of a Zinc Coating Cross-Sectioned at a Nominal Magnification of 1000x of a Size 36 Grit Non-Clean Coupon (Spot 1)	85
Figure 63. SEM Backscattered Image of a Zinc Coating Cross-Sectioned at a Nominal Magnification of 1000x of a Size 36 Grit Non-Clean Coupon (Spot 2)	85
Figure 65. Interface of Non-Clean 80 Grit Coupon (# 086)	87
Figure 66. SEM Backscattered Image of a Textured Steel Substrate at a Nominal Magnification of 100x of a Size 80 Grit Non-Clean Coupon	88
Figure 67. SEM Backscattered Image of a Zinc Coating Cross-Sectioned at a Nominal Magnification of 1000x of a Size 80 Grit Non-Clean Coupon (Spot 1)	89
Figure 68. SEM Backscattered Image of a Zinc Coating Cross-Sectioned at a Nominal Magnification of 1000x of a Size 80 Grit Non-Clean Coupon (Spot 2)	89
Figure 69. SEM Backscattered Image of a Zinc Coating Cross-Sectioned at a Nominal Magnification of 1000x of a Size 80 Grit Non-Clean Coupon (Spot 3)	90
Figure 70. Average Bond Strength vs. Substrate Ra	91
Figure 71. Percentage of Exposure of Textured Surface	94

LIST OF TABLES

Table 1. Average of Coating Properties.....	13
Table 2. Cutoff and Evaluation Values for Surface Profile Using Ra.....	24
Table 3. Coupon Matrix.....	36
Table 4. Average Roughness of Grits.....	56
Table 5. Average Bead Blast Roughness Before and After Cleaning	57
Table 6. Bond Strength Results of Coupons for SEM Examination.....	59
Table 7. Average Results of Substrate Roughness and Bond Strength	91

GLOSSARY OF ACRONYMS

ANSI – American National Standards Institute

ASME – The American Society of Mechanical Engineers

ASTM – The American Society for Testing and Materials

CDA – Dry Compressed Air

EDS – Energy Dispersive Spectrum

SEM – Scanning Electron Microscope

TWAS - Twin Wire Arc Spray

CHAPTER ONE

1. INTRODUCTION

1.1. Thermal Spray Technology

Thermal spray coating is an established industrial method for modifying component surfaces. The process of thermal spray coating is shown in Figure 1. A torch is used to heat material into a molten or semi-molten state. A gas is used to propel the material to the substrate [1]. The benefits are lower cost, improved engineering performance, and increased component life. In addition, thermal spray coatings repair worn parts and those damaged in service, and restore dimensions to mis-machined components [2].

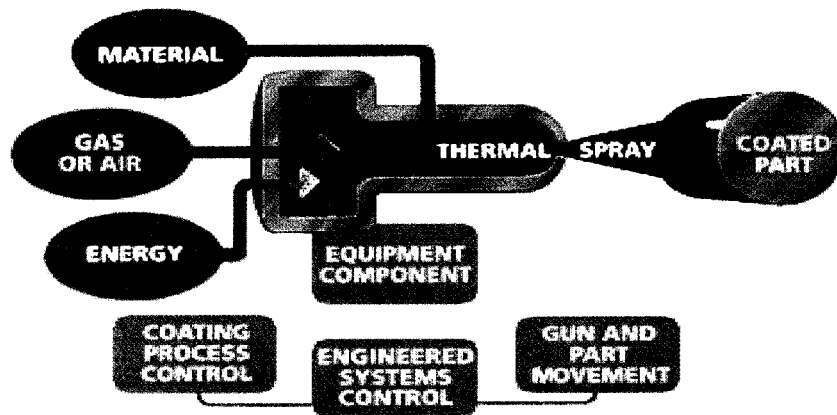


Figure 1. Process of Thermal Spray Coating [1].

walk-in acoustical spray enclosure as shown in Figure 3. This isolates the thermal spray operations from the rest of the work environment with a large view window so that operators can remain outside while viewing coating operations.

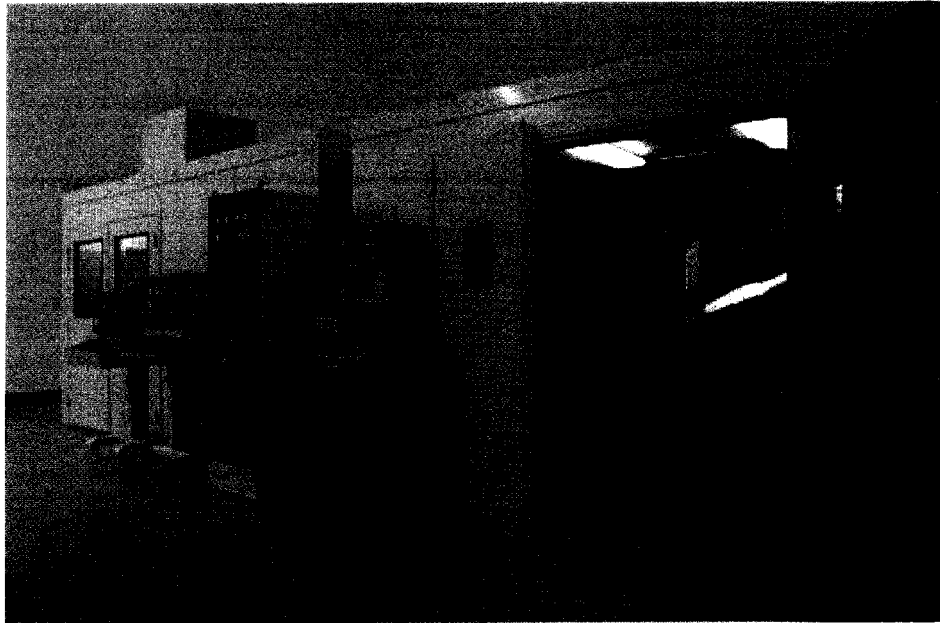


Figure 3. Spray Booth [5].

Thermal spray technology is distinguished by its ability to deposit overlays of metals, ceramics, polymers, and composites of these materials to form a coating on layers of substrates [8] as shown in Figure 4. Thermal spraying is a generic term that describes several material spraying processes: plasma spraying, combustion spraying, nozzle aspirated spraying, and twin-wire arc spraying [9].

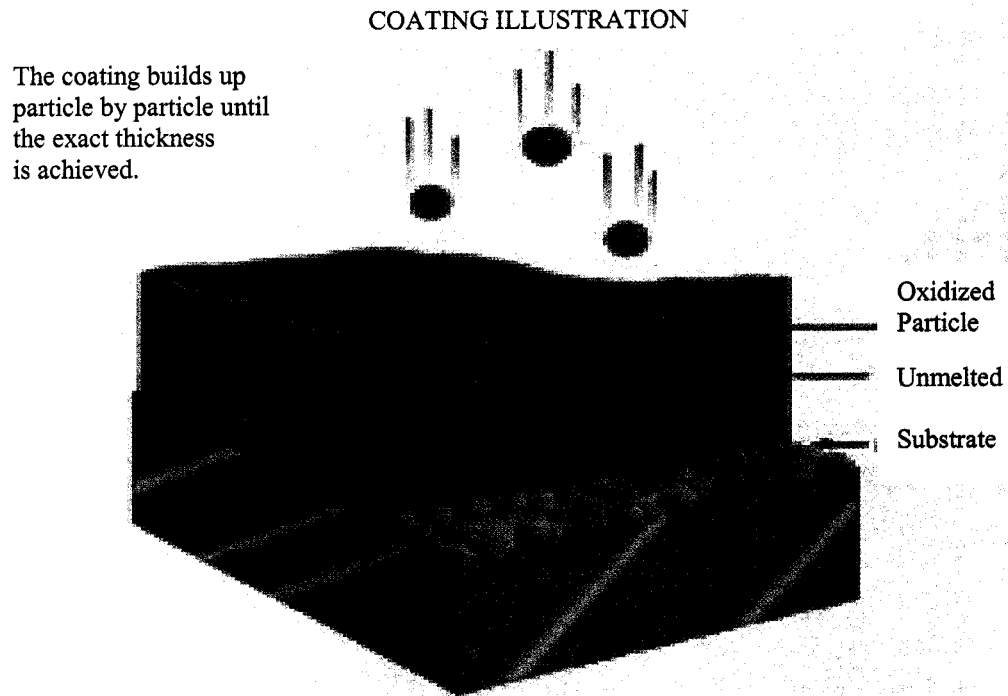


Figure 4. Thermal Spray Coating Illustration [5].

1.2. Concept of Twin-Wire Arc Spray (TWAS)

TWAS is utilized only for metallic coating of substrates. In this process, there is no external heat source. Heating and melting occur when two electrically opposed charged wires are fed together. A controlled arc occurs at the intersection [10]. Two wires that are consumable electrodes are drawn from spools. The electrodes form a liquid droplet due to arc heating and are blown by compressed gas as shown in Figure 5. The jet of gas acts to atomize the melted wire and to propel the atomized particles to the substrate. If the wires are of different materials, pseudo-alloy coatings can be produced

[4]. The two current-carrying and electrically conductive wires are fed into a common arc point where melting occurs [11]. Then molten material is continuously atomized by compressed air to form a molten spray with a high material throughput. As material is removed, additional material is supplied by a controlled means of delivering the wires [6]. Controlled feed rates of the wire ensure uniform melting. The operational temperature approaches 4000°C (7230°F) and particle velocities approach 50 to 150m/s (140 to 540 ft/sec) [2]. The requirements for a typical TWAS system are shown in Figure 6.

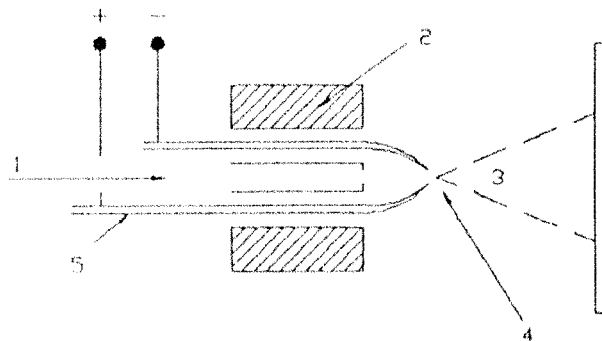


Figure 5. Sketch of Twin-Wire Arc Spraying [4].

1. Atomizing gas flow.
2. Torch outer shield.
3. Stream of molten particles.
4. Electric arc.
5. Consumable electrodes.

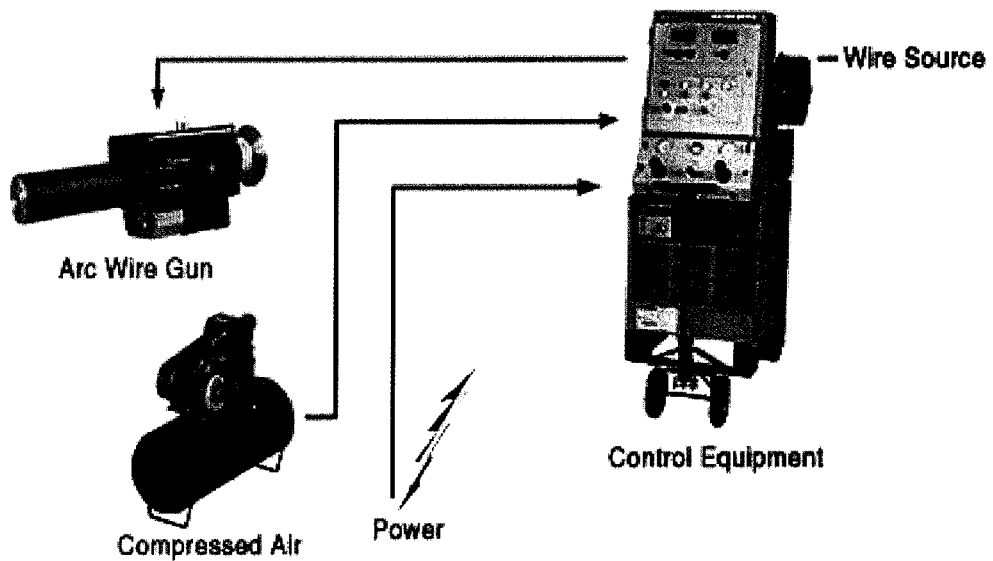


Figure 6. Requirement for a Typical Electric Wire Arc Spray System [1].

Figure 7 is an example of coating of spray by the Twin-Wire arc method.

Coatings are formed by particles flattening and piling up on the substrate. At the time of impact, the sudden deceleration of the particle causes a pressure buildup at the particle-surface interface; the high pressure inside the particle forces melted material to flow laterally and ductile material to deform. The particle spreads outward from the point of impact and forms a splat [12]. In the arc spray process, the molten particles are cooled along their trajectory from gun to substrate [13].



Figure 7. An Example of the Twin-Wire Arc Method of Spray Coating [14].

1.2.1. Advantages of Twin-Wire Arc Spraying

TWAS is easy to use, simple to learn, portable, and easy to maintain. The arc process also yields higher deposition rates and, in general, has higher bond strength than low-velocity combustion coatings. It also provides thicker coatings and has a lower operating cost than plasma spray coating. The TWAS process is able to spray materials at high spray rates while the substrate remains relatively cool. Some major aerospace engine manufacturers have shown that arc coatings can result in higher bond strength and lower residual stress for coating thicknesses similar to those of plasma. In some cases, the arc process can replace plasma because of lower cost and improved performance [2]. The capital costs for TWAS equipment is about \$15,000 compared to \$250,000 for

plasma spray equipment. The cost of labor, operation, and consumables for plasma spraying is approximately four times higher than that for arc wire spraying. Twin-wire arc spraying is a low cost process for coating large areas in a reasonable time [15].

1.2.2. Disadvantages of Twin-Wire Arc Spraying

The disadvantage of the twin-wire arc process is that coatings typically have higher levels of porosity, oxides, and unmelted particles. TWAS coatings are generally rougher than other processes. The types of materials that can be applied by the arc process are limited to conductive solid wires and cored wires that have powder fill surrounded by a metal sheath [2]. It is also noted that in the TWAS process, asymmetry in droplet formation and atomization result in remarkable inhomogeneity in the coating microstructure, which is detrimental to coating properties [16].

1.3. Applications of Twin-Wire Arc Spraying

One application area for the TWAS process is for dimensional restoration and repair of many different types of jet engine components. The arc spray technique is also used for spraying of bridges and marine structures with zinc and aluminum. Zinc and aluminum are used on structural steel to prevent corrosion (rust). Bridges and buildings are made of carbon steel, which will rust over time. Zinc and aluminum oxidize differently. Both of those materials form a very thin oxide layer, which prevents any

additional oxidation from taking place. TWAS can also be applied in the paper and pulp industry, where boiler tubes are protected against hot corrosion. Medical device applications are being developed, such as spraying of titanium wire in inert environments, and rapid prototyping. The inert Ti coatings are applied to orthopedic and dental implants as a very rough and porous coating. This coating allows the bone to grow into the pores of the coating and that creates a very strong bond between the bone and the implant. Other applications of TWAS are in automobile/marine diesel components, where low-carbon steel, molybdenum, and other types of corrosion/scuff-resistant alloys are being considered for valve lifter and piston ring applications. Copper base wires are also suitable for repair of car bodies [2]. In the electronics industry, TWAS aluminum, tin, zinc, and other materials are used for both electrical conductivity and resistivity. For example, aluminum coating on metal oxide varistors creates an electrical conductivity contact surface on the face of the varistors. Tin coatings are often used on nonmetallic parts because of their ability to accept solders [17].

1.4. Coating Material

In general, any material that is electrically conductive and can be made into a wire can be sprayed with a twin-wire electric arc device [9]. Experiments in this study will focus on zinc coatings. Zinc coatings have widespread applications in the automotive, transportation, and aircraft industries as an anticorrosion layer. A zinc sprayed coating is commonly applied to steel for corrosion protection. The coating acts

as both physical and chemical barrier to corrosion. Zinc has lower electrochemical potential than steel. Thus, if a crack occurs in the coating, a galvanic couple is created between the zinc coating and the steel. The coating will act as the anode, preferentially corroding the zinc and providing cathodic protection to the steel [18].

CHAPTER TWO

2. LITERATURE REVIEW

Several researchers have studied the TWAS coating bond strength and the major factors that affect the bond strength such as coating roughness and thickness. The effectiveness of the coating is determined primarily by the bond strength of the coating and substrate [19]. In order to achieve maximum bond strength for the optimum performance of the coating in a process chamber, understanding the parameters that affect the bond strength of the coating is important.

2.1. Bond Strength

The bond strength is the adhesive strength between the coating-substrate interfaces. Cohesive failure which is when failure occurs inside the coatings indicates the bond is stronger than the strength of the coating. From the microscopic point of view, adhesion is due to physico-chemical surface forces such as van der Waals, covalent and ionic forces. These forces can be established at the coating-surface interface and corresponds to the strength of adhesion. The energy dissipation rate corresponding to interfacial fracture energy determines the physical bond strength. It is a macroscopic property including all energy dissipation from mechanical, electrical and thermal sources due to substrate differences. The adherence of coatings is estimated as the stress to separate the coating from its substrate [20].

D.J. Varacalle et al. conducted experiments of TWAS of zinc/aluminum alloy coatings to determine the highest corrosion resistance that could be obtained with the process. They tried to develop a methodology to generate baseline data to optimize the previously mentioned material systems for the corrosive protection of steel. They used 85Zn/15Al and 70Zn/30Al to display the range of processing conditions and their effect on the coating. The purpose was to demonstrate the suitability of the systems for anticorrosion applications [21]. The researchers also investigated the mechanisms involved in the formation of twin-wire electric arc coatings by determining how process parameter variations affect the process dynamics, the subsequent coating properties, and the coating performance.

In the study, thickness was measured by image analysis with a metallograph. The image system was equipped with a ruler tool. Coating roughness was determined using a WYKO RST white light interferometer and was calculated per ANSI standard B46.1. The bond strength measurements were conducted following the test procedure described by ANSI/ASTM standard C633-79 and ASTM standard D4541. The average values are summarized in Table 1.

Table 1. Average of Coating Properties [21].

Average	Thickness mils	Roughness microin	Bond Strength psi
<i>85/15 system</i>	8 - 21	232.28 - 366.14	1467
<i>70/30 system</i>	6.6 - 20	255.91 - 519.68	1140

The Zn/Al alloy coatings' attributes evaluated were porosity, roughness, oxide content, bond strength, and corrosion resistance. The optimum coating was based on the highest corrosion resistance that could be obtained for each material. Low porosity and low oxide content were a secondary consideration in the optimization process. Bond strength was discounted because of relatively small variance.

2.2. The Major Parameters Affecting Bond Strength

Previous work found that the bond strength of the coating is highly dependent on surface preparation [22]. It is also strongly suggested that the bond strength also depends on the coating surface's roughness since the roughness of the substrate influences, to a degree, the coating surface's roughness which greatly influences the mechanical and physical properties of contacting parts [4, 23],

2.2.1 Substrate Surface Preparation

With most surface engineering procedures, it is necessary to create good initial surface conditions [24]. Surface preparation prior to thermal spraying is a key step to ensure good adhesion of the coating [25]. It has been suggested that surfaces should be properly prepared prior to being sprayed to ensure a strong mechanical bond between the substrate and the coating. Surface cleanliness and roughness are the most critical factors of the pre-spray preparation [3]. Grit blasting with hard abrasive particles like Al_2O_3 (Alumina) is the most common method of surface preparation [26]. Figures 8 and 9 are SEM micrographs of Alumina of various grit sizes. Coating adhesion quality is directly related to the cleanliness and roughness of the substrate surface [27].

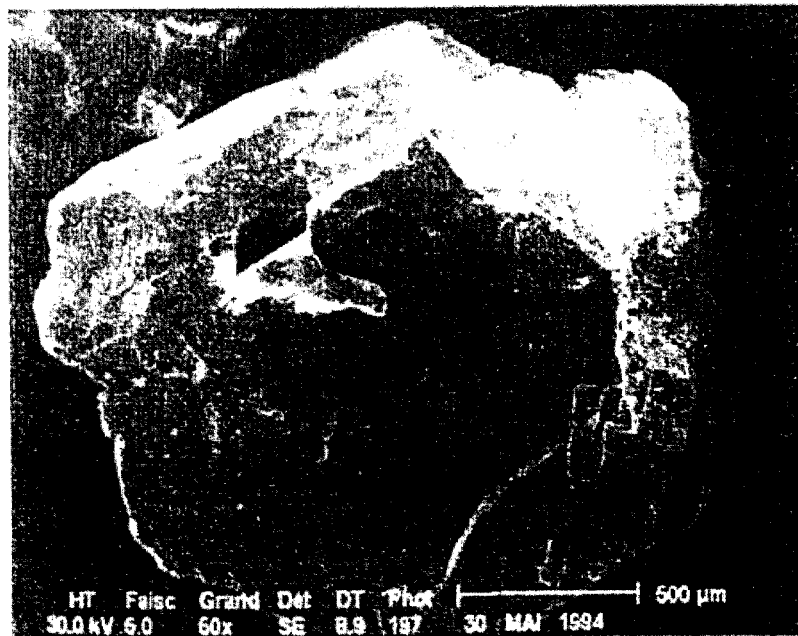


Figure 8. SEM Micrograph of Alumina 1400 Microns Grit Size [27].

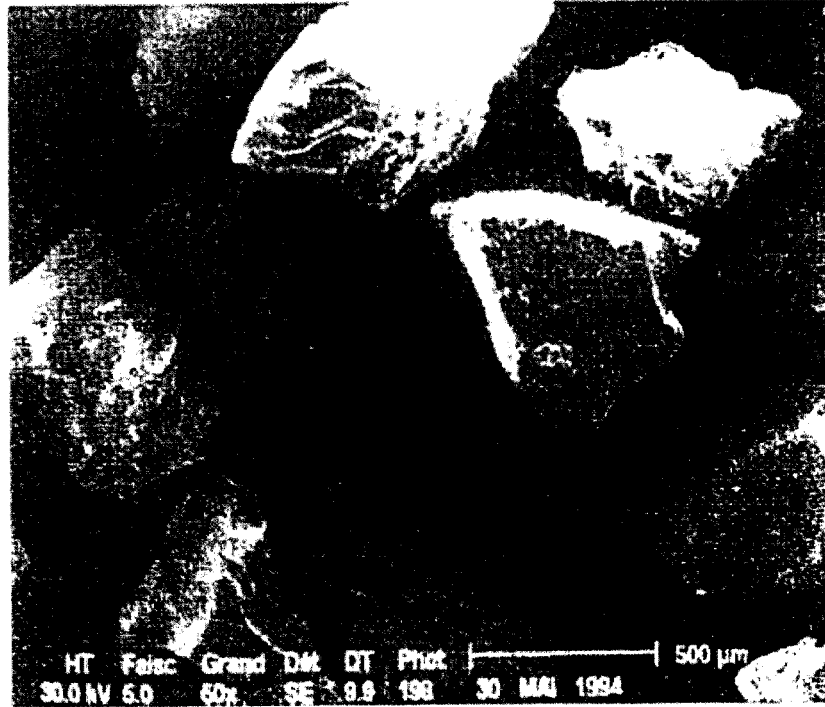


Figure 9. SEM Micrograph of Alumina 500 Microns Grit Size [27].

2.2.1.1 Substrate Surface Cleanliness

Grit blasting always leaves grit residue entrapped in the material [25]. The amount of grit residue increases with grit size, and is due to an increase in grit fragmentation with respect to grit size [27]. Grit blasting methods typically embed fine grit inclusions into the substrate due to fracture of grit asperities upon impact. These grit inclusions contaminate the interface between substrate and coating [26]. The quantity of embedded abrasive particles and grit residue can negatively affect coating adhesion [27]. Therefore, it is recommended that the substrate is cleaned before grit blasting to remove

residual dust and ensure that it remains uncontaminated by lubricants, oils, and moisture. It should also be cleaned after grit blasting to remove blast residue and embedded grit by vapor degreasing, rinsing with common organic solvents, or air drying using clean, dry compressed air (CDA) [3]. Well-prepared, clean substrate surfaces are essential for good bonding [6]. It was found that without cleaning, the grit residue was more than twice that measured after cleaning [27].

2.2.1.2 Substrate Surface Roughness

Grit blasting is the standard technique of surface roughening. Substrate surface roughness plays an integral role in the adhesive mechanism; without it there is no adhesion [28]. It is important to select the relevant grit for blasting. Selection of grit size depends on the substrate thickness. If the substrate is thin, finer grit should be selected. It is also noticed that the grit size decreases as a result of blasting parameters. The grit should be changed depending on the pressure of the blast and the hardness of the blasted pieces [10]. After grit blasting, the prepared surface needs to be coated as soon as possible (within five minutes) to prevent surface oxidation or contamination, which reduces the adhesion of the coating [19]. A delay in spraying of four hours or more after surface preparation causes deterioration in bond strength [22].

The substrate roughness is usually described by the average roughness R_a . However, in applications where it is important to know the values of the greatest

irregularities on the surface, R_{max} , maximum roughness depth parameter is used to quantify the surface (Figure 10) [4].

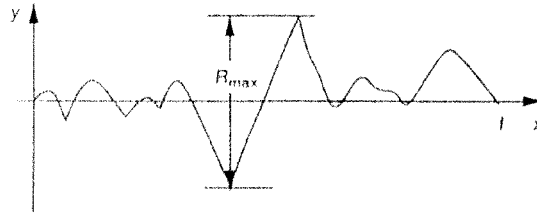


Figure 10. Profile of Roughened Surface [4].

2.2.2 Coating Thickness

Coating thickness buildup is dominated by wire feed rate, which is dictated by the system current. Higher current results in faster wire feed and thicker coatings. It was also discovered that a slower gun traverse rate was the most significant contributor to increasing thickness [10].

In the work done by R.L. Apps for flame-sprayed aluminum coatings on mild steel, coating thickness has a major influence on bond strength with strength falling rapidly from coatings of around 0.05 mm (1.97 mils) to a much lower level at thicknesses above about 0.15 mm (5.91 mils) as shown in Figure 11. This effect is caused by adhesive penetration of the spray coating, which could artificially strengthen thin

coatings. It was found that the adhesive penetration is highly influenced in thin-spray coating up to 0.15 mm. However, it has no effect on coating thicknesses above that since at a coating thickness above 0.15 mm, bond strength is independent of thickness [22].

The deposition characteristic of flame spray is very similar to TWAS; the difference is the way the energy is generated to melt the powder. In flame spray, a flame is generated using oxygen and acetylene gases; the power is injected into the flame. Flame spray tends to deposit a lot of materials in a very short time. Typically flame spray is used for low melting point metallic materials to rebuild steel substrate, while twin-wire-arc spray, as mentioned previously, uses two wires that have high voltage sent to them - one positively and one negatively charged. When the wires touch, they arc and melt, thus producing liquid particles.

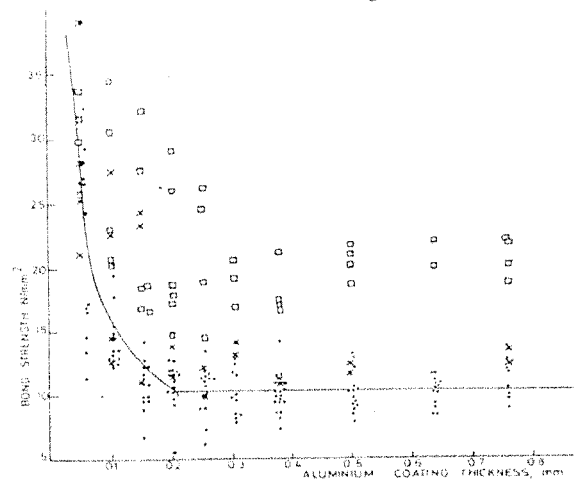


Figure 11. Variation of Bond Strength with Coating Thickness [22].

□ Alumina grit; × Copper slag grit; ● Chilled-iron angular grit.

The coating is the build-up from the individual particles that strike the substrate as in Figure 12. The phenomena occurring at the time beginning particles impact the substrate determine the adhesion of the coating to the substrate. The final coating thickness is the result of lamella deposited during passes of the spraying torch that moves over the substrate (Figure 13). At the beginning the particles impact the substrate. The phenomena occurring at this stage determine the adhesion of the coating to the substrate. The transformation of a molten particle, while striking the substrate, into a lamella is associated with the processes of deformation and solidification. Starting from the moment of the first contact with the substrate, the particle begins to deform. Initially, it takes the form of a cylinder. The impact creates a shock wave inside the lamella and in the substrate. Later, the cylinder expands in a radial direction taking the form of a pancake and, at the same time, the solidification process occurs [4].

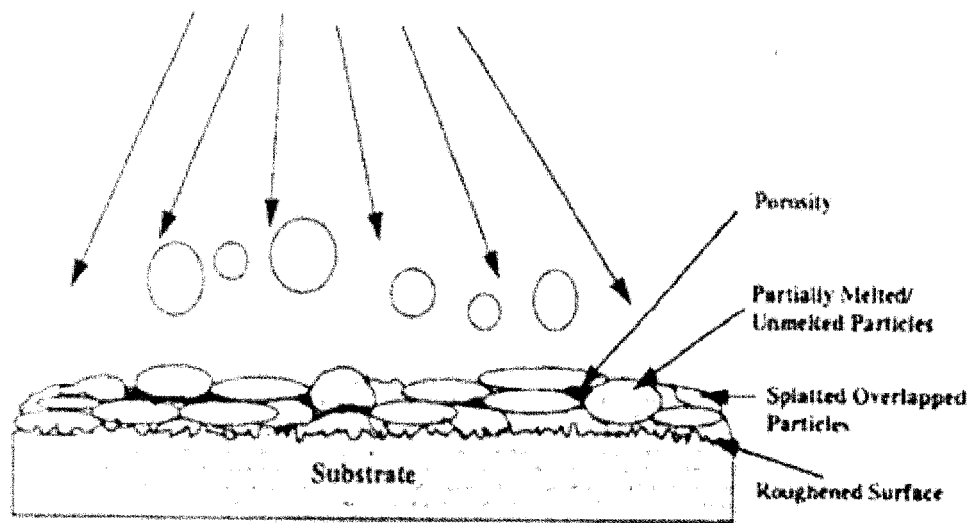


Figure 12. Schematic of Coating Deposition [7].

Lamella thickness depends on the degree of splashing of the particles which depend on many factors such as substrate surface roughness and particle size, velocity, and temperature [16]. Particle velocity and temperature at the point of impact on substrate depends strongly on particle size [18]. In general, a larger particle tends to produce a weaker splashing and hence a larger lamella thickness [16].

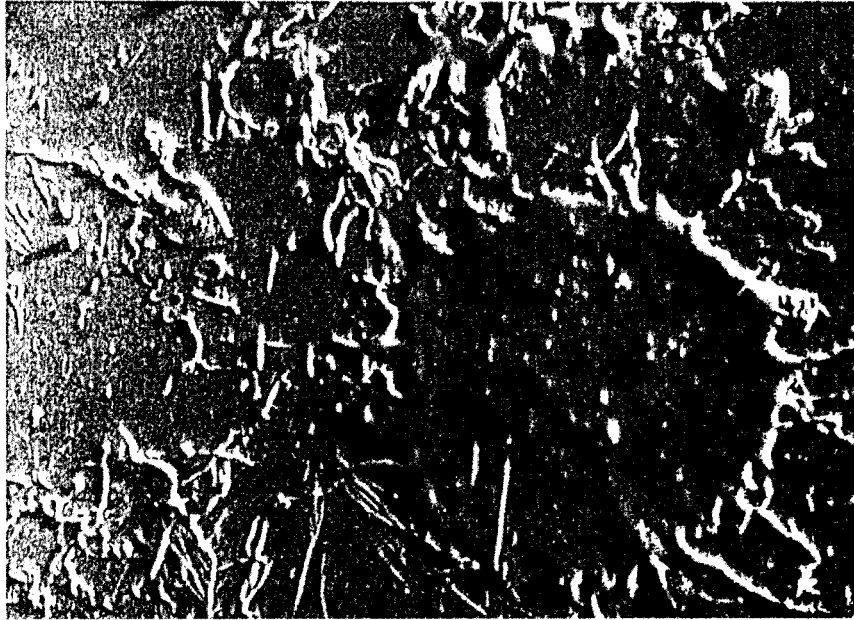


Figure 13. The Lamella after Impact of Sprayed Particles [4].

2.2.2.1 Spray Particles

It was found that the spray particles affect the coating quality; therefore, it is essential to measure their behavior on the coating characteristics such as roughness and bond strength to produce high quality coatings. In general, particle size decreases with decreasing current and increasing gas pressure. As the particles travel downstream along the centerline of the plume, the average centerline particle size decreases and then increases as the flow proceeds downstream. The largest particles at any particular cross section are at the centerline of the spray. The standard spray pattern is shown in Figure

14. One side of the spray plume has slightly larger particles, possibly due to the asymmetric melting behavior of the cathode and the anode wire. The anode melts slowly, resulting in elongated, relatively large droplets. Some large droplets are broken up by atomizing gas. At the cathode, melting is more localized, and the molten droplets are immediately blown away by the atomizing gas flow, resulting in relatively small droplets [29]. The drop size distribution is determined by a balance between aerodynamic shear forces, which tend to break up the drops and the surface tension of the molten material, which tends to hold the drops together.

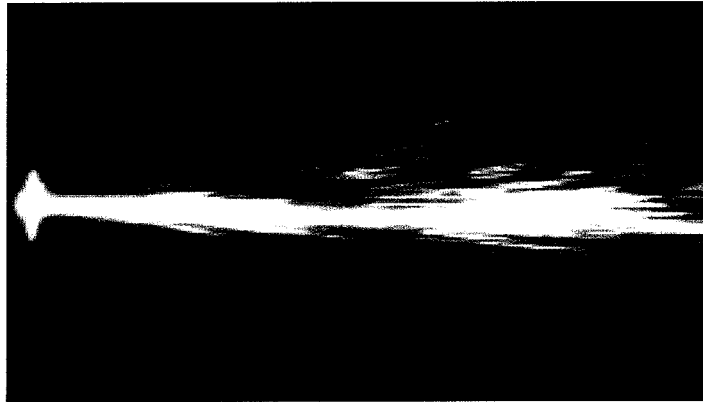


Figure 14. Standard Spray Pattern [17].

The particle size also depends on the desired sprayed coating roughness since finer grit results in finer sprayed coatings. The coating roughness increases with the powder particle size [4]. Compressed air is commonly used in the twin-wire arc process because of its low cost and availability. However, the oxide content of such sprayed

coatings is relatively high due to the oxidation of molten droplets. Thus interlamellar bond strength and machinability of coatings are reduced due to their oxide content [30].

The microstructure and properties of deposited coating of arc spray depend on the thermal and kinetic energy of the particles entered in the hot gas jet. Particle size is one of the main characteristics that controls adhesion [31]. For a given coating and substrate material combination, greater bond strength is achieved by the larger values of the particle sizes [19]. Moreover, the particles are not mono-sized and the big particles are accelerated to lower velocities than the small particles [4].

2.2.3 Coating Surface Characterization

The coating surface is composed of lamellae formed of molten, partially molten, and unmelted particles [4]. Surface roughness is very important from the point of view of such fundamental problems as friction, contact deformation, heat and electric current conduction, tightness of contact joints, and positional accuracy [32]. The surface is often characterized through the use of parameters such as R_a , R_{sk} , R_{da} , R_{ku} , and R_{pc} (usually using statistical techniques) which attempt to provide an indication of some attribute of the surface such as amplitude variation [23].

2.2.3.1. 2-D Surface Profile

The coating surface morphology is characterized generally based on the average roughness parameter R_a . Other parameters such as R_{sk} -a measure of the skewness or the symmetry of the profile about the mean line, R_{da} -a measure of the surface profile, R_{ku} - a measure of the sharpness of the surface profile, and R_{pc} -a count of the number of peaks that project beyond the mean line have been used to characterize surface roughness. Because the 2-D parameter R_a measurement results are highly dependent on cut-off and evaluation lengths, surface roughness evaluation cannot be based on only R_a measurement. Cut-off and evaluation lengths for 2-D R_a measurement are summarized in Table 2. Figure 15 explains how cut-off length and evaluation length are defined. Since the surface geometry is so complicated that a finite number of parameters cannot provide a full description, roughness description results will be clearer and more extensive if the number of parameters used is increased [31].

Table 2. Cutoff and Evaluation Values for Surface Profile Using R_a [33].

R_A Range (μm)	Cut-off Length (inches)	Evaluation Length (inches)
0.02 – 0.8	0.03	0.016
0.10 - 4	0.010	0.05
2.0 - 80	0.03	0.16
10 - 400	0.10	0.5
Above 400	0.3	1.6

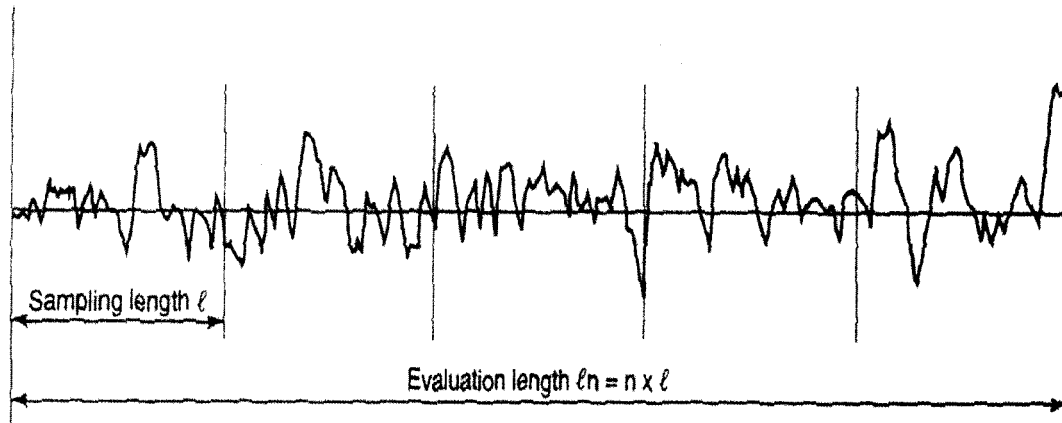


Figure 15. Sampling (or Cut-off) Length and Evaluation Length [34].

However, the above 2-D roughness parameters have a very limited value in relating the coating surface to its functional effectiveness. They are inherently unstable and only provide an average value of a single line or trace on a 3-D surface, which is unlikely to be representative of that surface as a whole [35]. Further, the commonly used parameter R_a had no direct functional significance and is less significant in statistics than the root-mean-squares (RMS) deviation R_q of 3-D amplitude parameters [36]. They cannot provide adequate and reliable information for the analysis of intrinsically 3-D topography [35] since 3-D analysis gets information on one more spatial dimension than a 2-D profile [37]. Therefore, it is necessary to evaluate coating surface topography through 3-D data collection and analysis to avoid the problems that occur with 2-D parameter variation.

2.2.3.2. 3-D Surface Topography

3-D surface topography greatly influences not only the mechanical and physical properties of contacting parts, but also optical and coating properties of some non-contacting components. 3-D surface topography of engineered surfaces is complex and cannot be described completely by a single or a few parameters. Each parameter can only describe one aspect of the topography [36].

Unlike 2-D parameters, 3-D topographic measurements do not impose the traditional cut-off defined in the standards because the spatial relationships between the parallel profiles have to be maintained. It was also discovered that the mapped area in 3-D and mapped profiles in 2-D are different. The mapped area contains parallel profiles that are usually obtained by raster scan logging. Specified cut-off should only apply whenever it is necessary after the whole area has been mapped [35].

In 2-D analysis it is stressed that the determination of a suitable reference line is fundamental to the characterisation of the surface, while in 3-D analysis this requirement is extended to the establishment of a suitable reference, or datum, plane so that roughness, waviness and form of a 3-D surface as in Figure 16 can be analyzed. The average roughness parameter R_a is a measure of the absolute deviation of the profile ordinate heights from the mean line in 2-D analysis, while in 3-D analysis, it is defined as

the absolute deviation of the profile height ordinates from the mean plane [35]. R_a is proposed in the parameter set for describing the statistical property of surface height [38].

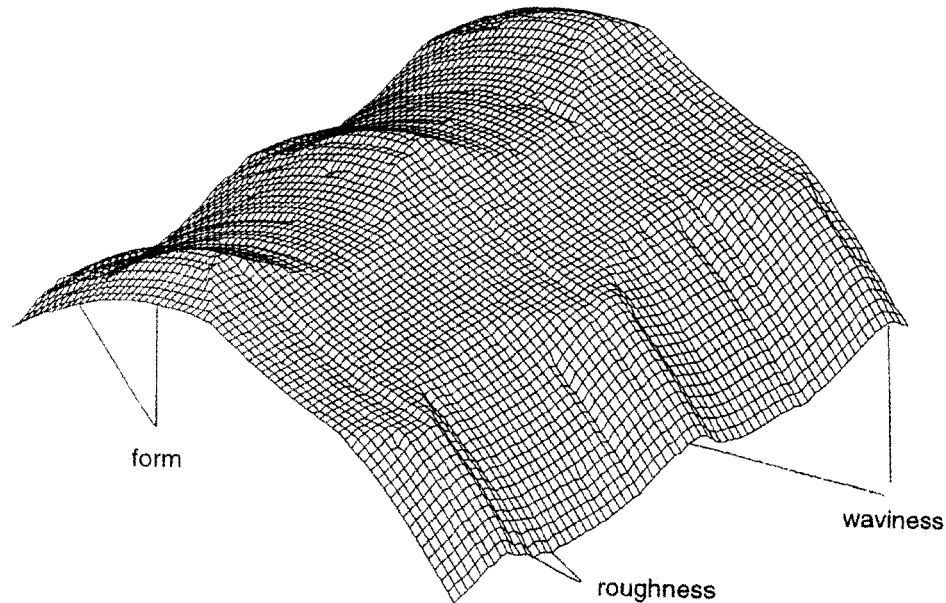


Figure 16. Roughness, Waviness, and Form of a 3-D Surface [35].

There are four independent 3-D amplitude parameters in the primary parameter set: S_q , S_z , S_{sk} , and S_{ku} . S_q is root-mean-square deviation of surface topography or a height description in statistics. S_z is ten point height of surface topography or an extreme description in statistics. S_{sk} is skewness of topography height distribution or a measure of asymmetry of surface deviation about the mean plane as in Figure 17. From a surface function point of view, S_{sk} can give some indication of the existence of “spiky” features.

S_{ku} is kurtosis of topography height distribution or a measure of the peakedness or sharpness of the topography height distribution as in Figure 18. This parameter is always presented in conjunction with the skewness to describe the shape of the topography height distribution [38]. More functional parameters can also be obtained from the 3-D data such as volume of logged area and total interfacial area in addition to extensions of 2-D parameters [35]. It is recognized that if different areas of a surface are logged, different surface features will be involved and a different trend of parameter variation will be obtained [39].

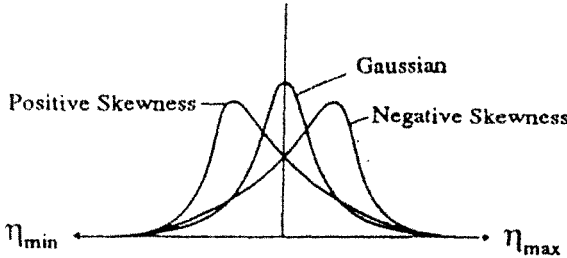


Figure 17. Skewness of Surfaces [35].

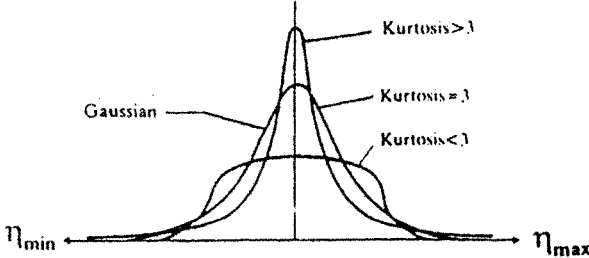


Figure 18. Kurtosis of Surfaces [35].

Since 3-D surface characterisation is based on digital areal topographic data, sampling conditions for 3-D topography as in Figure 19 are represented by the sampling interval $\Delta x/\Delta y$ in the two orthogonal directions, the size of sampling matrix $M \times N$, and the sampling area $A = l_x \times l_y$ while cut-off and evaluation lengths are standardized as the sampling conditions for a 2-D profile [35]. It should be noted that whenever the parameters are used, the conditions under which the parameter values are obtained have to be specified. All parameters are defined in one sampling area, which is in contrast to most 2-D parameters that are defined in one evaluation length consisting of several cut-off or sampling length [39].

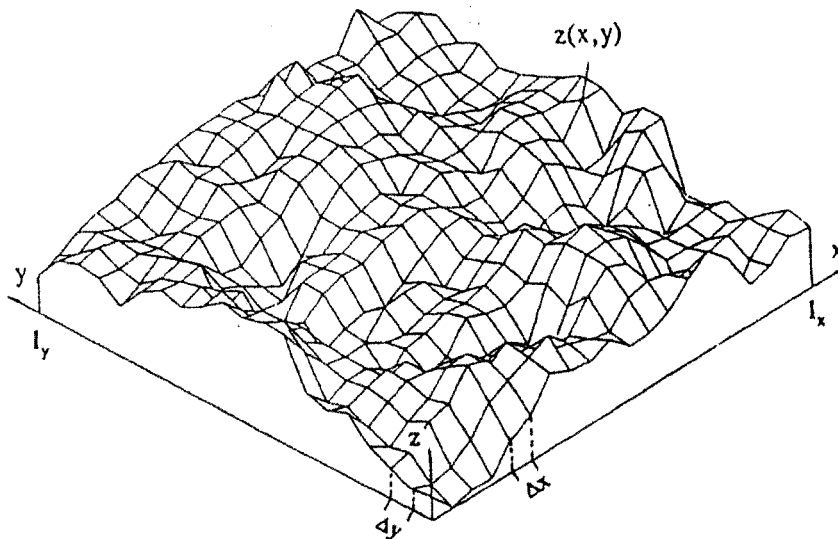


Figure 19. Coordinate System Used for Surface Topography Representation [35].

2.3 Summary

In summary, researchers have investigated TWAS Zn/Al coatings. The bond strength, roughness, and thickness were measured for various metal coatings. For the 85Zn/15Al system, thickness ranges from 8 -12 mils, roughness ranges from 232.28 – 366.14 μ inches and bond strength is 1467 psi. For the 70Zn/30Al system, thickness ranges from 6.6 – 20 mils, roughness ranges from 255.91 – 519.68 μ inches, and bond strength is 1140 psi. The relationship of bond strength and coating thickness of aluminum flame spray has also been studied. It was found that coating thickness from 2 mils to 5.9 mils has a major influence on bond strength. At a coating thickness above 5.9 mils, bond strength is independent of thickness.

TWAS coatings are currently the most common thermal spray coating technique used in industry. Zinc TWAS coatings have widespread applications. Most of the research related to Zn/Al TWAS coating focuses on corrosion of the film. Not much work has been done to study the bond strength of TWAS coatings and how the substrate surface roughness affects the coating's bond strength.

CHAPTER THREE

3. RESEARCH FOCUS

As a cost effective thermal spray technique, the twin-wire-arc process has gained widespread use as an application against corrosion and wear [16]. In response to increasing demand for productivity, more sophisticated control techniques must be developed to improve the coating's performance for specific applications. The performance of the coating is highly dependent upon the coating's bond strength since a coating with low bond strength can prematurely break or flake off in service [19].

In this research, we focus on investigating factors that affect the coating's bond strength. The coating's bond strength is one of the important keys for success in the TWAS process. The relationship between the substrate preparation and bond strength of the TWAS process on a substrate are investigated. The microstructure of the coating interface and cross-section is also examined.

3.1. Hypothesis

Literature has shown that there is a relationship between surface roughness of the substrate and the adhesion strength of subsequently deposited films. Increasing the roughness has shown to increase the adhesion strength of the film. However, there should be a limit to the effectiveness of increasing the surface roughness on the adhesion

strength. Increasing the roughness past a certain value should result in lower adhesion strength. At this point, the surface has become too rough for the film adheres.

Literature has also shown that cleaning the particles embedded into the surface during the roughening process alters the surface topography of the substrate. It stands to reason that the adhesion strength of the film would be affected by the cleaning process. Additionally, the size of the particle used in the roughening process should also affect the adhesion strength. Removal of large particles versus small particles during the cleaning process should produce different adhesion strength values.

3.2. Objective

The objective of this effort is to investigate the influences of substrate preparation and surface morphology on the bond strength between the coating and substrate. These factors can be used to optimize the control of the operating process resulting in optimum coating bond strength. With the understanding that it is primarily that bond strength determines the coating's success, the major factors affecting bond strength of the coating are analyzed for the purpose of achieving effective TWAS coating on a substrate and minimizing failures of the coating. The surface roughness of the substrate will be determined from three different grit blast particle sizes. The variation of the grit size will produce varying degrees of roughness on the surface. These roughened coupons will then be divided into two subsets: not cleaned and cleaned after grit blasting. Each subset

undergoes a TWAS coating process. The adhesion strength of the film will be measured and the underlying microstructure of the substrate surface will be investigated.

3.3. Justification

The success of any application relies upon effective coating. The effectiveness of a coating is determined by its bond strength. Lack of sufficient bond strength can be detrimental to the coating. Literature review indicates that the bond strength is highly dependent on coating thickness and substrate preparation, which includes substrate roughness and cleanliness. Therefore, it is crucial to understand how these factors affect the coating's bond strength to help produce desired coatings.

CHAPTER FOUR

4. EXPERIMENTAL METHODOLOGY

4.1. Approach

The approach is to analyze the coating's physical properties using various analytical instrumentation and techniques. Surface roughness and bond strength is characterized as a function of grit size and cleaning procedure. The blasting size is identified as a function of the substrate's roughness and bond strength. The bond strength of the coating is evaluated as a function of the substrate's roughness, coating thickness, and surface morphology.

4.2. Substrate Materials

Steel test coupons as shown in Figure 20 are identified by serial number on one side and are subjected to TWAS with 2 mm diameter zinc wire on the other side by a thermal spray shop using industry standard equipment. The steel coupons are bead blasted with No. 24 (686 microns), 36 (483 microns), and 80 (165 microns) alumina grits before spraying. There are 90 one-inch diameter and 36 two-inch diameter coupons used in this testing.

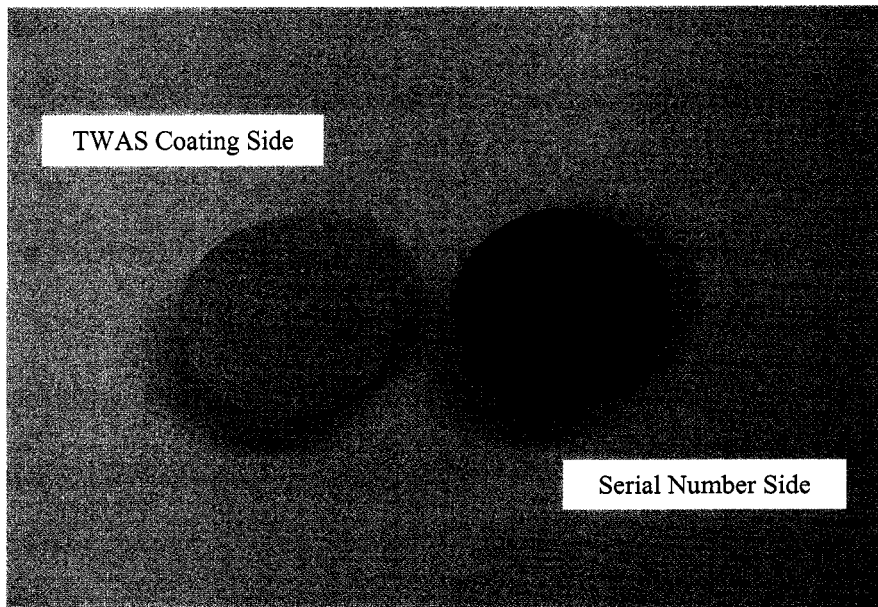


Figure 20. TWAS Test Coupon.

4.3. Experimental Design

Ninety one-inch diameter coupons are divided into six sets and fifteen one-inch diameter coupons (one is blasted/fourteen are sprayed) in each set. Thirty six two-inch diameter coupons are grit blasted. Eighteen of these coupons are held in reserve. The remaining eighteen two-inch diameters coupons are coated for morphology as summarized in Table 3. Since the coating roughness will be above 40 μ inches, the profilometer will be set at 0.3 inches for cut-off length and 1.6 inches for evaluation length as shown in Table 2. Only two-inch diameter coupons will be used for measuring coating roughness.

Table 3. Coupon Matrix.

Set # (6)	Substrate Roughness	Cleaning		Textured Coupons (6)		Sprayed Coupons (102)						
						Reser ved	Cross section	Testing Coupons		Tensil e Test	Tensile & SEM	Morph ology
		Yes	No	1" dia	2" di a	1" dia	1" dia	1" dia	2" dia	1" dia	1" dia	2" dia
		45	45	6	18	6	6	72	18	66	6	18
1	Low (80 grit, 60 psi)	15		1	3	1	1	12		11	1	
2			15	1	3	1	1	12	6	11	1	6
3	Nominal (36 grit, 60 psi)	15		1	3	1	1	12		11	1	
4			15	1	3	1	1	12	6	11	1	6
5	High (24 grit, 60 psi)	15		1	3	1	1	12		11	1	
6			15	1	3	1	1	12	6	11	1	6

4.3.1. Baseline Experiments

Figure 21 is a flow diagram of phase I grit blast coupons. There are thirty one-inch diameter and twelve two-inch diameter coupons blasted by 24, 36, and 80 grit sizes. Six two-inch diameter coupons are measured for roughness and held in reserve. Thirty one-inch diameter and six two-inch diameter coupons are measured for roughness and substrate thickness.

I – Grit Blast Coupons

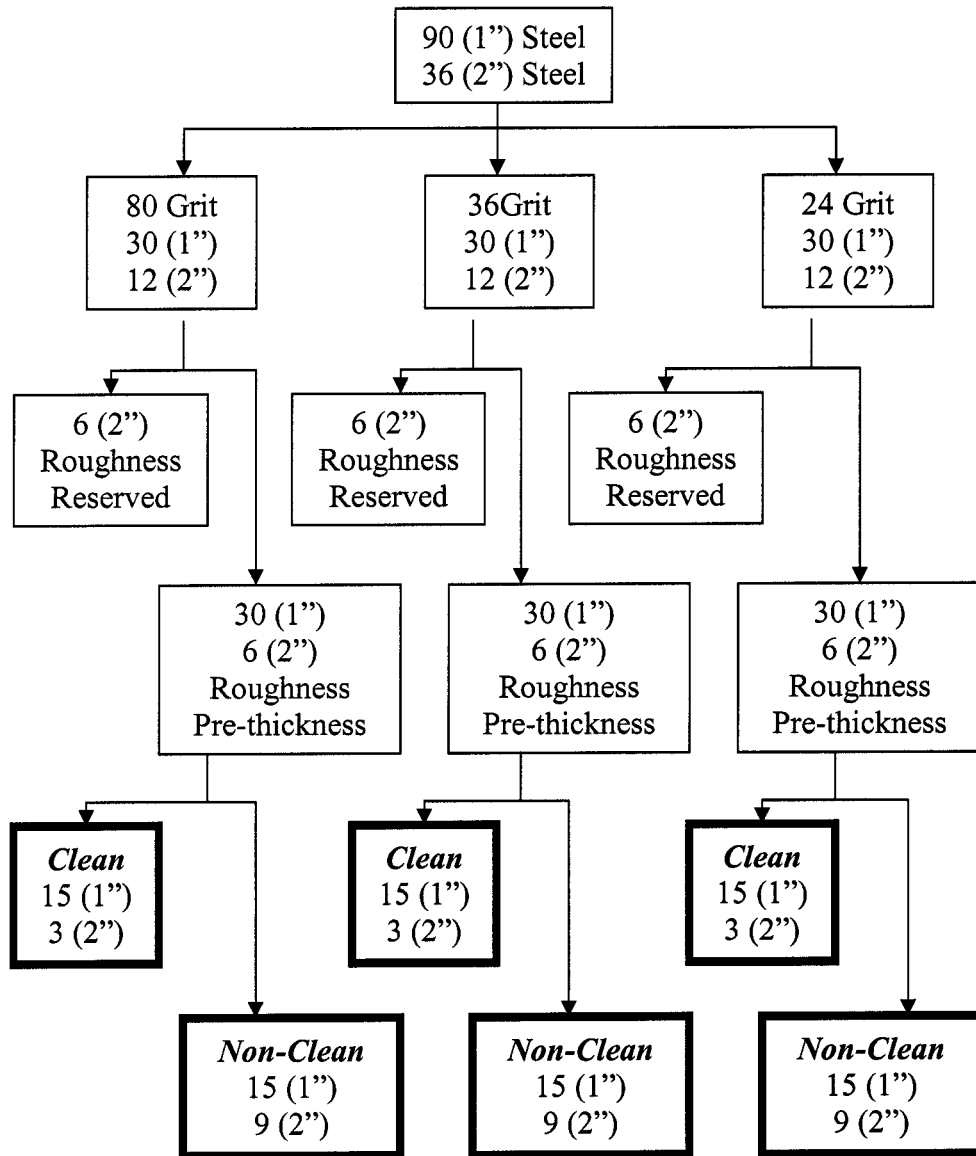


Figure 21. Experimental Procedure Flow Diagram Phase I.

In Figure 21, the bold boxes start phase II. Figure 22a is a flow diagram of phase II clean coupons. Fifteen one-inch diameter and three two-inch diameter coupons are cleaned and packaged in a class 1000 cleanroom. One one-inch diameter and three two-inch diameter coupons are reserved. Fourteen one-inch diameter coupons are sprayed and the thickness is measured. One coated one-inch diameter coupon is held in reserve. Eleven one-inch diameter coupons are adhesion tested. One one-inch diameter coupon is examined by an SEM. One one-inch diameter coupon is cross-sectioned and examined by an SEM.

II – Clean Coupons

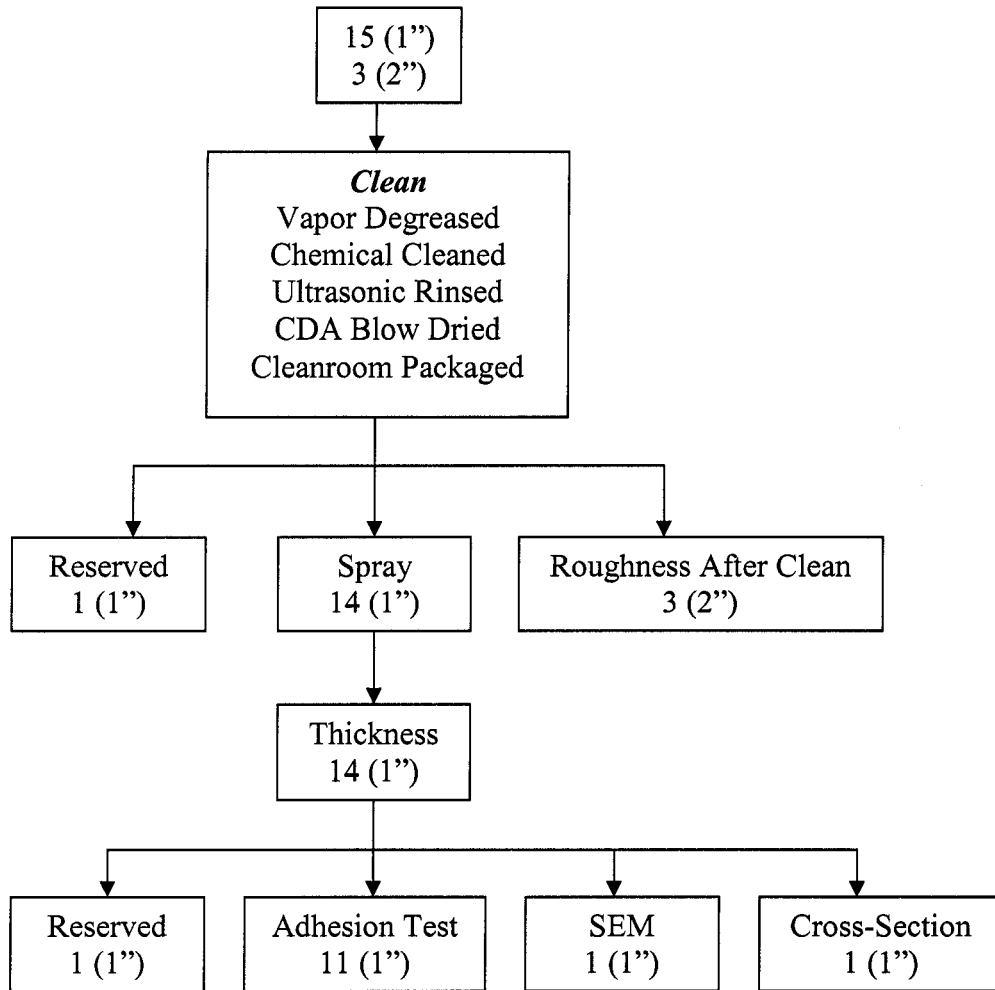


Figure 22a. Experimental Procedure Flow Diagram Phase II for Clean Coupons.

Figure 22b is a flow diagram of phase II non-clean coupons. Thirty one-inch diameter and three two-inch diameter coupons are subjected to CDA blow off. One one-inch diameter and three two-inch diameter coupons are held in reserve. Fourteen one-inch diameter and six two-inch diameter coupons are sprayed and the thickness is

measured. The roughness of six two-inch diameter coupons is measured. One one-inch diameter coupon is held in reserve. Eleven one-inch diameter coupons are adhesion tested. One one-inch diameter coupon is SEM examined. And one one-inch diameter coupon is cross-sectioned.

II – Non Clean Coupons

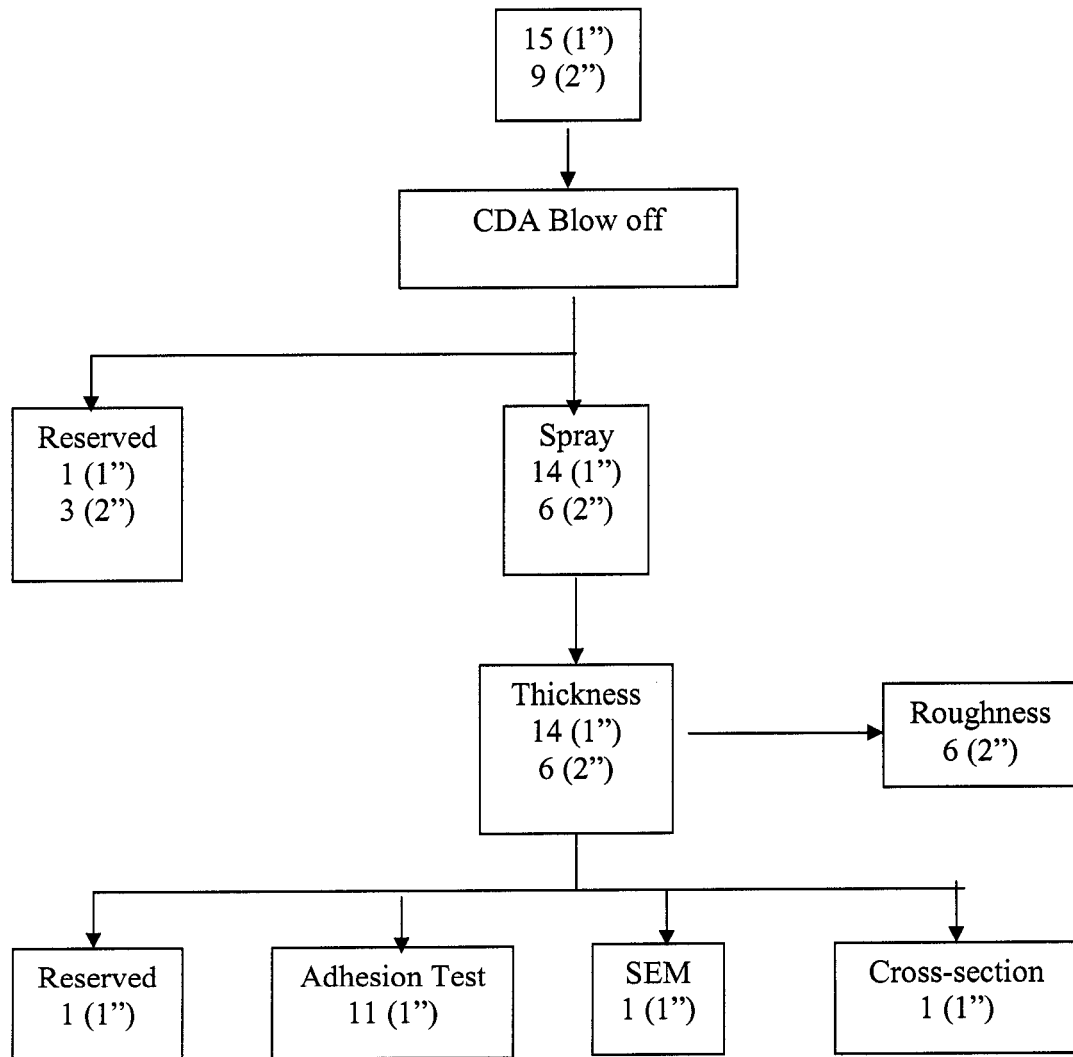


Figure 22b. Experimental Procedure Flow Diagram Phase II for Non-Clean Coupons.

4.3.2. Experimental Testing

Testing for the experiments is divided into a tensile adhesion test and surface characterization. The surface characterization includes surface roughness measurement and surface microstructure examination. The tensile adhesion test is conducted following the “Standard Test Method of Adhesion or Cohesive Strength of Flame-Sprayed Coatings”. Surface roughness is quantified using parameter Ra and measured using a profilometer. Surface microstructure is observed by an SEM with secondary and backscattered electron detectors.

4.3.2.1. Tensile Adhesion Test

The bond strength of the coating to the substrate if failure occurs at the coating to substrate interface is described by the tensile adhesion test according to ASTM C633-79 (1993). This test measures the strength in tension perpendicular to the surface [36]. Usually the failure mode should appear in the interface. The tensile test is conducted using two cylinders with a one-inch diameter coated coupon adhering between the two cylinders. Then the two cylinders are attached to the test apparatus via two universal link joints and pulled apart until a fracture occurs. The force (N) required to fracture the coating is measured in N/mm^2 (MPa) or psi [40] as shown in Figure 23.

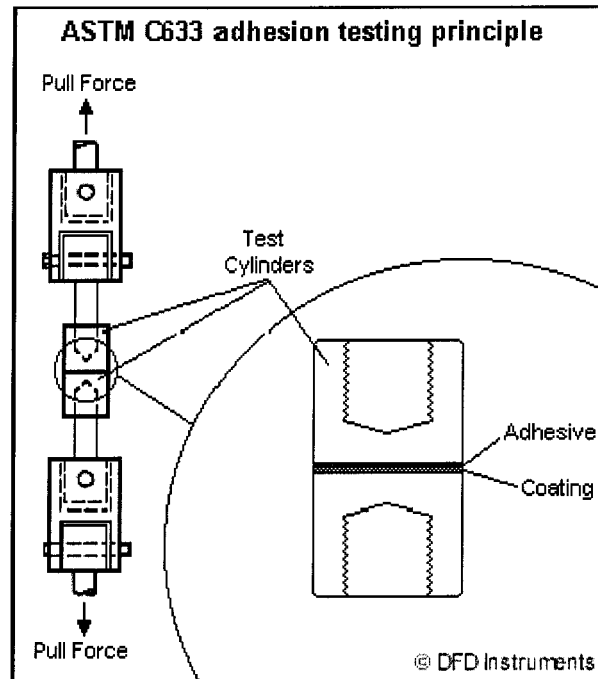


Figure 23. ASTM C633 Adhesion Testing Principle [40].

4.3.2.2. Surface Characterization

Surface characterization includes surface roughness measurement and surface microstructure examination.

4.3.2.2.1. Surface Roughness Measurement

Surface roughness is very important from the point of view of such fundamental problems as friction, contact deformation, heat and electric current deduction, tightness of contact joint, and positional accuracy. Among more than 30 parameters and functions

describing the surface roughness, Ra meets the demands of common use. Ra can be easily measured and has a significant relation to the useful properties of machine parts [32]. The Ra parameter provides a simple value for accept/reject decisions [41]. Hyosung Lee et al. use Ra as a parameter to measure surface roughness [42] and M. Amin also uses Ra parameter for studying surface roughness of arc spray coatings [19]. The average roughness parameter Ra is defined over the entire evaluation length L. It is the universally recognized and international parameter of roughness. Ra is the absolute value of the arithmetic mean of the absolute departures of the roughness profile from the mean line (Equation 1 and Figure 24) [42].

$$Ra = \frac{1}{L} \int_a^b |Z(x)| dx \quad \text{Equation 1}$$

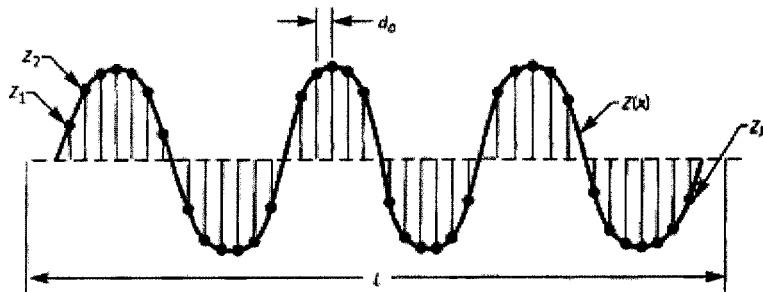


Figure 24. Illustration for the Calculation of Roughness Average Ra [33].

Ra = Average deviation or roughness profile Z(x) from the mean line.
 = Total shaded area/L.

The definition of surface roughness could probably be best understood on a causative basis. The measurement of surface roughness poses a problem in three-dimensional geometry, but for simplification purposes it is typically reduced to two-dimensional geometry by confining individual measurements to the profiles of plane sections taken through the surface. The direction of measurements is usually perpendicular to the direction of the predominant surface markings [41]. Figure 25 is a flow chart of the roughness measurement system.

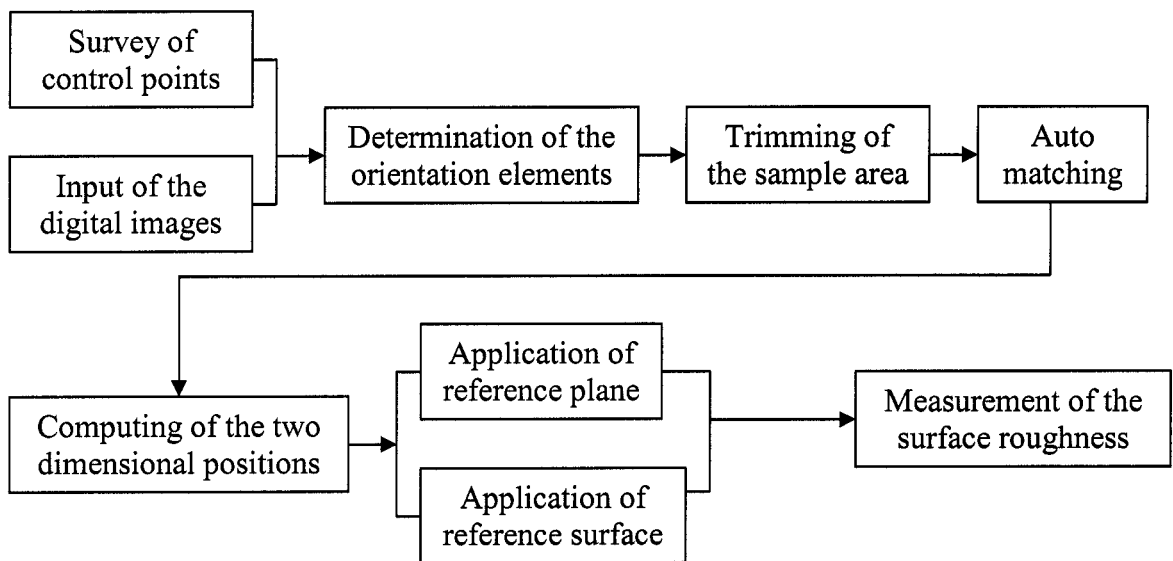


Figure 25. Flow Chart of the Roughness Measurement System [42].

4.3.2.2.2. Surface Microstructure Examination

Surface microstructure examination by an SEM with secondary electron and backscattered electron detectors is used as a method to observe the coating microstructure as in Figure 26. The SEM is a method for high resolution surface imaging. The SEM uses electrons for imaging, much as light microscopy uses visible light. An electron beam is produced at the top of the microscope by heating of a metallic filament. The beam follows a vertical path through the microscope's column and then goes through electromagnetic lenses. The lenses focus and direct the beam down towards the sample. When the beam hits the sample, either backscattered or secondary electrons are ejected from the sample. Detectors collect the ejected electrons and convert them to a signal. The signal is sent to a viewing screen like a television screen and produces an image [43]. The advantages of the SEM over light microscopy include greater magnification (up to 100,000X) and much greater depth of field. Imaging is typically obtained using secondary electrons for the best resolution of fine surface topographical features. Alternatively, imaging with backscattered electrons gives contrast based on an atomic number to resolve microscopic composition variations, as well as topographical information (Figure 27).

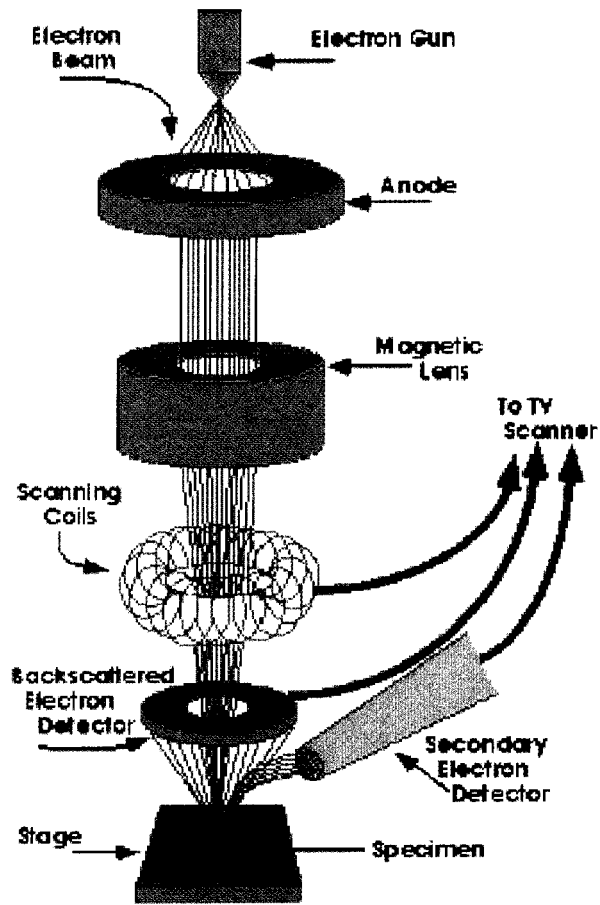


Figure 26. Scanning Electron Microscope (SEM) [43].

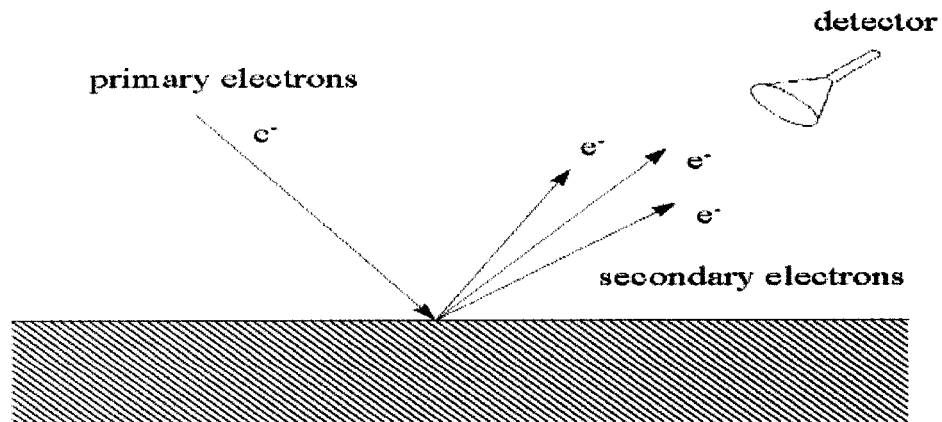


Figure 27. SEM Electrons [44].

4.4. Analytical Instrumentation

In this research, surface roughness is measured by a profilometer, microstructure is examined by an SEM, and thickness is measured by a micrometer.

4.4.1. Profilometer for Surface Roughness Measurement

Taylor Hobson's Talysurf Profilometer has a 90-degree conisphere diamond stylus with a tip width (or radius) of $2\mu\text{m}$ ($0.00008''/80\mu\text{inches}$) [44]. It is a 60 mm standard diamond stylus arm with a nominal range 10mm (0.4 in) as in shown Figure 28.

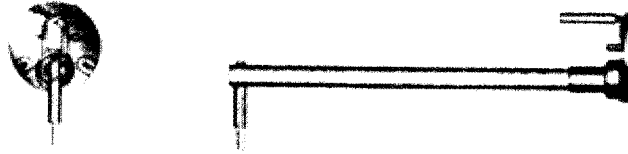


Figure 28. 60mm Standard Diamond Stylus Arm [45].

Figure 29 is a photo of the Talysurf profilometer that is used to characterize surface properties according to ASME B.46.1 – 1995, Standard Method for Roughness Measurement. It is a stylus profilometer that determines a numerical value for the surface finish by contact measurement technique. The instrument is shown schematically in Figure 30. There is a skid or shoe that is drawn slowly over the surface. The skid follows the general contours and provides a datum for measurements. The stylus movements are magnified and recorded. Algorithms are then used to compute the various roughness parameters [41].

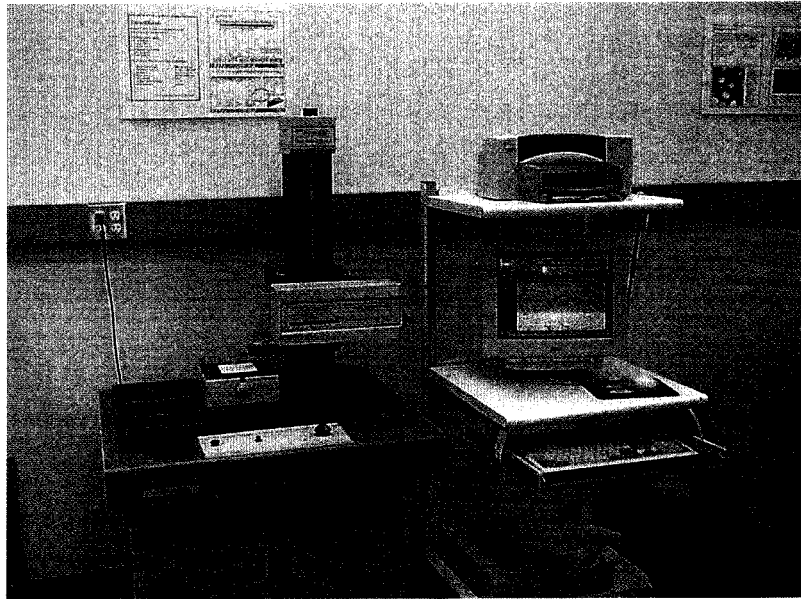


Figure 29. Taylor Hobson Talysurf Profilometer.

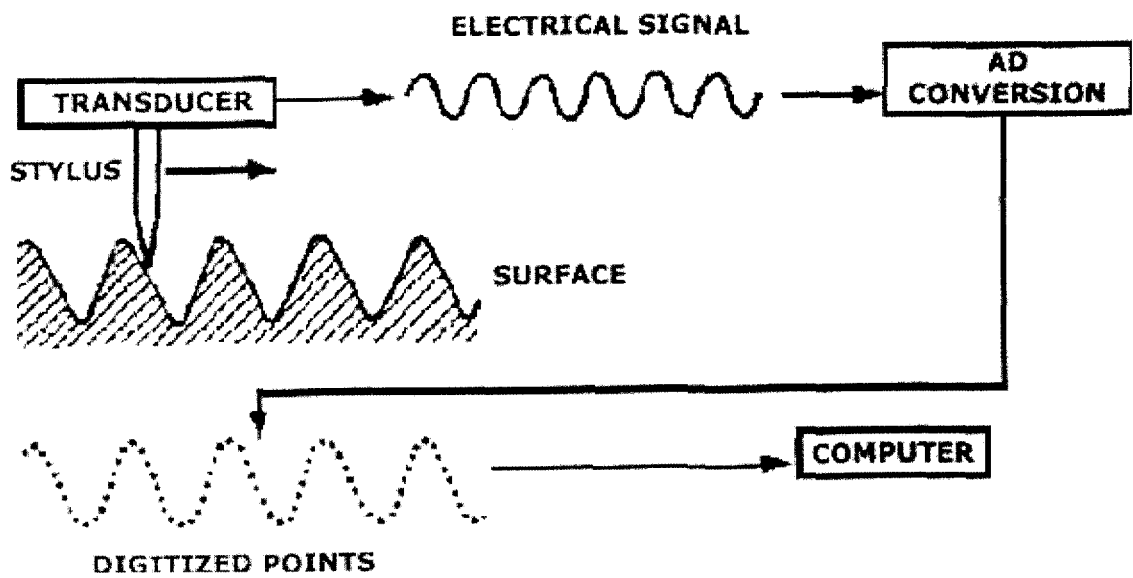


Figure 30. Schematic Diagram of a Computerized Stylus Instrument [46].

A schematic of the measurement system is shown in Figure 31. The first part of the sensor, a stylus, picks up surface undulation characteristics from the sample. Another part of the sensor looks up a reference surface; the transducer establishes the difference between the two and converts the information into an electrical signal. This signal is usually digitized and then processed. Hence, the measurement system has three important features: a sensor, a reference, and a means for comparison [41].

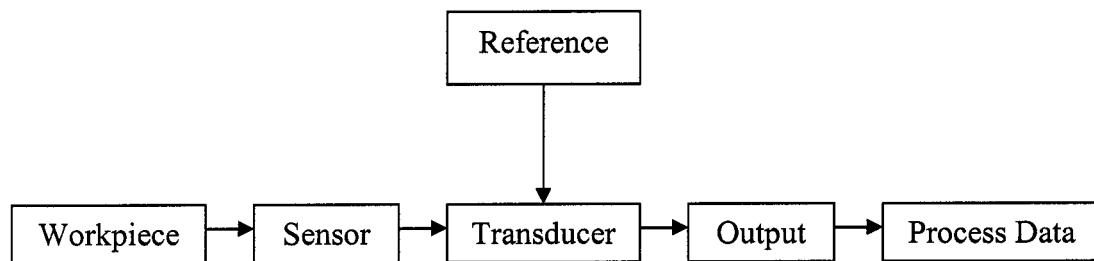


Figure 31. Schematic of Stylus Profilometer [41].

4.4.2. SEM for Surface Microstructure Examination

The R.J. Lee Instrument Personal Scanning Electron Microscope (SEM) in Figure 32 is used to study the structure of the coating and observe the individual features that contribute to the overall surface roughness and surfaces of cross-sectioned samples, it is also used to examine fractured surface and interfacial failure of the sprayed coupons after tensile testing.

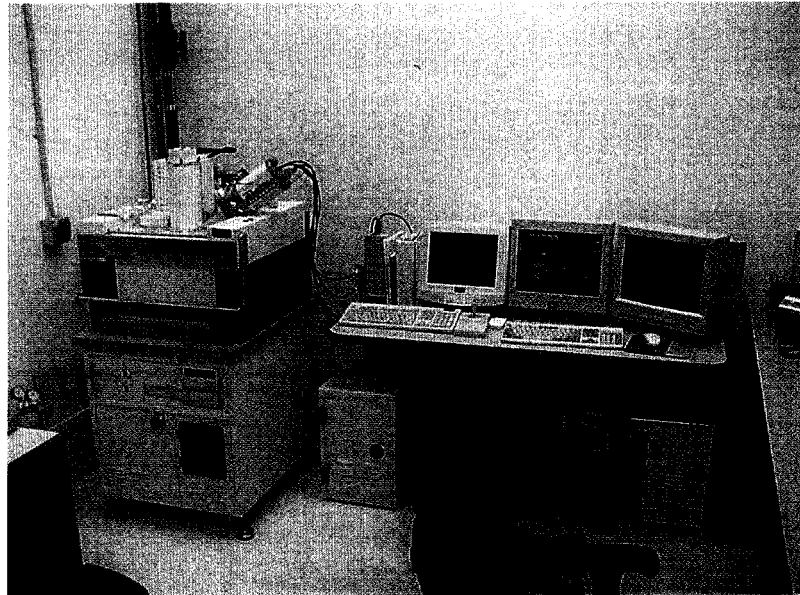


Figure 32. R. J. Lee Instrument Personal SEM.

4.4.3. Micrometer for Thickness Measurement

The Mitutoyo Micrometer as shown in Figure 33 is used to determine the coating's thickness.

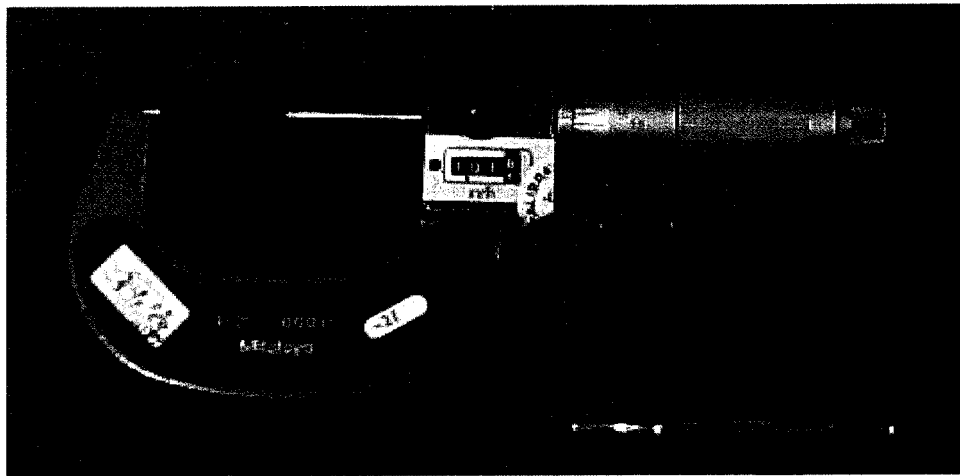


Figure 33. Mitutoyo Micrometer.

4.5. Experimental Procedure

The substrate of the test coupons is well prepared before being measured for roughness and thickness. Then they are coated and analyzed for coating bond strength, surface profile, and microstructure.

4.5.1. Substrate Preparation

All the test coupons are vapor degreased, ultrasonic rinsed, and dried by CDA to ensure the substrate surface is free from contaminations before grit blasting. After being cleaned, the coupons are Al_2O_3 bead blasted by three different size grits.

4.5.2. Measuring Substrate Roughness and Pre-Coating Thickness and Cleaning

Substrate roughness measurements are taken using a profilometer after grit blasting the surface but before cleaning it. Then, the pre-coating thickness of the coupons is measured using a micrometer. Since the cleaned test coupons are bead blasted and the roughness measured in a non-Cleanroom environment before coating, it is necessary to re-clean by vapor degreasing, chemical cleaning with 20% HNO_3 + 80% DI water solution, and ultrasonic rinsing. After that, the coupons are very carefully and gently final rinsed in high quality deionized water to remove remaining uncontaminated blast residue and embedded grit. Then the coupons are air blow-dried and packed in class 1000 Cleanroom prior coating. The non-cleaned coupons are only CDA blown-off.

4.5.3. Coating

The coating operation must be carried out as soon as possible after surface preparation for the test coupons to reduce growth of the oxide layer and to avoid deposition of dust and moisture. The testing coupons are sprayed at a thermal spray shop using standard industry equipment with the process parameter and spray condition as for spraying actual parts.

4.5.4. Analyzing Coating Bond Strength, Thickness, Surface Profile, and Microstructure

A micrometer is used to measure the post-coating thickness of the coupons, then subtract the pre-coating thickness of the coupons to determine the thickness of the coating. Then a 2-D Rank Taylor Hobson profilometer is used to evaluate the coated surface profile of the coupons. After that, it is followed by the ASTM C633-79 (1993), “Standard Test Method for Adhesion or Cohesive Strength of Flame-Sprayed Coatings” to determine the bond strength of the coating and the substrate. The coating microstructure of the coupons is examined by an SEM.

CHAPTER FIVE

5. RESULTS AND DISCUSSION

5.1. Roughness as a Function of Grit Size

As seen in Figure 34, substrate surface roughness decreases with a smaller grit size. The coupons were blasted by Al_2O_3 media with 60 psi pressure, 4 inches distance, and a 90-degree angle. The average grit blast roughness is indicated in Table 4. The 24 grit has a size of 686 microns; average roughness of the substrate surface is 185 ± 18 μ inches. The 36 grit has a size of 483 microns; the average roughness of the substrate surface is 100 ± 10 μ inches. The 80 grit has a size of 165 microns; the average roughness of the substrate surface is 60 ± 10 μ inches. The coupons blasted by size 24 grit have a greater variation in roughness than that of size 36 and size 80 grit.

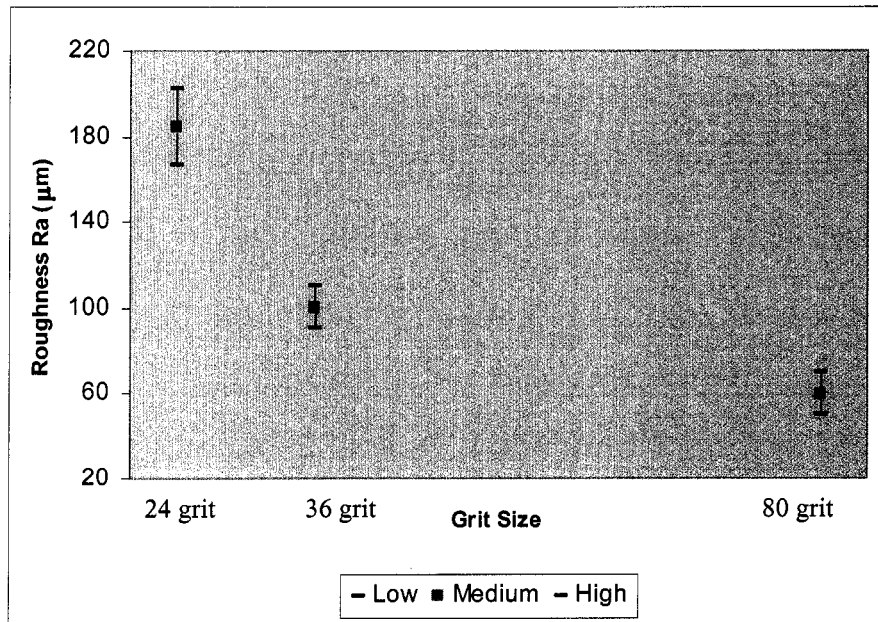


Figure 34. Average Substrate Roughness vs. Grit Size.

Table 4. Average Roughness of Grits.

Grit	Size (microns)	Ave Ra (µ-in)
80	165	59.516 +/- 9.816
36	483	99.943 +/- 9.754
24	686	184.578 +/-17.682

5.2. Ra Before and After Cleaning

Cleaning of blasted coupons can result in some changes in surface roughness as shown in Table 5. It should be noted that cleaning of coupons blasted with size 24 and size 36 grit results in an increase in roughness. However, cleaning of the coupons blasted

with size 80 grit reduces roughness. The results are an average of three (3) coupons for each size. Two measurements were taken on each sample. Appendix A details the results of bead blast roughness before and after cleaning.

Table 5. Average Bead Blast Roughness Before and After Cleaning.

Grit	Ave Ra before cleaning (μ-in)	Ave Ra after cleaning (μ-in)
80	64.744 +/- 3.432	62.495 +/- 1.716
36	122.772 +/- 3.384	129.282 +/- 4.290
24	178.608 +/- 6.451	190.451 +/- 10.147

From data analysis, the changes of roughness before and after cleaning are statistically insignificant. A t-test indicates that the average roughnesses of clean and non-clean coupons are identical to 95% confidence criteria. Details of an F-Test Two-Sample for Variances and a t-Test Two-Sample Assuming Equal Variances are in Appendix B.

5.3. Results of Clean Coupons

Results of clean coupons include result of adhesion vs. roughness and SEM analysis of clean coupons.

5.3.1. Adhesion vs. Roughness

Figure 35 indicates that from a statistical standpoint, clean coupons blasted by size 24 and size 80 grit have the same bond strength. Details of an F-Test Two-Sample for Variances and a t-Test Two-Sample Assuming Equal Variances of clean coupons are in Appendix C. Coupons blasted by size 36 grit have a higher bond strength and greater variation. It is suggested that cleaning with size 36 grit is the proper grit size for this substrate.

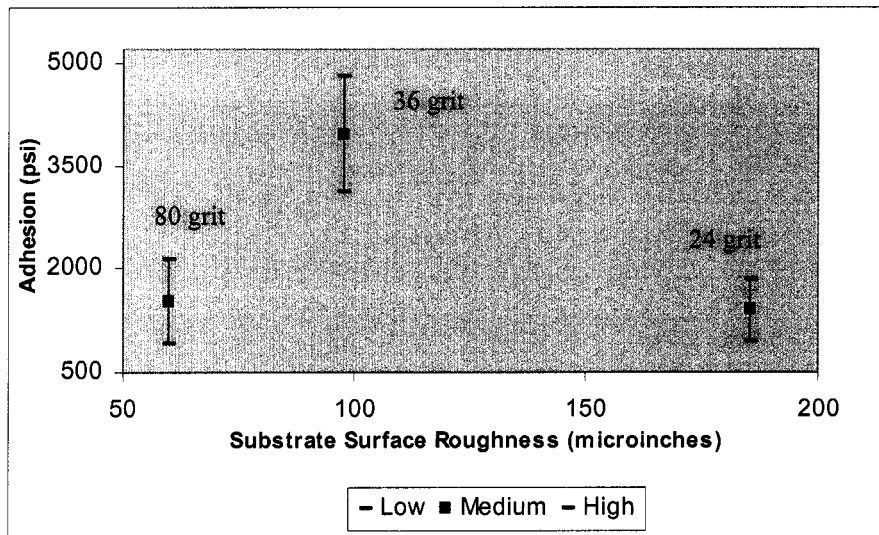


Figure 35. Average Adhesion vs. Clean Substrate Roughness.

5.3.2. SEM Images Analysis

One coupon in each set was further examined with an SEM after tensile tests to explore the microscopic aspect of fractured interfaces. Table 6 summarizes the bond strength results of clean and non-clean coupons used for SEM examination.

Table 6. Bond Strength Results of Coupons for SEM Examination.

Grit Size	Clean		Non-Clean	
	Coupon #	Bond Strength	Coupon #	Bond Strength
24	041	1974	056	4379
36	021	4493	006	318
80	071	1306	086	4108

5.3.2.1. Clean 24 Grit

Interfacial and cross-sectional images of the test coupons are analyzed by an SEM.

5.3.2.1.1. Interface

As seen in Figure 36, the adhesion failure of a clean coupon blasted by size 24 grit does not occur solely at the interface. Failure occurs both at the interface (adhesive) and within the coating itself (cohesive). The bond strength of this coupon is 1974 psi.

Although the coupon was cleaned, it is noticed from SEM examination that there are some remaining embedded grit residues on the substrate.

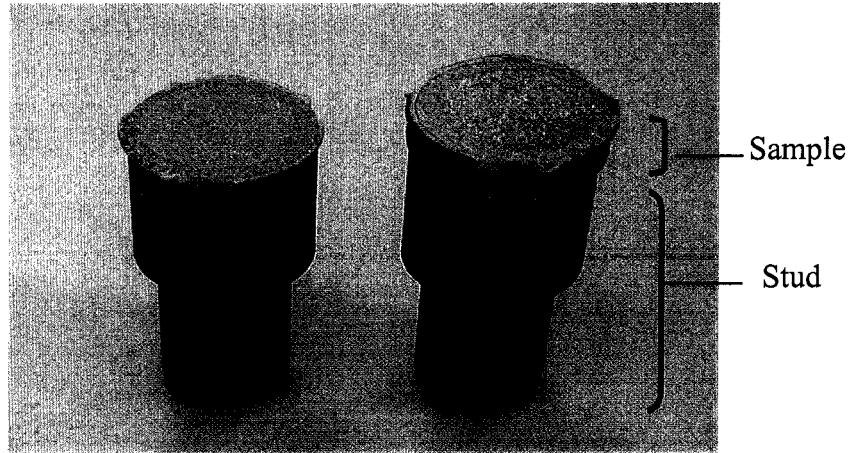


Figure 36. Interface of Clean 24 Grit Coupon (# 041).

In order to examine the interface between the coating and substrate after the tensile test, one coupon in each set is observed by an SEM. An image software package is used to analyze the SEM secondary and backscattered images.

Figure 37a is an SEM secondary image of a textured steel substrate at a nominal magnification of 100x and Figure 37b is a backscattered image of a size 24 grit clean coupon. Clearly shown in Figure 37b is the zinc (white areas) remaining on the substrate (dark gray areas).

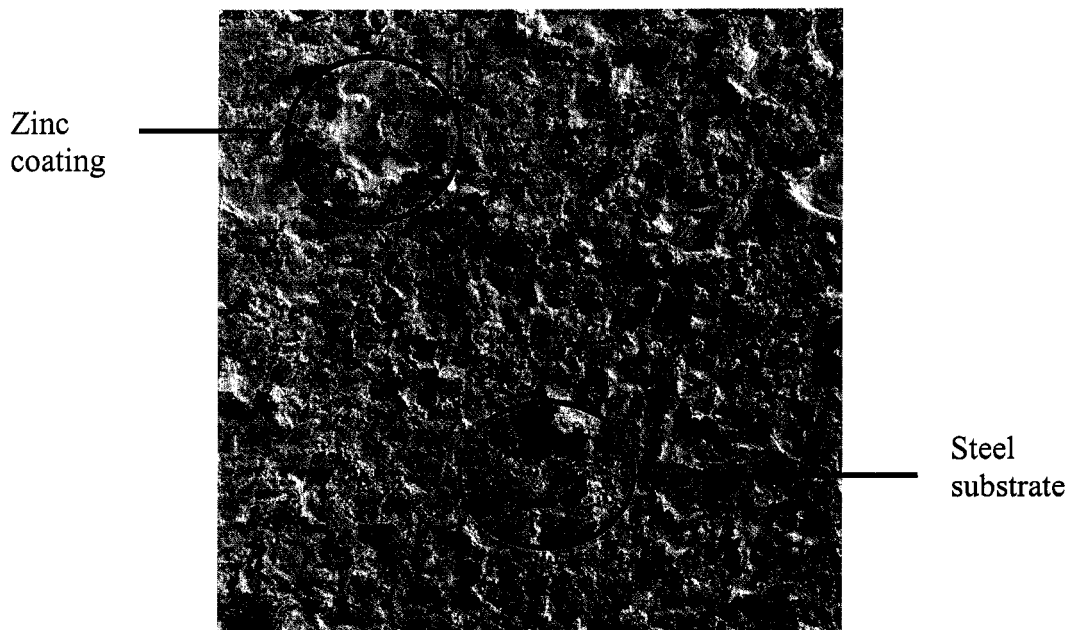


Figure 37a. SEM Secondary Image of a Textured Steel Substrate at a Nominal Magnification of 100x of a Size 24 Grit Clean Coupon.

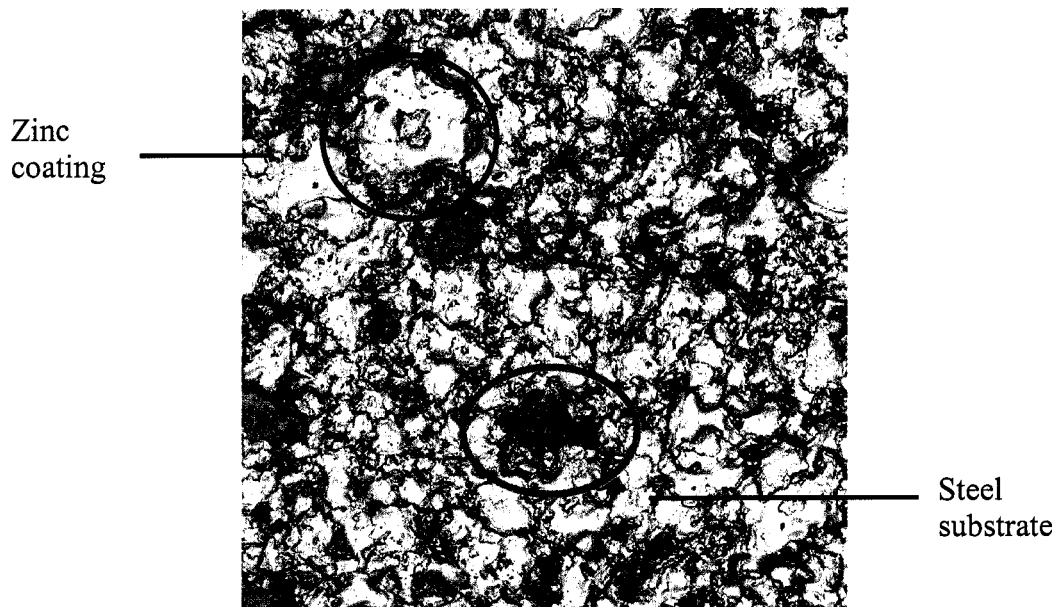


Figure 37b. SEM Backscattered Image of a Textured Steel Substrate at a Nominal Magnification of 100x of a Size 24 Grit Clean Coupon.

Figure 38a is an SEM secondary image of a textured steel substrate at a nominal magnification of 500x and Figure 38b is a backscattered image of a size 24 grit clean coupon. The black spots are the remaining alumina grit.

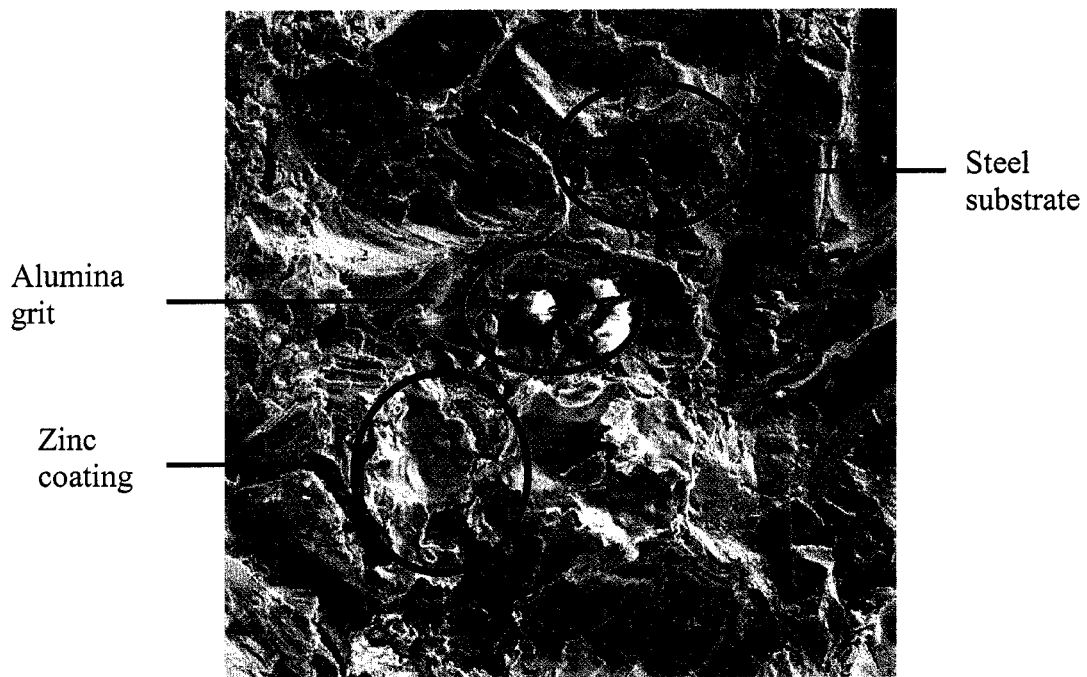


Figure 38a. SEM Secondary Image of a Textured Steel Substrate at a Nominal Magnification of 500x of a Size 24 Grit Clean Coupon.

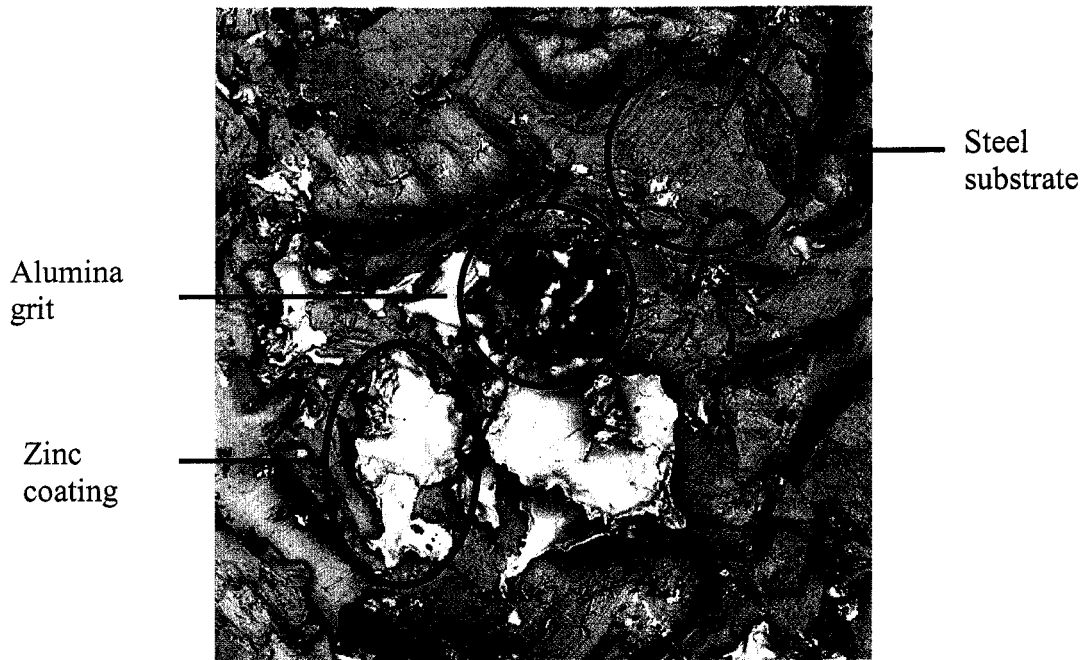


Figure 38b. SEM Backscattered Image of a Textured Steel Substrate at a Nominal Magnification of 500x of a Size 24 Grit Clean Coupon.

Energy Dispersive Spectrum (EDX) analysis confirms that there is alumina grit residue (black spots) embedded on the substrate. Figures 39, 40, and 41 show typical spectrums for substrate (dark gray areas), alumina grit (black spots), and sprayed zinc coating (white areas). The substrate is made of steel which is compounded of iron and chrome as shown in the EDX spectrum in Figure 39. The energy levels of the shells vary in a discrete fashion in atomic number so that the difference in energy between shells changes significantly even with adjacent atomic numbers. When a vacancy is created in a shell by ionization, the transition to fill that vacancy can often occur from more than one outer shell. These shells are at different energies; the X-rays created are at different

energies and are designated differently [47]. Therefore, it is expected to see more than one X-ray of electrons in the EDX analysis.

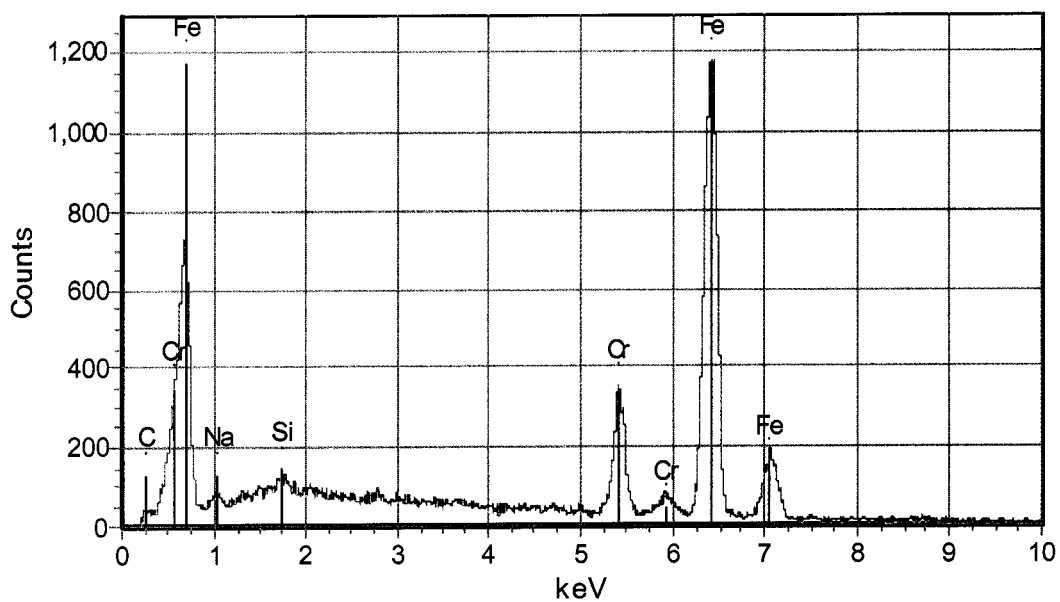


Figure 39. EDX Spectrum of Substrate (Dark Gray Areas).

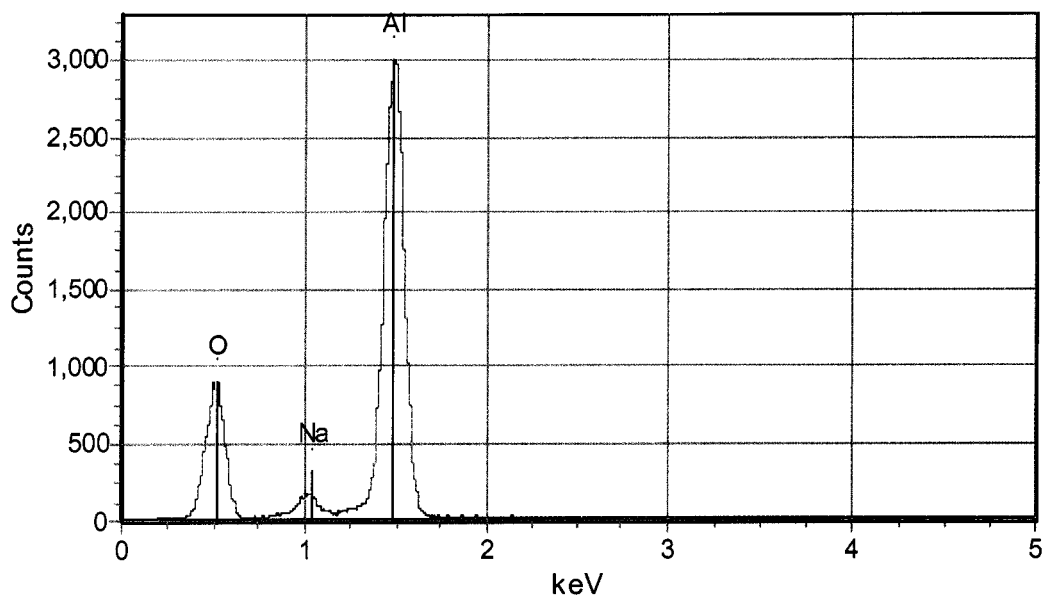


Figure 40. EDX Spectrum of Alumina Grit (Black Spots).

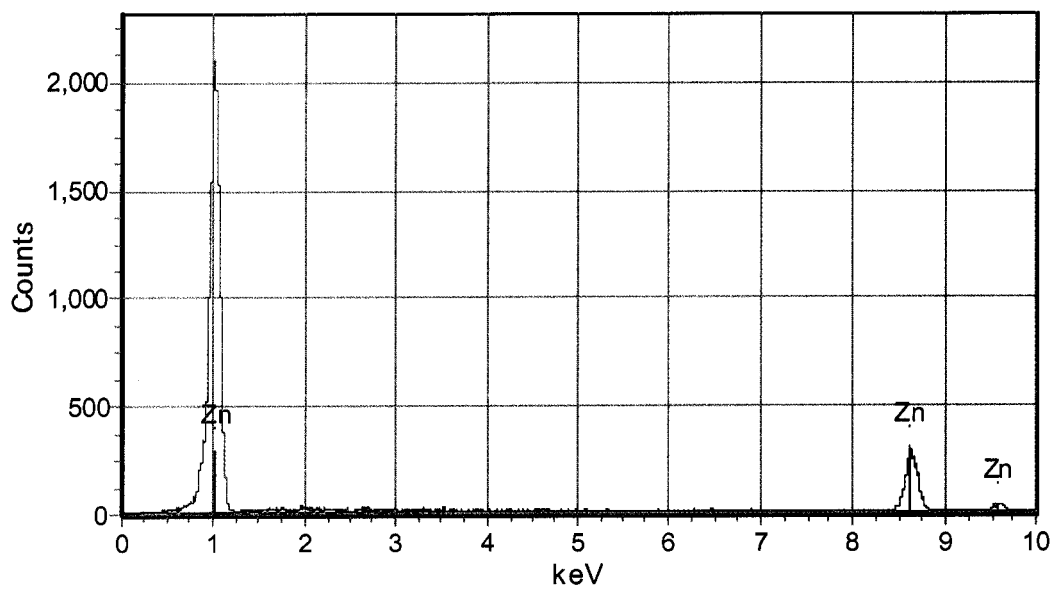


Figure 41. EDX Spectrum of Sprayed Zinc Coating (White Areas).

5.3.2.1.2. Cross-Sectional Images

Cross-section analyses of computerized image analyses are shown in Appendix D. Individual frames of the coating are captured and stored in the computer. The thickness of the film is evaluated based upon the number of pixels of coating compared to the total pixel count of the system. SEM and EDX images analyses show that there are small grits remaining on the substrate of clean coupons. Figures 42 and 43 are SEM backscattered images of a zinc coating cross-sectioned at a nominal magnification of 1000x of a size 24 grit clean coupon at different spots.

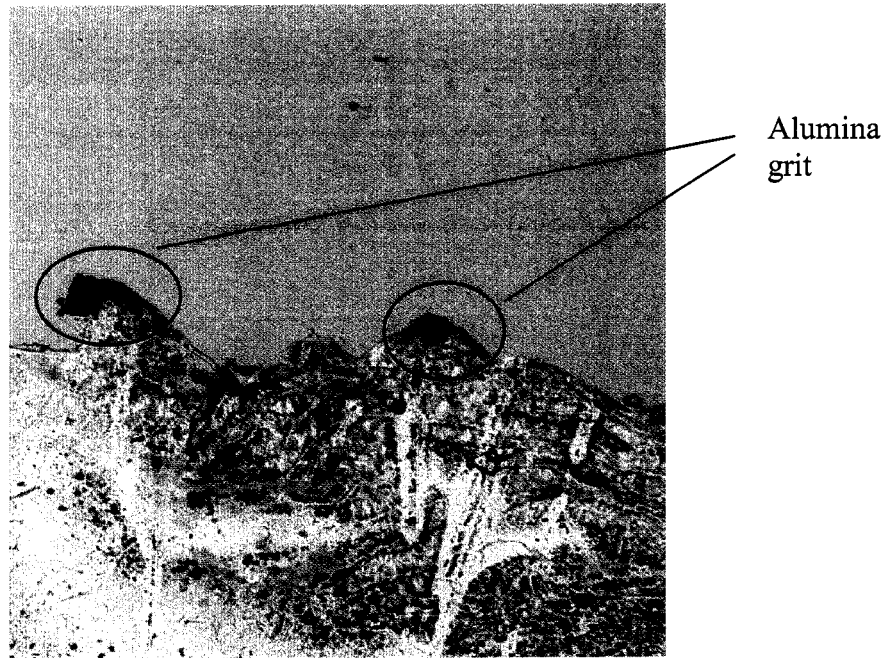


Figure 42. SEM Backscattered Image of a Zinc Coating Cross-Sectioned at a Nominal Magnification of 1000x of a Size 24 Grit Clean Coupon (Spot 1).

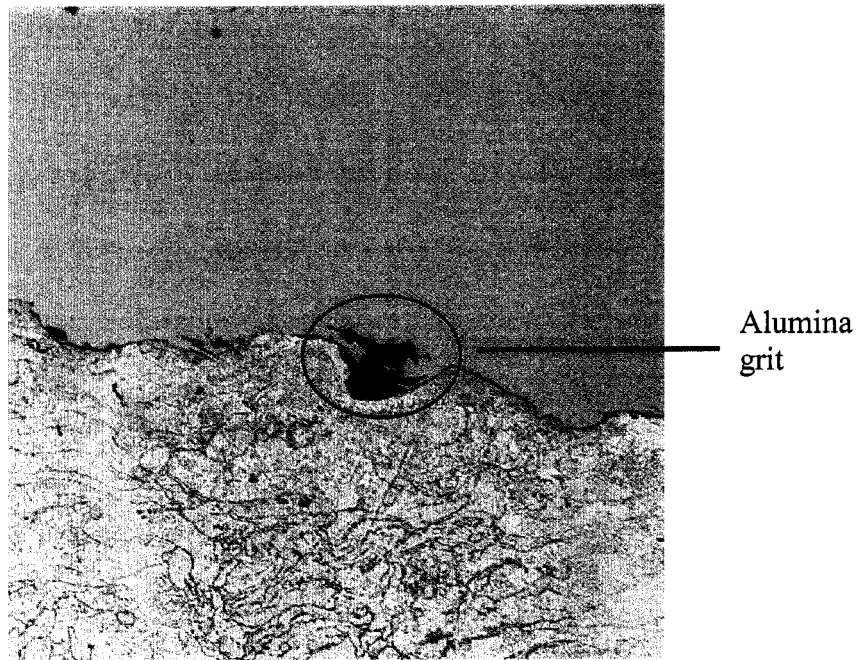


Figure 43. SEM Backscattered Image of a Zinc Coating Cross-Sectioned at a Nominal Magnification of 1000x of a Size 24 Grit Clean Coupon (Spot 2).

5.3.2.2. Clean 36 Grit

Interfacial and cross-sectional images of the test coupons are analyzed by an SEM.

5.3.2.2.1. Interface

In Figure 44, the bond strength failure mode of a clean coupon blasted by size 36 grit is visually cohesive. However, SEM imaging (Figures 45a and 45b) indicates a small

amount of adhesive failure. The bond strength of this coupon is 4493 psi; therefore, the adhesive must be higher than that.

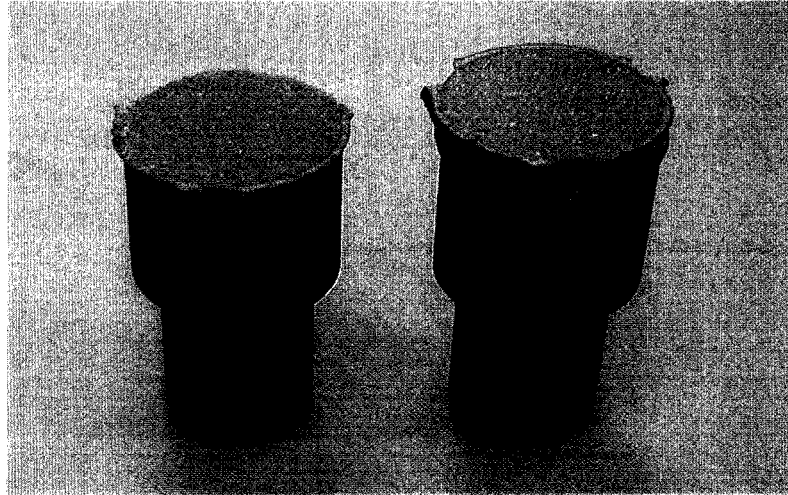


Figure 44. Interface of Clean 36 Grit Coupon (# 021).

Figure 45a is an SEM secondary image of a textured steel substrate at a nominal magnification of 100x and Figure 45b is a backscattered image of a size 36 grit clean coupon.

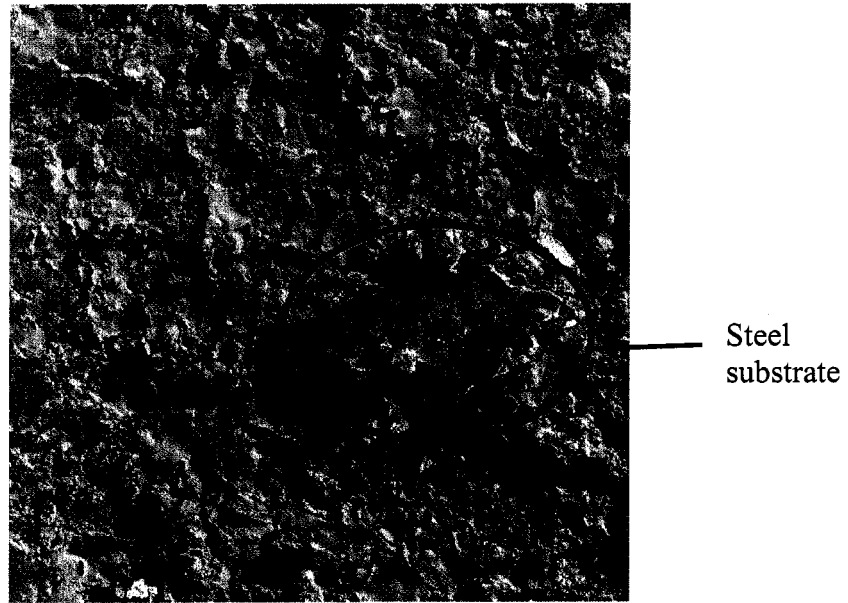


Figure 45a. SEM Secondary Image of a Textured Steel Substrate at a Nominal Magnification of 100x of a Size 36 Grit Clean Coupon.

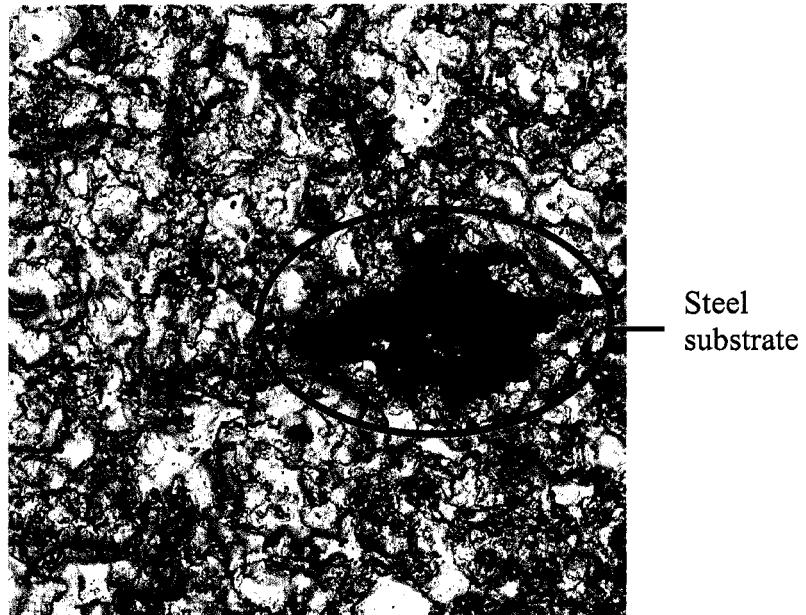


Figure 45b. SEM Backscattered Image of a Textured Steel Substrate at a Nominal Magnification of 100x of a Size 36 Grit Clean Coupon.

5.3.2.2.2. Cross-Sectional Images

Figures 46 and 47 are SEM backscattered images of a zinc coating cross-sectioned at a nominal magnification of 1000x of a size 36 grit clean coupon at different spots.

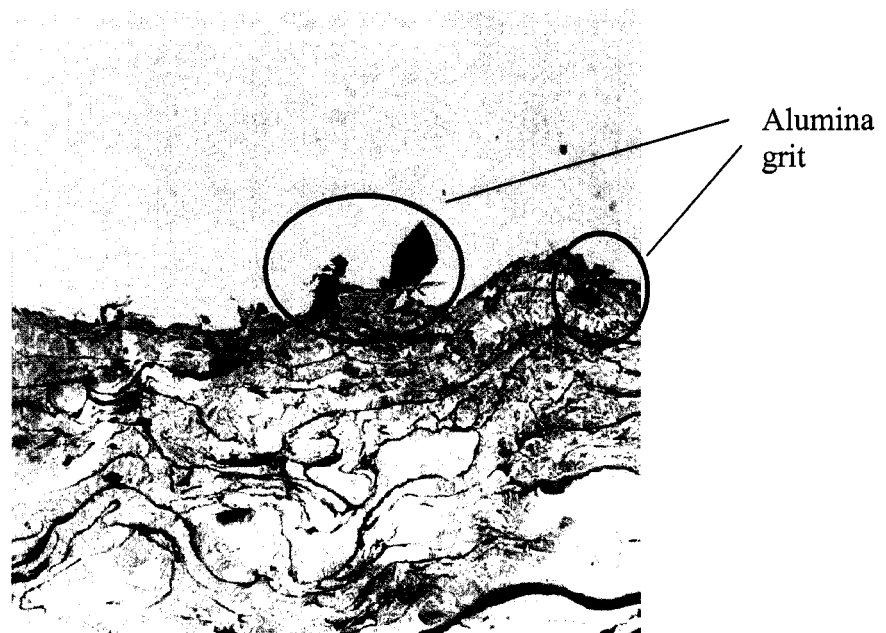


Figure 46. SEM Backscattered Image of a Zinc Coating Cross-Sectioned at a Nominal Magnification of 1000x of a Size 36 Grit Clean Coupon (Spot 1).

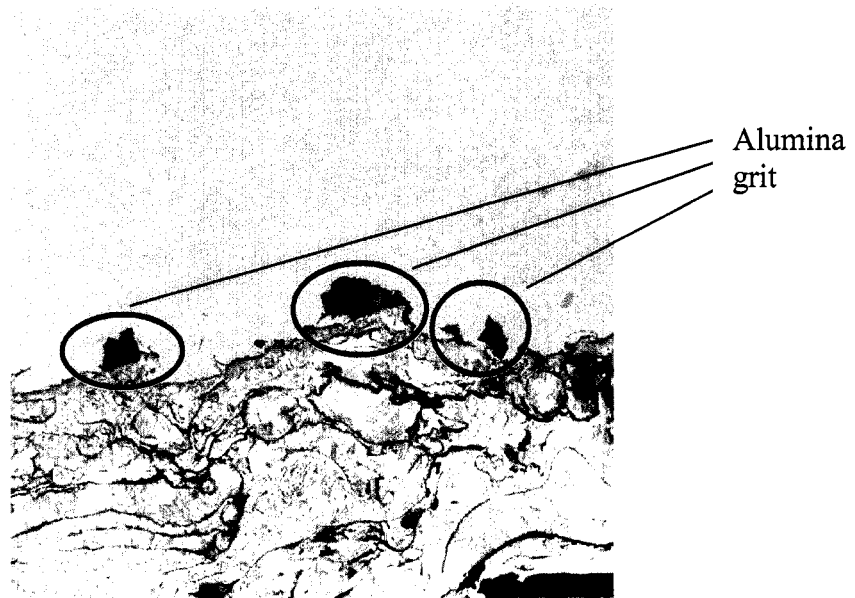


Figure 47. SEM Backscattered Image of a Zinc Coating Cross-Sectioned at a Nominal Magnification of 1000x of a Size 36 Grit Clean Coupon (Spot 2).

5.3.2.3. Clean 80 Grit

Interfacial and cross-sectional images of the test coupons are analyzed by an SEM.

5.3.2.3.1. Interface

As seen in Figure 48, the bond strength of a clean coupon blasted by size 80 grit is visually cohesive. The bond strength of this coupon is 1306 psi. There are small grits

remaining on the substrate and some little adhesive as showed in SEM and EDX images analyses.

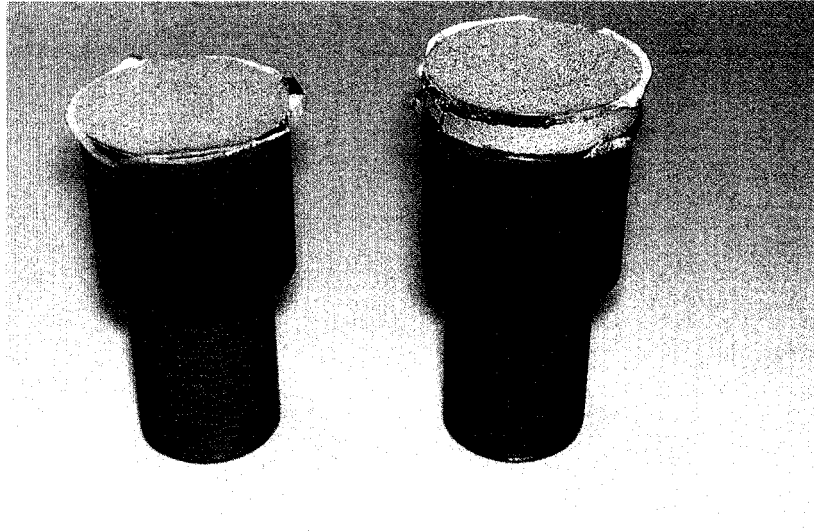


Figure 48. Interface of Clean 80 Grit Coupon (# 071).

Figures 49 and 50 are SEM backscattered images of a size 80 grit clean coupon at difference spots.

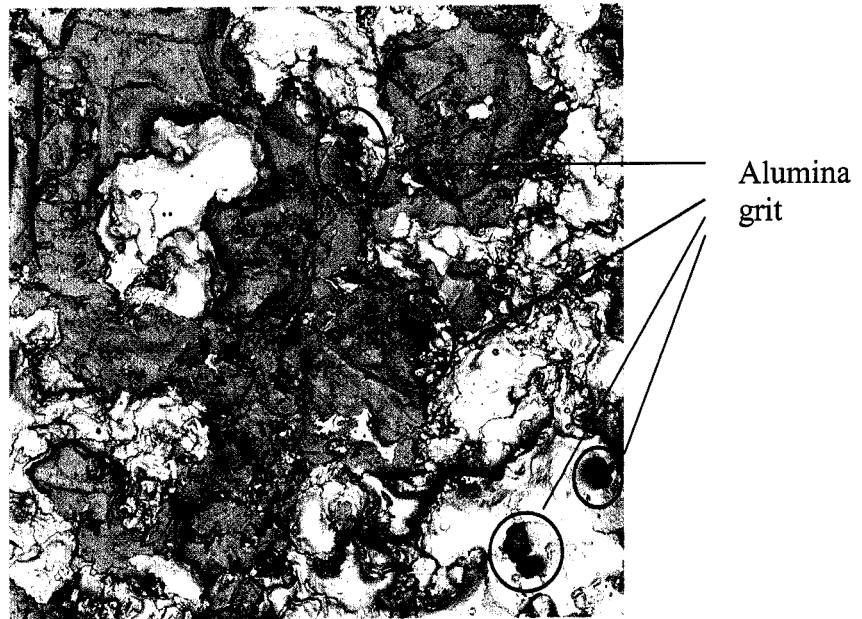


Figure 49. SEM Backscattered Image of a Textured Steel Substrate at a Nominal Magnification of 250x of a Size 80 Grit Clean Coupon (Spot 1).

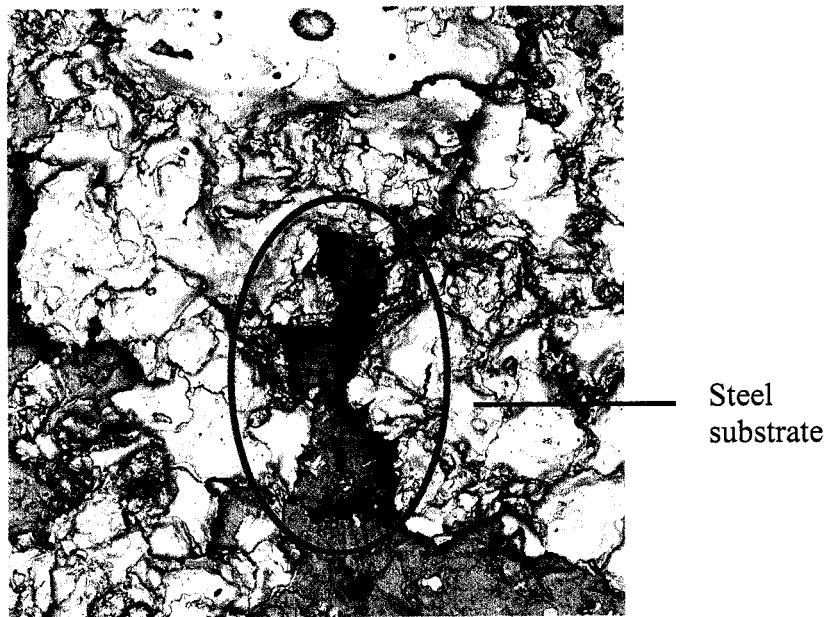


Figure 50. SEM Backscattered Image of a Textured Steel Substrate at a Nominal Magnification of 250x of a Size 80 Grit Clean Coupon (Spot 2).

5.3.2.3.2. Cross-Sectional Images

Figures 51 and 52 are SEM backscattered images of a zinc coating cross-sectioned at a nominal magnification of 1000x of a size 80 grit clean coupon at different spots.

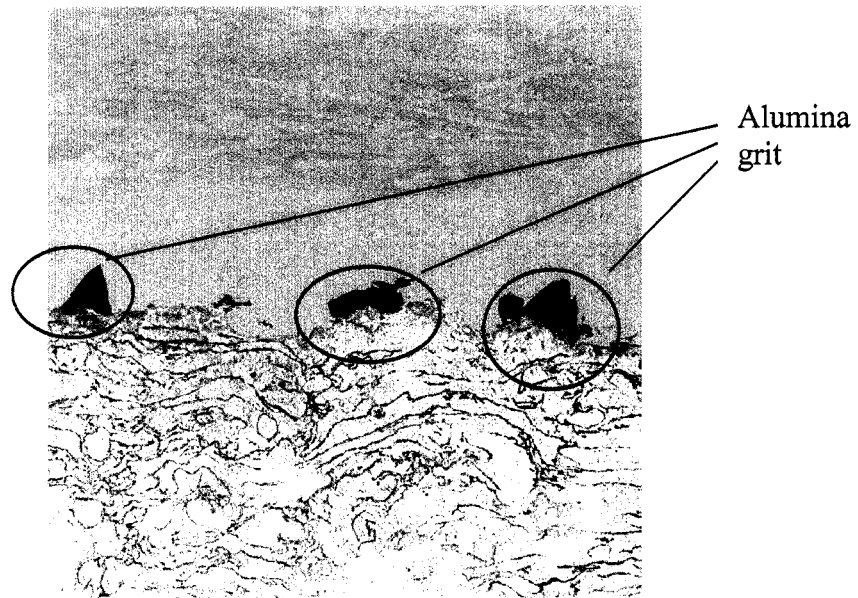


Figure 51. SEM Backscattered Image of a Zinc Coating Cross-Sectioned at a Nominal Magnification of 1000x of a Size 80 Grit Clean Coupon (Spot 1).

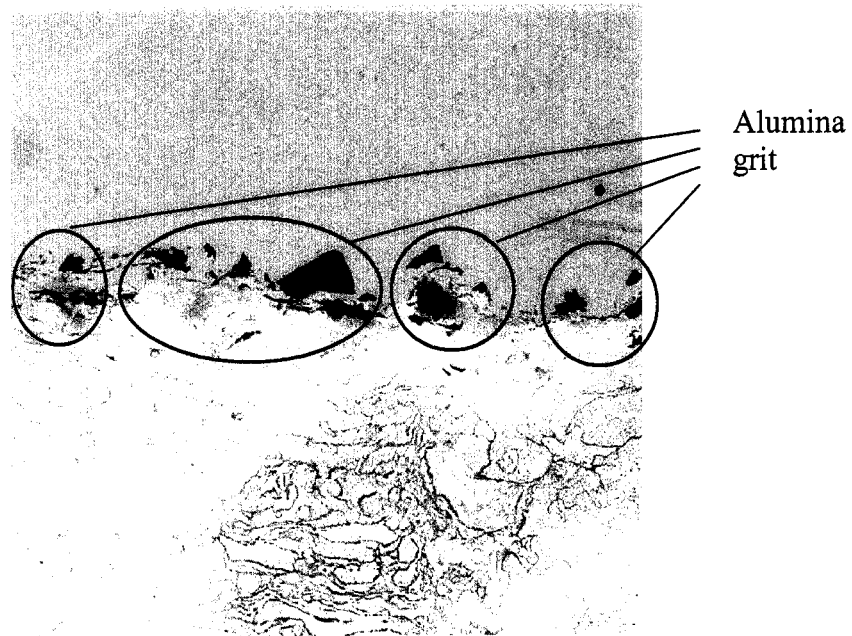


Figure 52. SEM Backscattered Image of a Zinc Coating Cross-Sectioned at a Nominal Magnification of 1000x of a Size 80 Grit Clean Coupon (Spot 2).

5.4. Results of Non-Clean Coupons

Results of non-clean coupons include result of adhesion vs. roughness and SEM analysis of non-clean coupons.

5.4.1. Adhesion vs. Roughness

Figure 53 indicates that non-clean coupons blasted by size 24 and size 80 grits statistically have the same bond strength. However, non-clean coupons blasted by size 36 grit have a lower bond strength and less variation. Details of an F-Test Two-Sample

for Variances and a t-Test Two-Sample Assuming Equal Variances of non-clean coupons are in Appendix C.

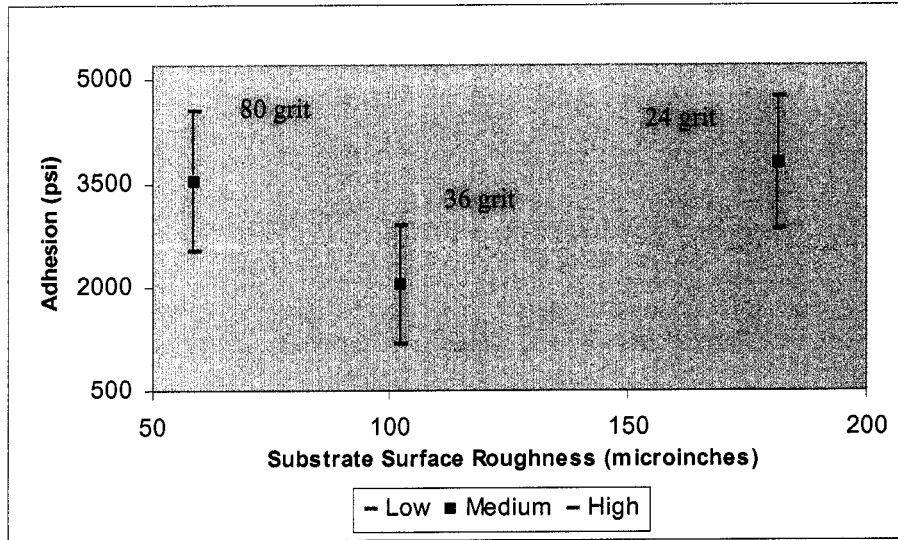


Figure 53. Average Adhesion vs. Non-Clean Substrate Roughness.

5.4.2. SEM Images Analysis

One coupon in each set was further examined with an SEM after tensile tests to explore the microscopic aspect of fractured interfaces.

5.4.2.1. Non-Clean 24 Grit

Interfacial and cross-sectional images of the test coupons are analyzed by an SEM.

5.4.2.1.1. Interface

As seen in Figure 54, the bond strength of a non-clean coupon blasted by size 24 grit is completely cohesive. The bond strength of this coupon is 4379 psi.

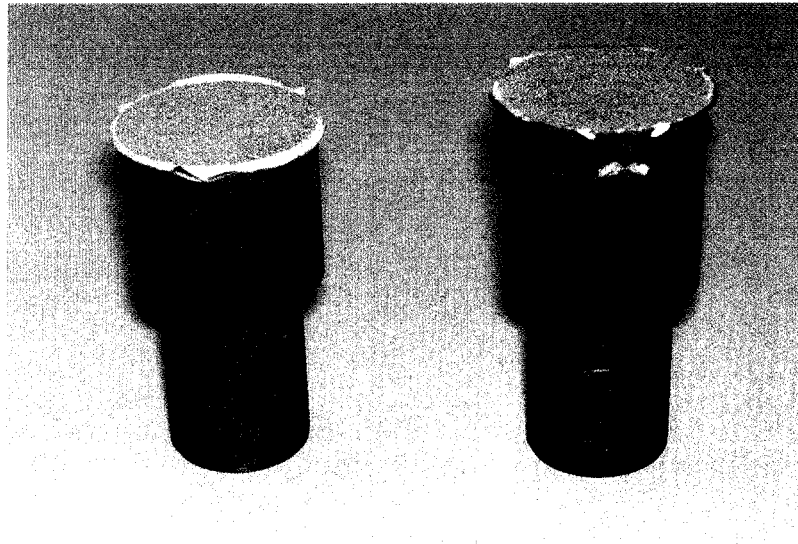


Figure 54. Interface of Non-Clean 24 Grit Coupon (# 056).

Figure 55 is an SEM backscattered image of a size 24 grit non-clean coupon.

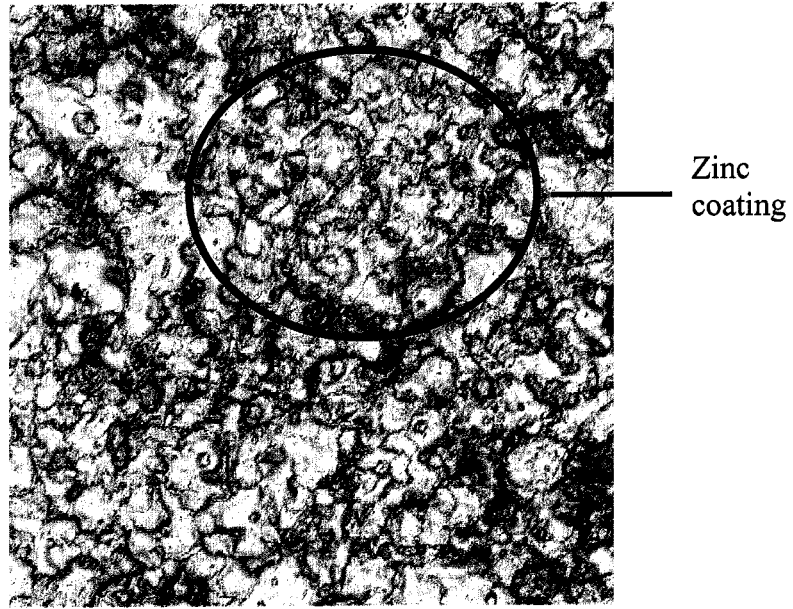


Figure 55. SEM Backscattered Image of a Textured Steel Substrate at a Nominal Magnification of 100x of a Size 24 Grit Non-Clean Coupon.

5.4.2.1.2. Cross-Sectional Images

There are not only small grits but also big grits remaining on the substrate for the non-clean samples. Figures 56, 57, and 58 are SEM backscattered images of a zinc coating cross-sectioned at a nominal magnification of 1000x of a size 24 grit non-clean coupon at different spots.

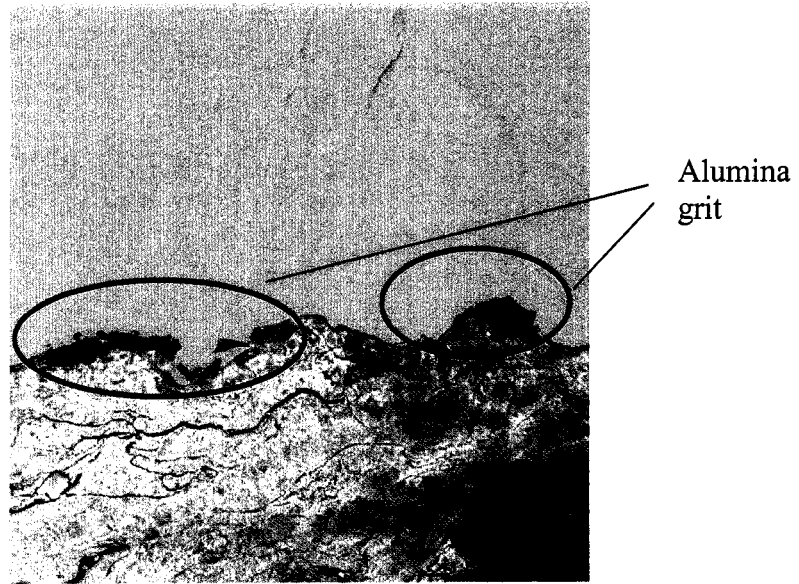


Figure 56. SEM Backscattered Image of a Zinc Coating Cross-Sectioned at a Nominal Magnification of 1000x of a Size 24 Grit Non-Clean Coupon (Spot 1).

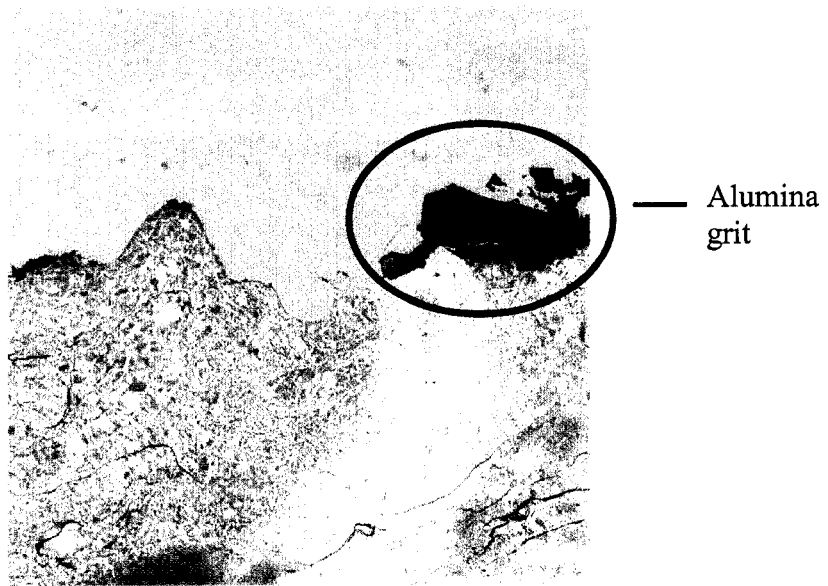


Figure 57. SEM Backscattered Image of a Zinc Coating Cross-Sectioned at a Nominal Magnification of 1000x of a Size 24 Grit Non-Clean Coupon (Spot 2).

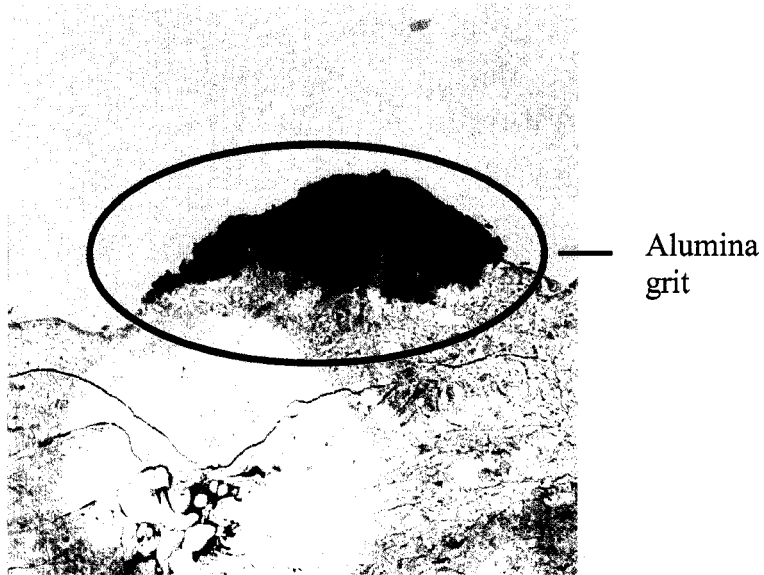


Figure 58. SEM Backscattered Image of a Zinc Coating Cross-Sectioned at a Nominal Magnification of 1000x of a size 24 Grit Non-Clean Coupon (Spot 3).

5.4.2.2. Non-Clean 36 Grit

Interfacial and cross-sectional images of the test coupons are analyzed by an SEM.

5.4.2.2.1. Interface

As seen in Figure 59, the bond strength of a non-clean coupon blasted by size 36 grit is adhesive. The bond strength of this coupon is 318 psi. EDX analysis shows that there are some alumina grits at the interface.

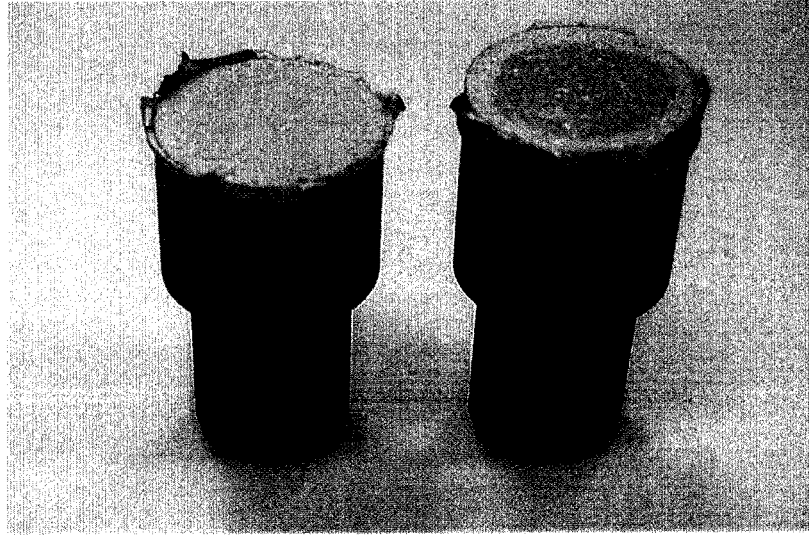


Figure 59. Interface of Non-Clean 36 Grit Coupon (# 006).

Figure 60a is an SEM secondary image of a textured steel substrate at a nominal magnification of 100x and Figure 60b is a backscattered image of a size 36 grit non-clean coupon. As seen in the image, the interface is at the substrate.

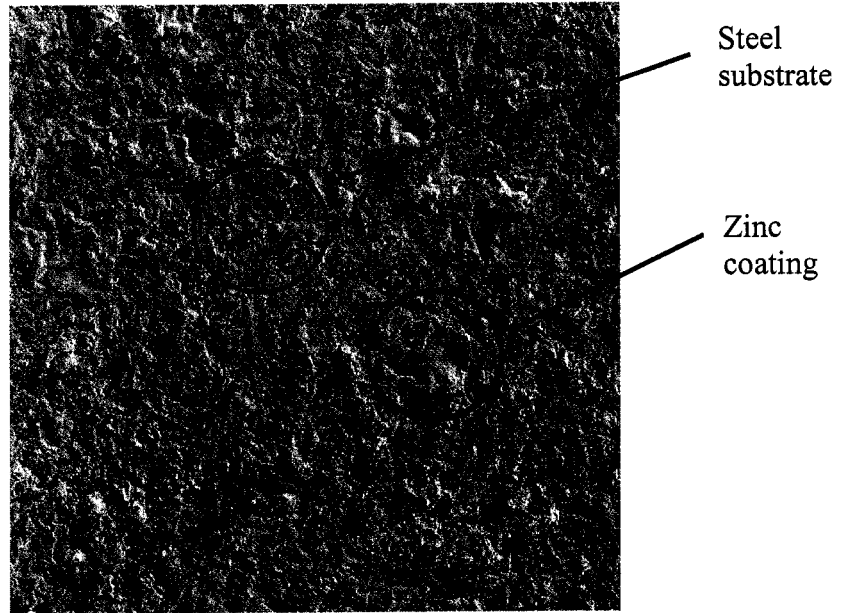


Figure 60a. SEM Secondary Image of a Textured Steel Substrate at a Nominal Magnification of 100x of a Size 36 Grit Non-Clean Coupon.

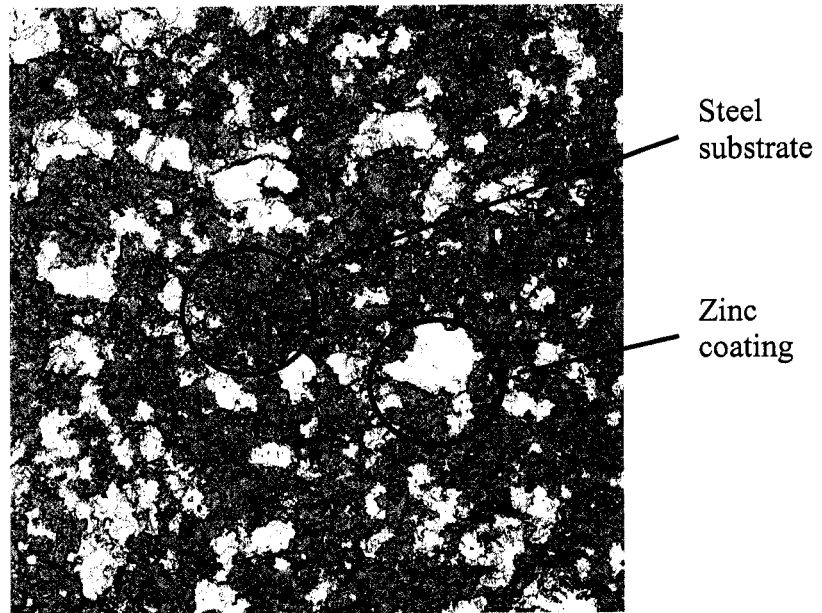


Figure 60b. SEM Backscattered Image of a Textured Steel Substrate at a Nominal Magnification of 100x of a Size 36 Grit Non-Clean Coupon.

Figure 61a is an SEM secondary image of a textured steel substrate at a nominal magnification of 500x and Figure 61b is a backscattered image of a size 36 grit non-clean coupon. As seen in Figure 61b, there are some alumina grits remaining on the substrate. It is more difficult to recognize the remaining alumina grit in the secondary image (Figure 61a).

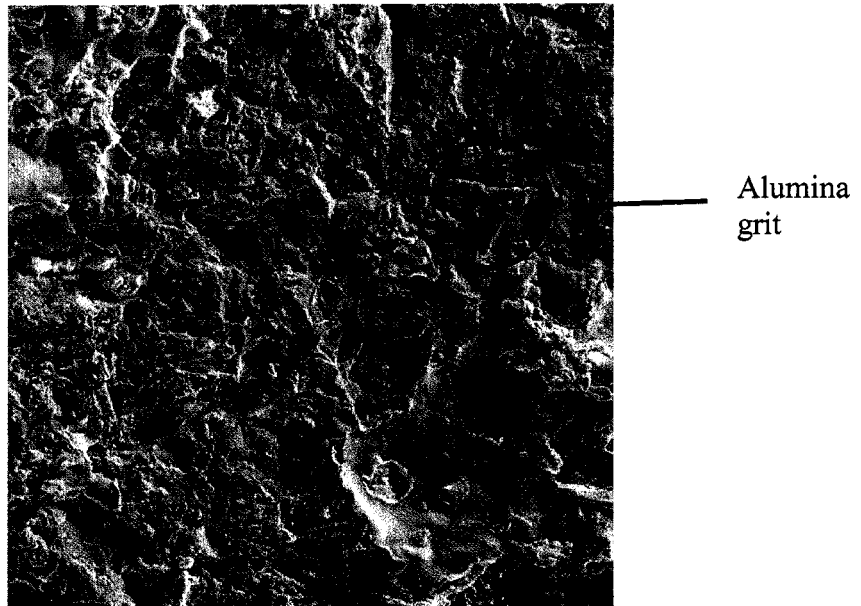


Figure 61a. SEM Secondary Image of a Textured Steel Substrate at a Nominal Magnification of 500x of a Size 36 Grit Non-Clean Coupon.

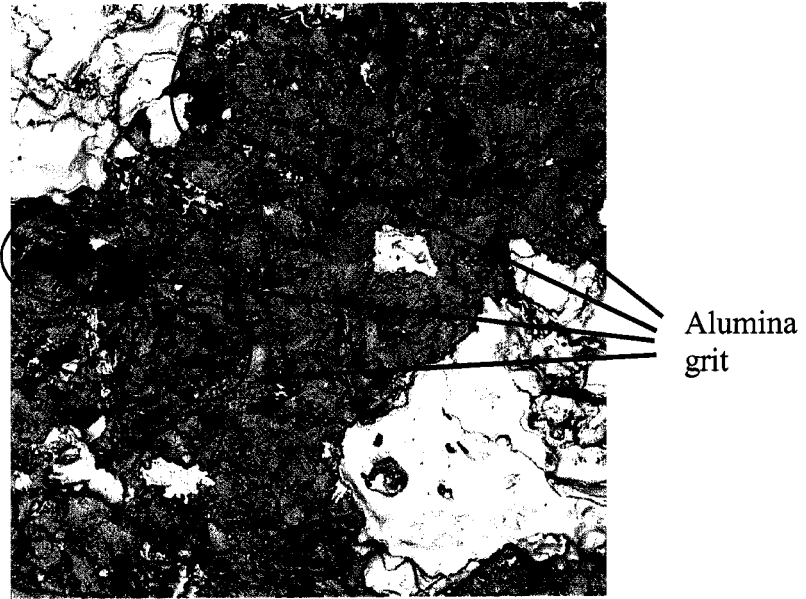


Figure 61b. SEM Backscattered Image of a Textured Steel Substrate at a Nominal Magnification of 500x of a Size 36 Grit Non-Clean Coupon.

5.4.2.2.2. Cross-Sectional Images

Figures 62, 63, and 64 are SEM backscattered images of a zinc coating cross-sectioned at a nominal magnification of 1000x of a size 36 grit non-clean coupon at different spots.

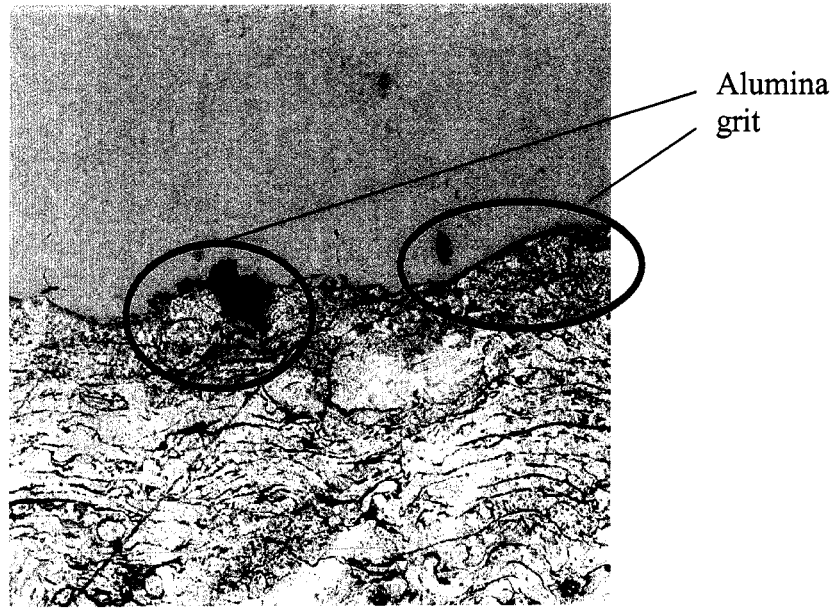


Figure 62. SEM Backscattered Image of a Zinc Coating Cross-Sectioned at a Nominal Magnification of 1000x of a Size 36 Grit Non-Clean Coupon (Spot 1).

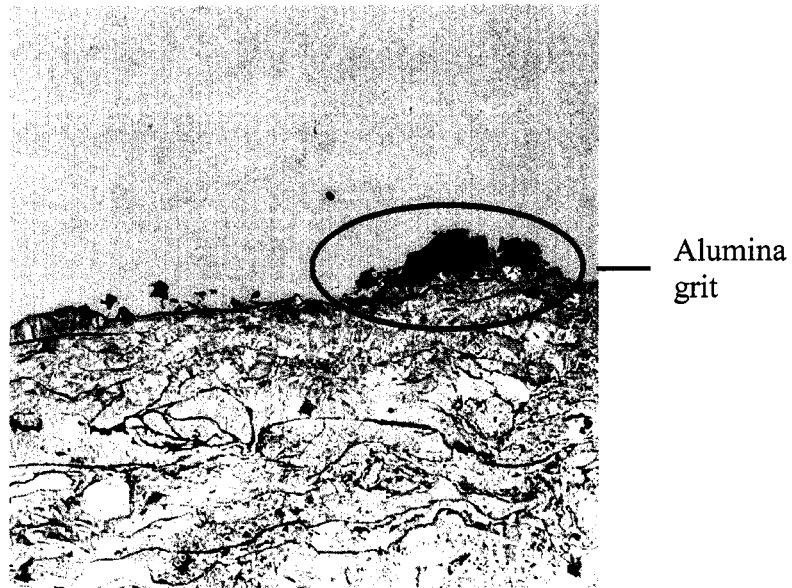


Figure 63. SEM Backscattered Image of a Zinc Coating Cross-Sectioned at a Nominal Magnification of 1000x of a Size 36 Grit Non-Clean Coupon (Spot 2).

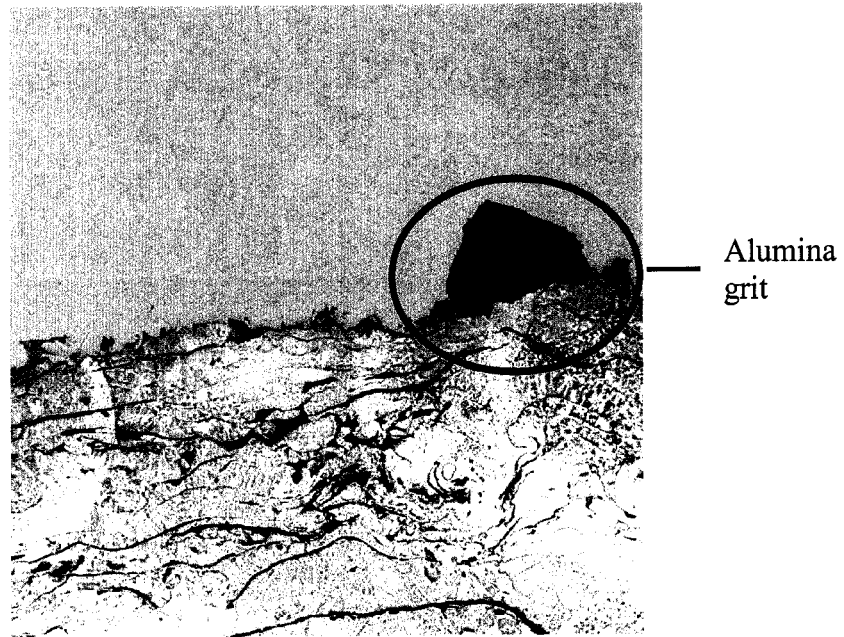


Figure 64. SEM Backscattered Image of a Zinc Coating Cross-Sectioned at a Nominal Magnification of 1000x of a Size 36 Grit Non-Clean Coupon (Spot 3).

5.4.2.3. Non-Clean 80 Grit

Interfacial and cross-sectional images of the test coupons are analyzed by an SEM.

5.4.2.3.1. Interface

As seen in Figure 65, the bond strength failure mode of a non-clean coupon blasted by size 80 grit is visually cohesive. However, further investigation by EDX and SEM indicates that there is a portion of the failure inside the coating as shown in Figure 66. The bond strength of this coupon is 4108 psi.

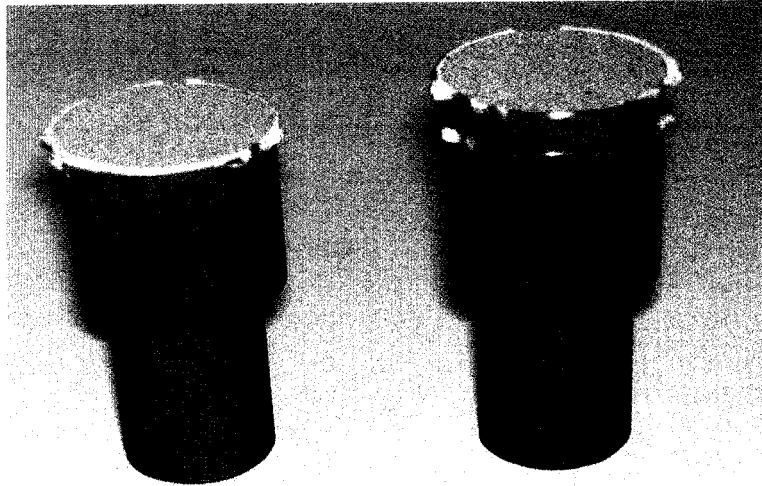


Figure 65. Interface of Non-Clean 80 Grit Coupon (# 086).

Figure 66 is an SEM backscattered image of a size 80 grit non-clean coupon.

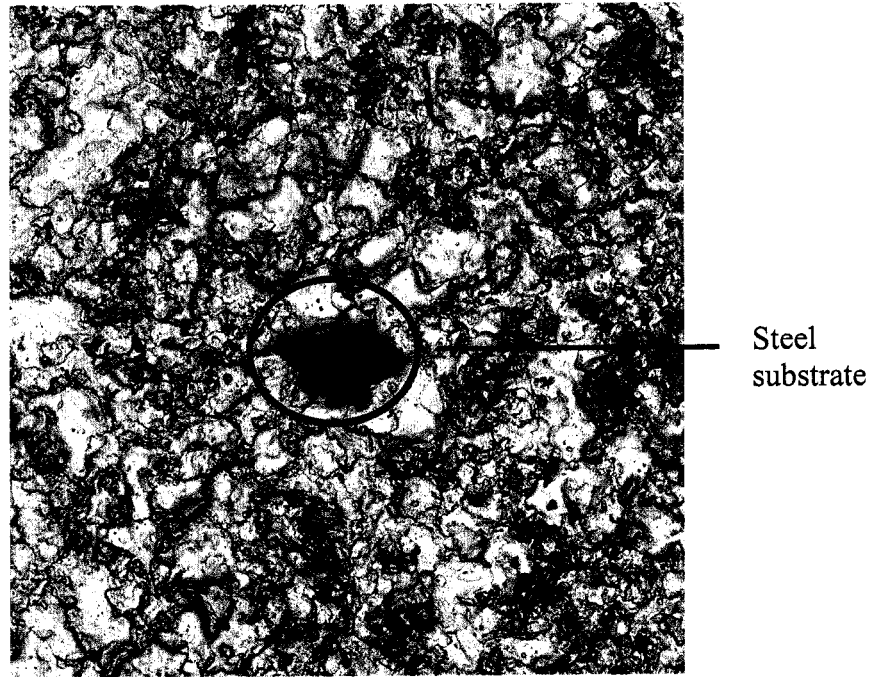


Figure 66. SEM Backscattered Image of a Textured Steel Substrate at a Nominal Magnification of 100x of a Size 80 Grit Non-Clean Coupon.

5.4.2.3.2. Cross-Sectional Images

Figures 67, 68, and 69 are SEM backscattered images of a zinc coating cross-sectioned at a nominal magnification of 1000x of a size 80 grit non-clean coupon at different spots.

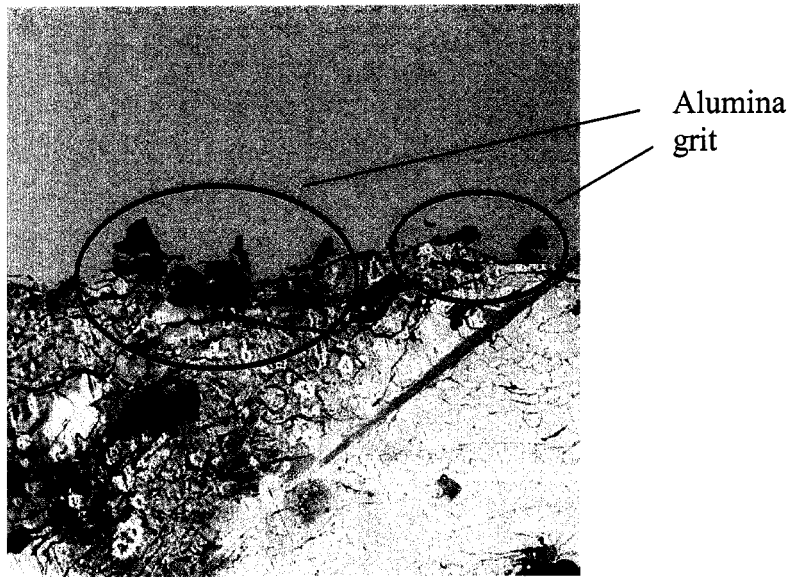


Figure 67. SEM Backscattered Image of a Zinc Coating Cross-Sectioned at a Nominal Magnification of 1000x of a Size 80 Grit Non-Clean Coupon (Spot 1).

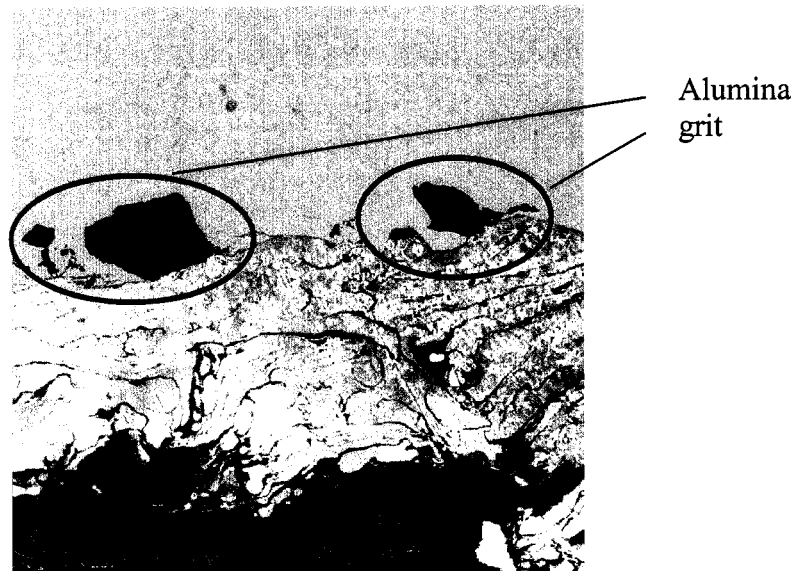


Figure 68. SEM Backscattered Image of a Zinc Coating Cross-Sectioned at a Nominal Magnification of 1000x of a Size 80 Grit Non-Clean Coupon (Spot 2).

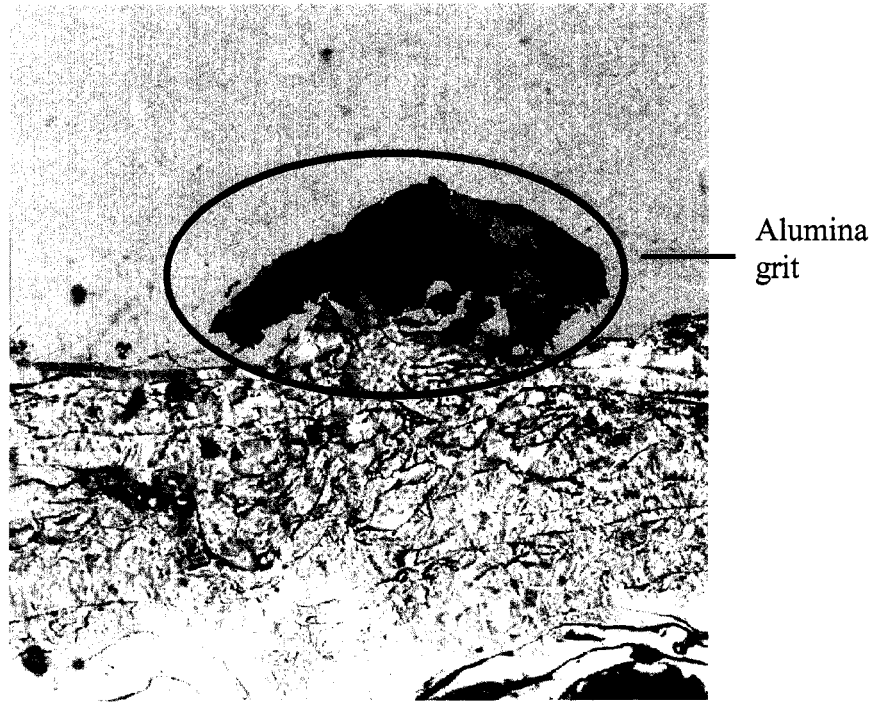


Figure 69. SEM Backscattered Image of a Zinc Coating Cross-Sectioned at a Nominal Magnification of 1000x of a Size 80 Grit Non-Clean Coupon (Spot 3).

5.5. Results of Clean vs. Non-Clean Coupons

As seen in Figure 70, the bond strengths of size 24 and size 80 grit clean coupons are lower than that of non-clean coupons. In contrast, the bond strengths of size 36 grit clean coupons are higher than that of non-clean coupons. Table 7 summarizes the average results of substrate roughness and bond strength. Appendix D, E, and F detail results of coupons' roughness and bond strength.

Table 7. Average Results of Substrate Roughness and Bond Strength.

Average	Clean		Non-Clean	
Grit Sizes	Roughness (microin)	Bond Strength (psi)	Roughness (microin)	Bond Strength (psi)
80	60.051 +/- 11.115	1504 +/- 608	58.980 +/- 8.517	3528 +/- 1012
36	97.696 +/- 10.476	3955 +/- 844	102.189 +/- 9.031	2035 +/- 872
24	187.508 +/- 16.237	1398 +/- 450	181.647 +/- 19.126	3793 +/- 954

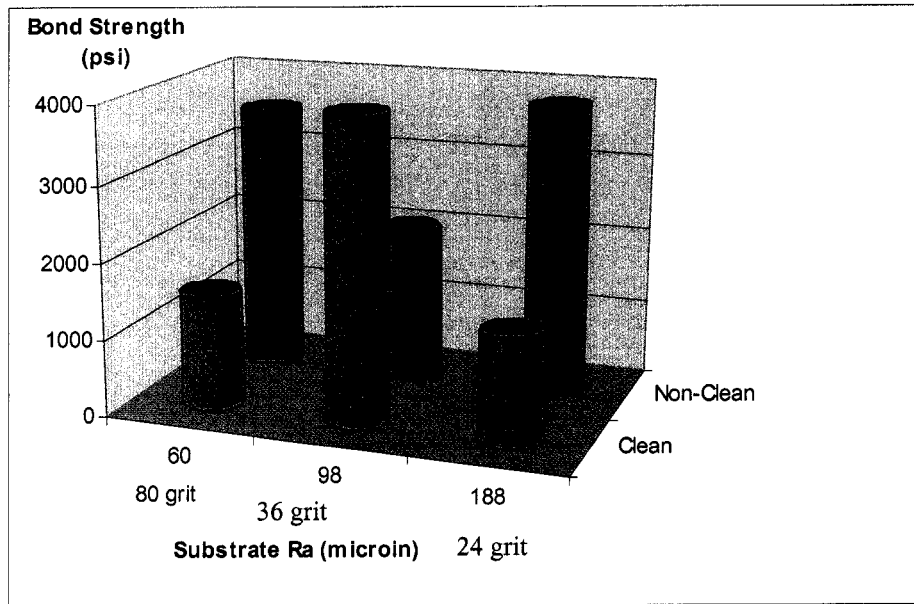


Figure 70. Average Bond Strength vs. Substrate Ra.

CHAPTER SIX

6. SUMMARY AND CONCLUSION

Substrate surface roughness decreases with smaller grit size. The desired roughness can be controlled by selecting proper grit size. Cleaning of blasted coupons can result in changes in surface composition that affect bond strength. Cleaning of coupons blasted with size 24 and size 36 grits results in increased roughness while the surface roughness decreases for coupons blasted with size 80 grit media. Cleaning removes the large size of grit residue from 24 and 36 sized grits. The smaller grit (size 80 grit) has a very small amount of grit residue remaining on the substrate that has no effect on the roughness. Cleaning also etches some substrate materials resulting in lower Ra.

Clean coupons blasted by size 24 and size 80 grit have the same bond strength. Coupons blasted by size 36 grit have a higher bond strength and greater variation. Cleaning with size 36 grit results in the maximum bond strength. Probably size 36 grit is the proper grit size to achieve optimum Ra for this substrate. The failure mode of clean coupons blasted by size 24 grit does not occur solely at the interface. Failure is a mix of adhesive and cohesive properties. The failure mode of clean coupons blasted by size 36 grit and size 80 grit is cohesive with small adhesive portions. Cohesive failures in clean coupons indicate that the bond strength is higher than that resulting from the tensile test. In the case of size 24 grit, the large amount of grit residues results in adhesion failure

occurring both at the interface and the coating and reduces the bond strength of the coating on the substrate

Non-clean coupons blasted by size 24 and size 80 grits have the same bond strength. Coupons blasted by size 36 grit have lower bond strength and less variation. The failure mode of non-clean coupons blasted by size 24 grit is completely cohesive. The failure mode of non-clean coupons blasted by size 36 grit is adhesive. The failure mode of non-clean coupons blasted by size 80 grit is cohesive with a small adhesive portion. Grit residues of non-clean coupons scatter within the coating resulting in cohesive failure in the cases of size 24 and size 80 grits. In the case of size 36 grit, bond strength is very low due to large amounts of grit residues.

The bond strength of size 24 and size 80 grit clean coupons is lower than that of non-clean coupons. The bond strength of size 36 grit clean coupons is higher than that of non-clean coupons. The average bond strength of size 36 grit clean coupons is the highest, so it is the proper preparation for the substrate.

Traditional visual inspection of fractured surfaces resulting from the tensile test may not be effective in differentiating the type of fracture mechanism: adhesive, cohesive, or mixed mode. In the cases of clean 36 grit coupon # 021 shown in Figure 44, clean 80 grit coupon # 071 shown in Figure 48, and non-clean 80 grit coupon # 086 shown in Figure 65, the bond strength is visually cohesive. However, SEM analysis

showing that there is some adhesion is given in Figures 45 b, Figure 50, and Figure 66. SEM in backscattered mode should be applied to assess the nature of the fracture mechanism. As seen in most images, backscattered images differentiate substrate, alumina grits, and zinc coating more clearly. Figures 38a and 38 b are examples of this statement.

Examining fractured surfaces of available coupons using SEM and EDX analyses showed that textured surfaces had more embedded grit media for coupons without cleaning prior to spray coating compared to that of coupons with cleaning. The observation indicated that most coupons without cleaning exhibited either interfacial or mixed modes as estimated in Figure 71. Based upon a scale from 0% to 100% for cohesion to adhesion, coupons with cleaning are exposed from 5% to 30% while coupons without cleaning are exposed from 25% to 95%.

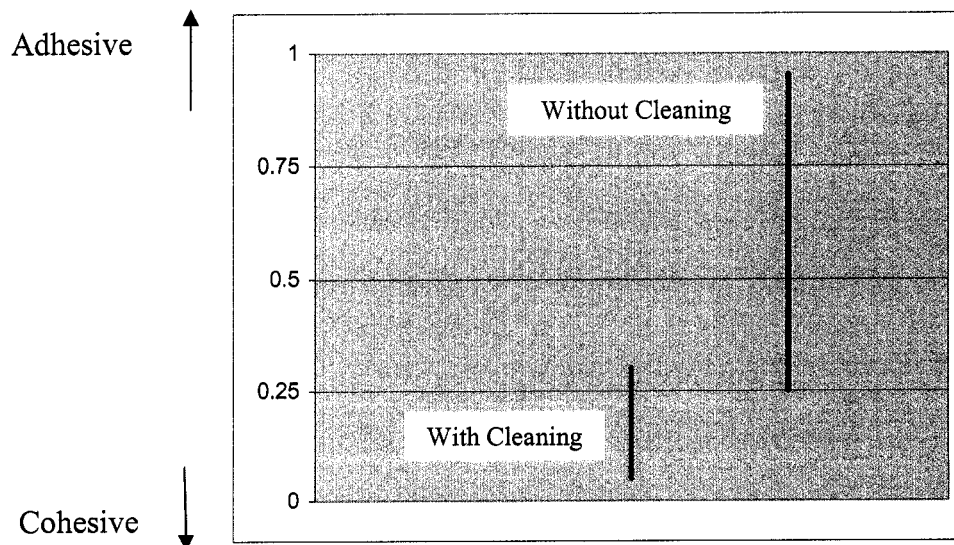


Figure 71. Percentage of Exposure of Textured Surface.

Cleaned coupons exhibited mostly cohesion. It was observed that some of them exhibited adhesion, which means the interface may have been altered due to surface topography of the substrate that can affect the failure mode. However, surface roughness topography is not the only factor that affects the coating bond strength.

From the examination of cross-sectioned coupons, it can certainly be concluded that there are more embedded grit media on non-clean coupons than on clean coupons on a semi-quantitative basis. Also, coupons blasted by larger grit size have more grit residue than coupons blasted by smaller grit size.

CHAPTER SEVEN

7. FUTURE WORK

Future work should be done exploring alternative film adhesion testing methods. The coating bond strength should be determined not only by tensile test but also by shear test to verify the accuracy of the results. It also is necessary to evaluate coating surface topography through 3-D data collection and analysis since 2-D parameter Ra used to measured roughness has a very limited value in relating the coating surface to its functional effectiveness; therefore, surface 3-D topography should be analyzed. Research should be conducted to study failure mechanism (cohesive vs. adhesive) to be able to control the coating bond strength. A better way to measure thickness to evaluate the relationship of thickness and bond strength should be determined. The interdependence between coating structures should also be investigated to understand how overlays of materials build up in the TWAS process.

REFERENCES

1. (2004). What is thermal spray. *Sulzer Metco*. <http://www.sulzermetco.com/> (2 January 2004).
2. M.R. Dorfman, Sulzer Metco (US) Inc., “*Thermal Spray Processes*,” *Advanced Materials & Processes*, (August 2002).
3. D.J. Varacalle Jr., R.S. Hartley, L.B. Lundberg, J. Walker and W.L. Riggs II, “*Surface Preparation via Grit-Blasting for Thermal Spraying*,” *Proceedings of the 8th National Thermal Spray Conference*, **11**, 359 (September 1995).
4. L. Pawlowski, “*The Science and Engineering of Thermal Spray Coatings*,” John Wiley & Sons, 1-9 (1995).
5. (2000). About thermal spray. *Hardface Alloys*. <http://www.harfacealloys.com/> (5 August 2003).
6. J. Mostaghimi, S. Chandra, R. Ghafouri-Azar and A. Dolatabadi, “*Modeling Thermal Spray Coating Processes: A Powerful Tool in Design and Optimization*,” *Surface and Coatings Technology*, **163**, 1-11 (2003).
7. E. Petrovicova and L.S. Schadler, “*Thermal Spraying of Polymer*,” *International Materials Reviews*, **47**, 169 – 189 (2002).
8. S. Sampath and R. McCune, “*Thermal-Spray Processing of Materials*,” *MRS Bulletin*, **12** (July 2000).

9. D.J. Varacalle, Jr., G.C. Wilson, R.W. Johnson, T.J. Steeper, G. Irons, W.R. Kratochvil and W.L. Riggs, "*A Taguchi Experimental Design Study of Twin-Wire Electric Arc Sprayed Aluminum Coatings*," *Journal of Thermal Spray Technology*, ASM International, **3**, 69 (March 1994).
10. R.C. Tucker, Jr., Praxair Surface Technologies, Inc., "*Thermal Spray Coatings*," *ASM Handbook – Surface Engineering*, 499-506 (2000).
11. H. Herman, S. Sampath and R. McCune, "*Thermal Spray: Current Status and Future Trends*," *MRS Bulletin*, 18 (July 2000).
12. A. Vardelle, C. Moreau and P. Fauchais, "*The Dynamics of Deposit Formation in Thermal-Spray Processes*," *MRS Bulletin*, 32 (July 2000).
13. D. Sacriste, N. Goubot, J. Dhers, M. Ducos and A. Vardelle, "*An Evaluation of the Electric Arc Spray and (HPPS) Processes for the Manufacturing of High Power Plasma Spraying MCrAlY Coatings*," *Journal of Thermal Spray Technology*, ASM International, **10**, 352-358 (June 2001).
14. (2000). Semiconductor equipment applications – metallic coatings. *APS Materials*. <http://www.apsmaterials.com/> (2 January 2004).
15. G.R. Heath, P. Heimgartner, G. Irons, R. Miller and S. Gustafsson, "*An Assessment of Thermal Spray Coating Technologies for High Temperature Corrosion Protection*," *Materials Science Forum*, **251**, 809-816 (1997).
16. Y.L. Zhu, H.L. Liao, C. Coddet and B.S. Xu, "*Characterization via image analysis of cross-over trajectories and inhomogeneity in twin arc spraying*," *Surface and Coatings Technology*, **162**, 307 (2003).

17. (2002). Arc spray equipment solutions. *Praxair surface technologies*.
<http://www.praxair.com/> (2 September 2003).
18. M. Li and P.D. Christofides, “*Modeling and analysis of HVOF thermal spray process accounting for powder size distribution*,” *Chemical Engineering Science*, **58**, 849 (2003).
19. M. Amin, “*Effects of Process Parameter on Surface Roughness and Porosity for Coatings Deposited using the Arc Spray Process*,” *A Review of Arc Spray Coating Process*, **2**, 273-276 (1996).
20. M. Laribi, N. Mesrati, A.B. Vannes and D. Treheux, “*Adhesion and residual stresses determination of thermally sprayed molybdenum on steel*,” *Surface and Coatings Technology*, **166**, 208 (2003).
21. D.J. Varacalle, Jr., D.P. Zeek, V. Zanchuck, E. Sampson, K.W. Couch, D. Benson and G.S. Cox, “*Experimental Studies of Twin-Wire Electric Arc Sprayed Zinc/Aluminum Alloy Coatings*,” *Journal of Thermal Spray Technology*, ASM International, **7**, 513-520 (December 1008).
22. R.L. Apps, “*The Influence of Surface Preparation on the Bond Strength of Flame-Sprayed Aluminum Coatings on Mild Steel*,” *J. Vac., Sci. Technol.*, **11**, 741-745 (July/August 1974).
23. W.P. Dong, P.J. Sullivan and K.J. Stout, “*Comprehensive study of parameters for characterizing three-dimensional surface topography - I: Some inherent properties of parameter variation*,” *Wear*, **159**, 161 (1992).

24. J.M. Guilemany, N.L. Isern and P.J. Szabo, "*Residual Stress Characterization of Grit Blasted Steel Surfaces*," *Surface Engineering*, **12**, 77-79 (1996).
25. C. Coddet, G. Montavon, S. Ayrault-Costil, O. Freneaux, F. Rigolet, G. Barbezat, F. Folio, A. Diard and P. Wazen, "*Surface Preparation and Thermal Spray in a Single Step: the PROTAL Process – Example of Application for an Aluminum-Base Substrate*," *Journal of Thermal Spray Technology*, **8**, 235-242 (June 1999).
26. J.K. Knapp and T.A. Taylor, "*Waterjet Roughened Surface Analysis and Bond Strength*," *Surface & Coating Technology*, **86**, 22-27 (1996).
27. M. Mellali, A. Grimaud, A.C. Leger, P. Fauchais and J. Lu, "*Alumina Grit Blasting Parameters for Surface Preparation in the Plasma Spraying Operation*," *Journal of Thermal Spray Technology*, **6**, 217-227 (June 1997).
28. C.A. Brown and S. Siegmann, "*Fundamental scales of adhesion and area-scale fractal analysis*," *International Journal of Machine Tools & Manufacture*, **41**, 1933 (2001).
29. D.L. Hale, W.D. Swank and D.C. Haggard, "*In-Flight Particle Measurements of Twin-Wire Electric Arc Sprayed Aluminum*," *Journal of Thermal Spray Technology*, ASM International, **7**, 58-63 (March 1998).
30. G. Jandin, H. Liao, Z.Q. Feng and C. Coddet, "*Correlations between operating conditions, microstructure and mechanical properties of twin wire arc sprayed steel coatings*," *Materials Science and Engineering*, **2**, 1-8 (2000).
31. J.R. Fincke and R.A. Neiser, "*Advanced Diagnostics and Modeling of Spray Processes*," *MRS Bulletin*, **26** (July 2000).

32. B. Nowicki, "*Multiparameter Representation of Surface Roughness,*" *Wear*, **102**, 161 (1985).
33. ANSI/AMSE B.46.1, "*Surface Texture (Surface roughness, Waviness, and Lay,)*" (1995).
34. Mitutoyo, SJ-201 Surface Roughness Tester, *published results* (1997).
35. K.J. Stout and L. Blunt, Development of Methods for the Characterisation of Roughness in Three Dimensions, *published results* (2000).
36. ASTM C633 – 79, Standard Test Method for Adhesion or Cohesive Strength of Flame-Sprayed Coatings, *published results* (1993).
37. W.P. Dong, P.J. Sullivan and K.J. Stout, "*Comprehensive study of parameters for characterizing three-dimensional surface topography - IV: Parameters for characterizing spatial and hybrid properties,*" *Wear*, **178**, 45 (1994).
38. W.P. Dong, P.J. Sullivan and K.J. Stout, "*Comprehensive study of parameters for characterizing three-dimensional surface topography - III: Parameters for characterizing amplitude and some functional properties,*" *Wear*, **174**, 29-35 (1994).
39. W.P. Dong, P.J. Sullivan and K.J. Stout, "*Comprehensive study of parameters for characterizing three-dimensional surface topography - II: Statistical properties of parameter variation,*" *Wear*, **167**, 16 (1993).
40. (2000). ASTM-C633 testing standard. *DFD instruments*.
<http://www.dfdinstruments.co.uk/> (2 October 2003).

41. S. Parthasarathi, K. Sampath and B.R. Tittmann, "*Metrology of Grit Blasted Surfaces*," Proceedings of the 8th National Thermals Spray Conference, 11-15 (September 1995).
42. H. Lee, Y. Eo, Y. Kim and K. Ahn, Korea, Object's Surface Roughness Measurement using a High Resolution Digital Camera, *published results* (1998).
43. (2004). How the SEM works. *Iowa State University*. <http://www.iastate.edu/> (21 November 2003).
44. D.L. Smith, "*Material Analysis*," *Methods of Thin Film Deposition*, **5**, 11 (2003).
45. Rank Taylor Hobson Manual, Precision, *published results* (1998).
46. (2001). Dimensional measurements. *NIST manufacturing engineering laboratory*. <http://www.mel.nist.gov/> (2 December 2003).
47. J.I. Goldstein, D.E. Newbury, P. Echlin, D.C. Joy and E. Lifshin, "*Scanning Electron Microscopy and X-ray Microanalysis*," A Text for Biologists, Materials Scientists, and Geologists, 101 (1981).

APPENDICES

APPENDIX A – RESULTS OF Ra BEFORE AND AFTER CLEANING

Grit Size	80 Grit		36 Grit		24 Grit	
	<i>Before Cleaning</i>	<i>After Cleaning</i>	<i>Before Cleaning</i>	<i>After Cleaning</i>	<i>Before Cleaning</i>	<i>After Cleaning</i>
<i>S/N</i>	31A		07A		19A	
	66.705	60.232	97.957	108.268	182.228	177.240
	68.449	64.079	103.654	114.917	189.020	197.146
<i>Ave</i>	67.577	62.156	100.806	111.593	185.624	187.193
<i>Std Dev</i>	1.233	2.720	4.028	4.702	4.803	14.076
<i>S/N</i>	32A		08A		20A	
	62.961	67.043	139.807	142.909	202.028	211.764
	67.878	64.579	138.945	150.028	191.929	196.937
<i>Ave</i>	65.420	65.811	139.376	146.469	196.979	204.351
<i>Std Dev</i>	3.477	1.742	0.610	5.034	7.141	10.484
<i>S/N</i>	33A		09A		21A	
	65.185	59.035	124.236	127.567	147.984	175.650
	57.287	60.004	132.035	132.000	158.461	183.969
<i>Ave</i>	61.236	59.520	128.136	129.784	153.223	179.810
<i>Std Dev</i>	5.585	0.685	5.515	3.135	7.408	5.882
Average	64.744	62.495	122.772	129.282	178.608	190.451
Ave S.D.	3.432	1.716	3.384	4.290	6.451	10.147

**APPENDIX B – F-TESTS AND T-TESTS OF THE CHANGES IN
ROUGHNESS BEFORE AND AFTER CLEANING**

t-Test: Two-Sample Assuming Equal Variances

	<i>Variable 1</i>	<i>Variable 2</i>
Mean	64.74417	62.49533
Variance	17.27498	10.16685
Observations	6	6
Pooled Variance	13.72092	
Hypothesized Mean Difference	0	
df	10	
t Stat	1.051541	
P(T<=t) one-tail	0.158878	
t Critical one-tail	1.812462	
P(T<=t) two-tail	0.317757	
t Critical two-tail	2.228139	

F-Test Two-Sample for Variances

	<i>Variable 1</i>	<i>Variable 2</i>
Mean	64.74417	62.49533
Variance	17.27498	10.16685
Observations	6	6
df	5	5
F	1.699148	
P(F<=f) one-tail	0.287434	
F Critical one-tail	5.050339	

80 Grit

t-Test: Two-Sample Assuming Equal Variances

	<i>Variable 1</i>	<i>Variable 2</i>
Mean	122.7723	129.2815
Variance	324.1972	254.8724
Observations	6	6
Pooled Variance	289.5348	
Hypothesized Mean Difference	0	
df	10	
t Stat	-0.66258	
P(T<=t) one-tail	0.26129	
t Critical one-tail	1.812462	
P(T<=t) two-tail	0.522579	
t Critical two-tail	2.228139	

F-Test Two-Sample for Variances

	<i>Variable 1</i>	<i>Variable 2</i>
Mean	122.7723	129.2815
Variance	324.1972	254.8724
Observations	6	6
df	5	5
F	1.271998	
P(F<=f) one-tail	0.399107	
F Critical one-tail	5.050339	

36 Grit

t-Test: Two-Sample Assuming Equal Variances

	<i>Variable 1</i>	<i>Variable 2</i>
Mean	178.6083	190.451
Variance	438.2381	195.3503
Observations	6	6
Pooled Variance	316.7942	
Hypothesized Mean Difference	0	
df	10	
t Stat	-1.15245	
P(T<=t) one-tail	0.137971	
t Critical one-tail	1.812462	
P(T<=t) two-tail	0.275942	
t Critical two-tail	2.228139	

F-Test Two-Sample for Variances

	<i>Variable 1</i>	<i>Variable 2</i>
Mean	178.6083	190.451
Variance	438.2381	195.3503
Observations	6	6
df	5	5
F	2.243345	
P(F<=f) one-tail	0.197974	
F Critical one-tail	5.050339	

24 Grit

**APPENDIX C – F-TEST AND T-TEST OF SIZE 24 AND SIZE 80 GRITS
COUPONS**

**C1. F-TEST AND T-TEST OF THE BOND STRENGTH OF CLEAN
COUPONS BLASTED BY SIZE 24 GRIT AND SIZE 80 GRIT**

t-Test: Two-Sample Assuming Equal Variances

	<i>Variable 1</i>	<i>Variable 2</i>
Mean	1504.27	1398.17
Variance	369190	202902
Observations	11	12
Pooled Variance	282087	
Hypothesized Mean Difference	0	
df	21	
t Stat	0.4786	
P(T<=t) one-tail	0.31858	
t Critical one-tail	1.72074	
P(T<=t) two-tail	0.63717	
t Critical two-tail	2.07961	

F-Test Two-Sample for Variances

	<i>Variable 1</i>	<i>Variable 2</i>
Mean	1504.273	1398.17
Variance	369189.6	202902
Observations	11	12
df	10	11
F	1.819543	
P(F<=f) one-tail	0.170174	
F Critical one-tail	2.853625	

**C2. F-TEST AND T-TEST OF THE BOND STRENGTH OF NON-CLEAN
COUPONS BLASTED BY SIZE 24 GRIT AND SIZE 80 GRIT**

t-Test: Two-Sample Assuming Equal Variances

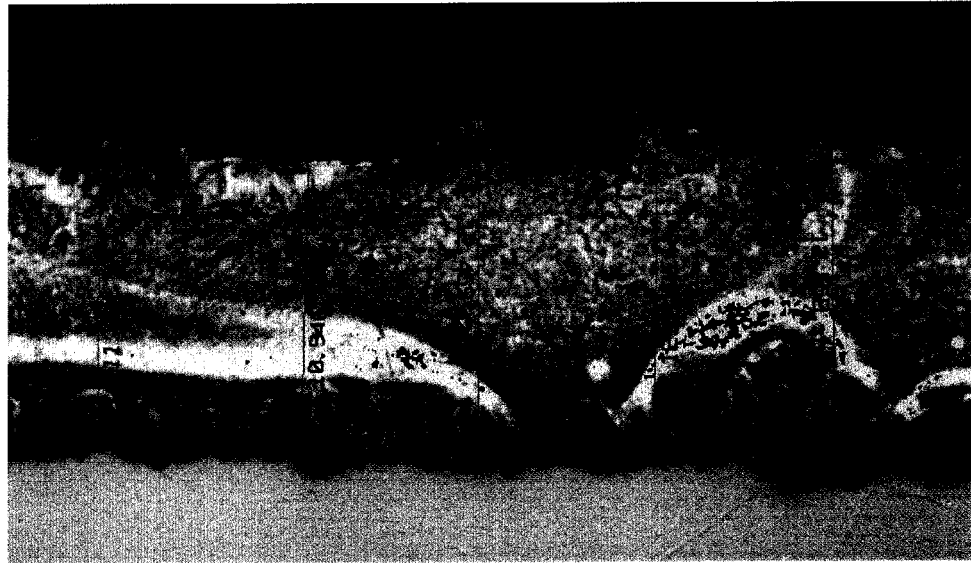
	<i>Variable 1</i>	<i>Variable 2</i>
Mean	3528.08	3792.67
Variance	1024364	911018
Observations	12	12
Pooled Variance	967691	
Hypothesized Mean Difference	0	
df	22	
t Stat	-0.65882	
P(T<=t) one-tail	0.25842	
t Critical one-tail	1.71714	
P(T<=t) two-tail	0.51685	
t Critical two-tail	2.07388	

F-Test Two-Sample for Variances

	<i>Variable 1</i>	<i>Variable 2</i>
Mean	3528.083	3792.67
Variance	1024364	911018
Observations	12	12
df	11	11
F	1.124417	
P(F<=f) one-tail	0.424637	
F Critical one-tail	2.817927	

APPENDIX D – CROSS-SECTIONED VIA COMPUTERIZED IMAGE ANALYSIS

D1. Clean 24 Grit: 100x (# 040)

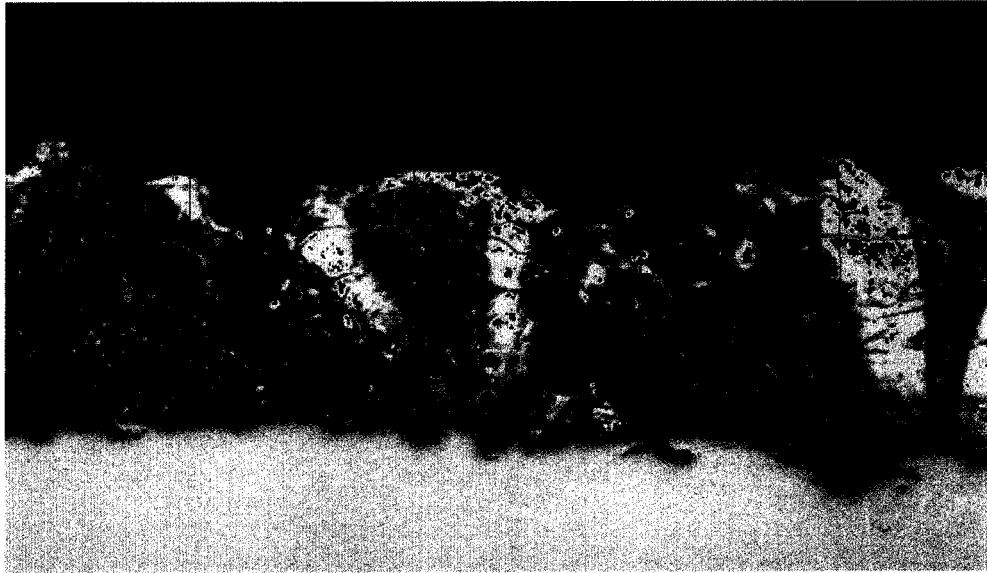


11.091 10.946 12.459 12.214 12.558



10.700 11.505 10.213 10.946 10.803

D2. Clean 36 Grit: 200x (# 020)



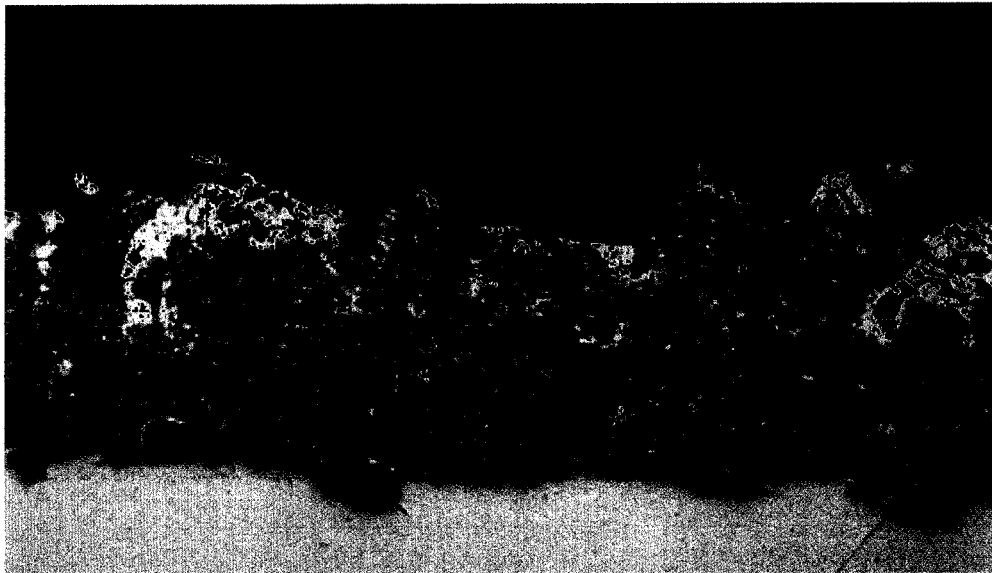
1.918

1.645

1.782

1.609

2.182



1.618

1.872

1.863

1.581

2.027

2.000

D3. Clean 80 Grit: 100x (# 070)

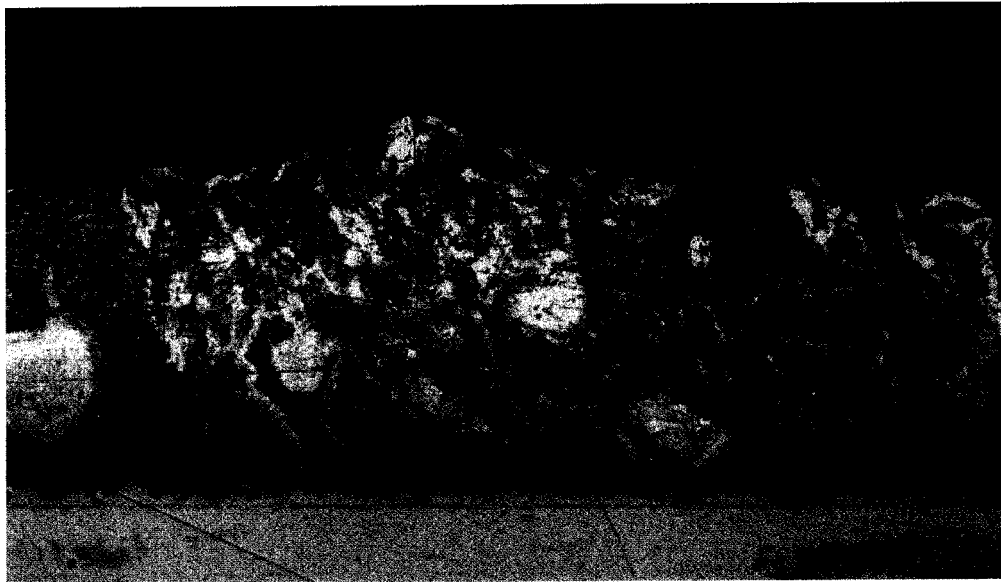


11.531

12.655

12.606

11.384



11.141

12.704

11.238

10.311

D4. Non-Clean 24 Grit: 200x (# 055)



1.863

2.009

2.145

2.281

2.109



2.136

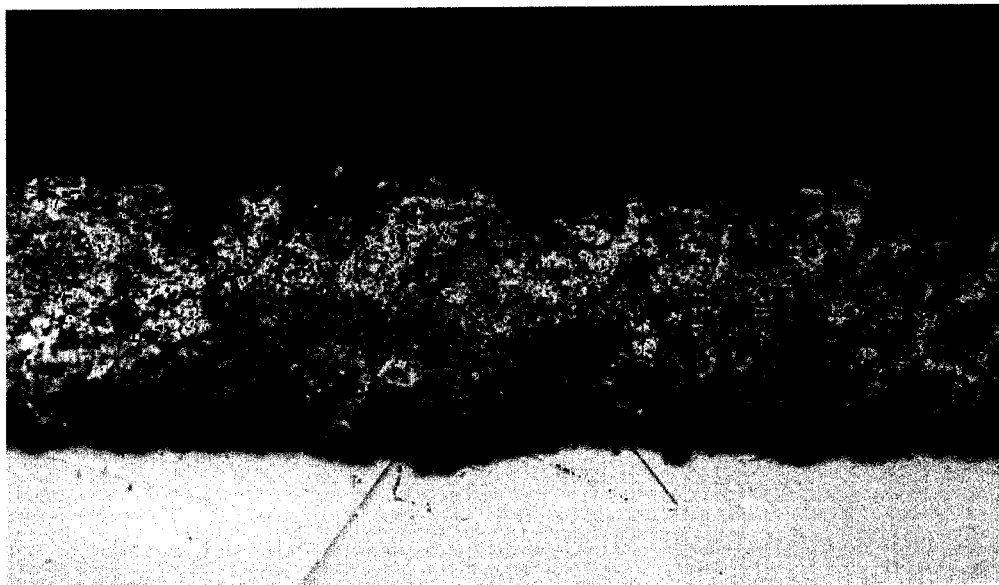
2.319

2.072

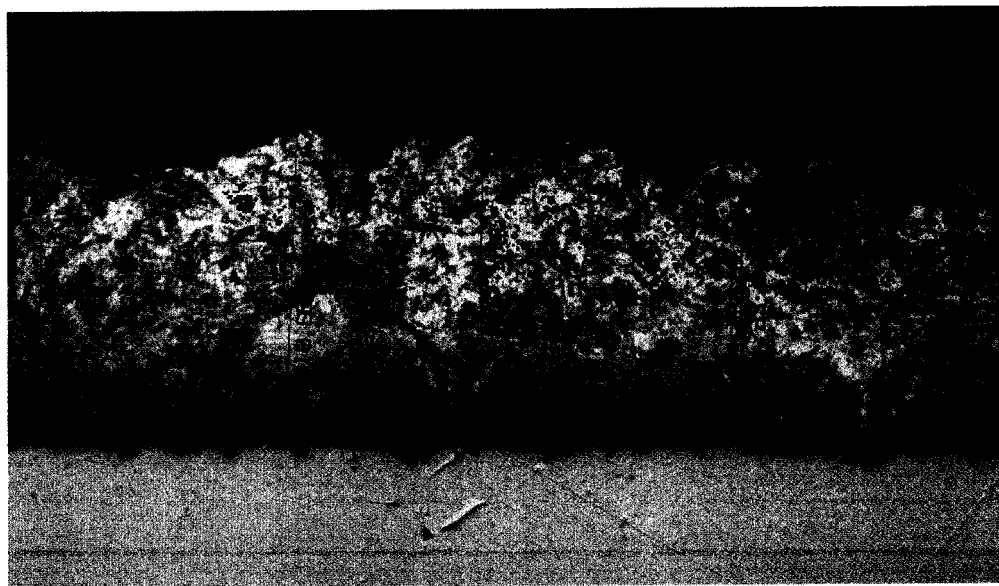
2.127

1.709

D5. Non-Clean 36 Grit: 100x (# 005)

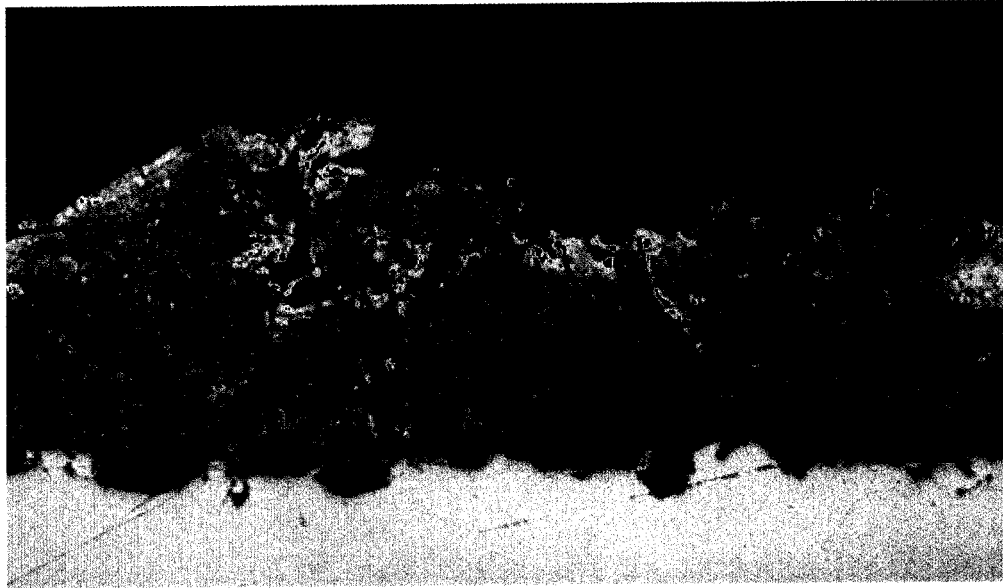


9.186 8.943 10.016 8.503 9.478



10.456 10.063 10.407 9.723 9.185

D6. Non-Clean 80 Grit: 200x (# 085)

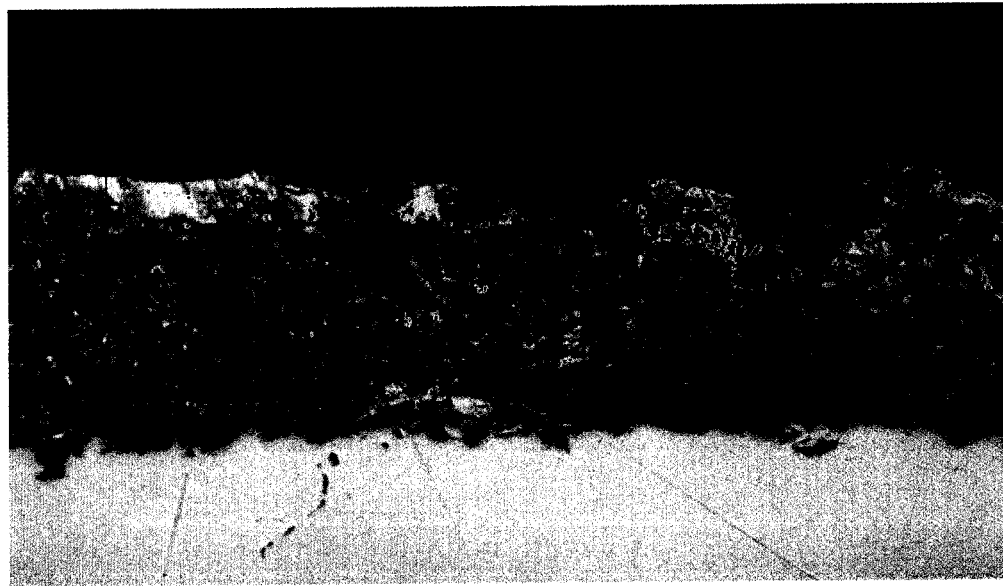


2.210

1.809

1.654

1.572



1.736

1.554

1.600

1.663

APPENDIX E - RESULTS OF SIZE 80 GRIT COUPONS

	Clean		Non-Clean	
	Roughness (microin)	Bond Strength (psi)	Roughness (microin)	Bond Strength (psi)
80 grit	55.291	1210	59.354	3853
	58.059	1847	48.004	4828
	54.488	1516	54.516	4051
	53.272	1529	71.047	4637
	57.425	764	78.551	1306
	53.720	2420	60.331	4306
	51.295	2325	54.500	3643
	84.114	1306	56.043	2624
	78.134	573	52.724	2580
	64.016	2038	53.972	2930
	50.744	1019	63.461	3471
			55.252	4108
Average	60.051	1504.273	58.980	3528.083
Stdev	11.115	607.610	8.517	1012.109

APPENDIX F – RESULTS OF SIZE 36 GRIT COUPONS

	Clean		Non-Clean		
	Roughness (microin)	Bond Strength (psi)	Roughness (microin)	Bond Strength (psi)	
36 grit	107.039	4013	116.689	3771	
	116.531	4917	96.307	2216	
	112.378	4076	105.437	1834	
	95.866	3694	99.980	2955	
	82.217	4446	84.106	1885	
	99.268	3981	98.319	1197	
	86.921	4688	95.126	2471	
	99.854	1783	97.768	2102	
	89.512	3599	110.933	2325	
	101.350	3822	106.531	2013	
	92.343	3503	101.496	1337	
	89.067	4943	113.579	318	
	Average	97.696	3955.417	102.189	2035.333
	Stdev	10.476	843.859	9.031	872.429

APPENDIX G – RESULTS OF SIZE 24 GRIT COUPONS

	Clean		Non-Clean	
	Roughness (microin)	Bond Strength (psi)	Roughness (microin)	Bond Strength (psi)
24 grit	169.004	1785	170.854	4280
	184.236	2293	188.185	3694
	186.457	968	190.433	3248
	194.961	1274	183.933	4267
	196.740	1051	179.469	4446
	175.358	1388	134.197	3949
	165.378	1478	211.335	5210
	168.417	1529	193.795	3694
	182.764	713	178.803	2790
	210.689	1274	189.646	1479
	207.898	1051	165.134	4076
	208.189	1974	193.984	4379
Average	187.508	1398.167	181.647	3792.667
Stdev	16.237	450.447	19.126	954.472